PhD Program in Bioengineering and Robotics

Curriculum: Bionanotechnology

Project title:

DEVELOPING DRUG DELIVERY SYSTEMS BASED ON ALGINATE AND BRUSHITE

Student: **Seyed Mohammad Hossein Dabiri**

Cycle: **XXX**

Tutors: **Laura Pastorino**

Year: **2014-2017**

TABLE OF CONTENTS

DEDICATION

This is dedicated to my family and Laura Pastorino

without whom nothing would have been possible

ACKNOWLEDGEMENTS

This journey would not have been possible without the support of my family, professors and mentors, and friends.

To my family, thank you for encouraging me in all of my pursuits and inspiring me to follow my dreams. I will never forget the emotional supports I got from you. I always knew that you believed in me and wanted the best for me.

To my advisor Prof. Laura Pastorino for the continuous support of my Ph.D study and related research, for her patience, motivation, and immense knowledge. Her guidance helped me in all the time of research and writing of this thesis. I could not have imagined having a better advisor and mentor for my Ph.D study.

My sincere thanks also goes to Prof. Elizabetta Finocchio, Prof. Bahar Aliakbarian Prof. Barberis, Dr.Alberto Lagazzo, and Dr. Mehdi Farokhi who gave me access to their laboratories and research facilities and provided me the opportunity to collaborate with them. Without their precious support it would not be possible to conduct this research.

Many thanks to my life-coach and eternal cheerleader, Arin: I will never forget our interesting and long-lasting conversation. My forever interested, encouraging and always enthusiastic friend, Mz: I will be very appreciative of your support. My big brother, movie mate, supporter, colleague, Amir(Reza): The time we spent together will

be unforgettable in my life. My guardian, tracker, and partner in crime, Hamed: hope to see you in Amsterdam.

With a special mention to Yalda, Sepehr, Hossein, Mahdiar, Reza, Elena, Ilaria, and Camilo. It was fantastic to have the opportunity to know you and spending time with you. I will be grateful for all the supports and help you gave during this period of time.

Hossein

February 5, 2018, Genova, Italy

Preface

Biomedical applications of polymer-composite materials have experienced an ascending trend during the last few decades. A composite is a material constituted by at least two separate phases (the matrix and the reinforcement) with different physical and chemical properties that result to a new material with a significant different properties compare to those of reference materials. Biopolymers-calcium phosphate is one of the most frequently used composite system in biomedical applications especially in the regeneration of hard tissue and drug delivery. Incorporation of inorganic materials like calcium phosphate into polymer matrix, or reverse, may enhance biocompatibility, mechanical properties and modified swelling and drug release behavior of individual components. Another significant factors which need to be taken into consideration are the type and content of reinforcement component to tailor these properties to specific demands.

Alginate is a promising polysaccharide polymer which has been extensively used owing to its biocompatibility low toxicity and mild gelation conditions. Alginate have been subjected to the incorporation with calcium phosphate materials specially hydroxyapatite for drug delivery application. This secondary phase not only improved mechanical properties such as compressive strength and toughness, but also it resulted to a sustained release profile. Recently dicalcium phosphates including brushite and

monetite have risen the attentions due to their superior biodegradability in physiological conditions respect to other calcium phosphates.

My PhD was oriented toward developing drug delivery system based on Alginate and brushite. Therefore, in the first chapter a brief information about alginate and brushite was provided. In addition, this chapter include a quick overview over different biomedical applications of these materials. This chapter was followed by three chapters which have their own introduction, materials and method, results and discussion, and conclusion.

In the second chapter, the process of in-situ formation of Alginate-brushite composite hydrogels for their prospective usage as drug delivery systems was investigated. This composite hydrogel could be of particular interest in oral drug delivery systems and hard tissue regeneration especially in dental and periodontal local treatment. The effect of initial pH and phosphate concentration on the in-situ formation of brushite inside the Alginate matrix were taken into account. The different samples were characterized by XRD, FTIR, SEM, TGA, DTA, and MTT

Evaluation of in-situ synthetized Alginate-Brushite hydrogel composites as a novel pH sensitive drug carriers was discussed in the third chapter. The different carrier formulations as well as the final composites have been fully characterized to understand the carriers-drug interactions. The mechanical properties and the swelling behaviors were evaluated with respect to changes in the content of raw materials to thoroughly investigate the mechanical property impacts on the release behavior of these composite

materials. Sodium salt of Ibuprofen (Ibu) was used as a model drug to perform release experiments.

The aim of fourth chapter was fabricating a functionalized bone cement substitute for the local delivery of Gentamicin sulfate. The effects of alginate concentration on microstructural, mechanical, and biological properties of brushite cement as a Gentamicin sulfate carrier was studied in the first part of this chapter. In the second part, the most adequate concentration of alginate according the obtained results in the first part was chosen to load Gentamicin with different concentrations through liquid phase or solid phase. Finally, different formulations of cement were examined in terms of setting time, chemical composition, and chemical, morphological and mechanical changes in response to soaking in PBS along with evaluation of Gentamicin release by these cements for a period of two weeks.

Finally, highlights of different part of my projects was reported as the final chapter entitled conclusion. It is noteworthy that the major part of this thesis has already been published in the form of research articles in international peer reviewed journals. Since all of those works were carried out by me under supervision of my tutor, I have freely used text, figures and tables in those publications.

CHAPTER 1

Introduction

In conventional drug administration methods, most drugs fail to achieve favorable clinical outcomes, because of the very fast release rate and the difficulty, represented by biological barriers, for the drug to reach its intended target. Therefore, these methods entail the administration of high drug dosages and a significant amount of these is 'lost' over healthy tissues and organs, with the risk of provoking severe side effects.

The idea of developing a DDS[1] that selectively kills unhealthy cells, while leaving healthy ones untouched, was first introduced by Paul Ehrlich over a century ago. Since then, the development of systems for the targeted delivery of drugs directly at the desired site of action and with a controlled release rate has been the object of several studies. Controlled drug delivery systems would offer significant advantages when compared to conventional methods, including higher therapeutic efficiency, lower toxicity and better patient compliance. This chapter is a quick overview over the Alg[2] and Bru[3] materials which have been used to develop DDS

1.1 Alginate

Alg is a conventional polysaccharide obtained from brown algae such as kelp. Alg is able to form hydrogel at mild pH and entrapping drugs, biomolecules, and cells.

---

[1] Drug Delivery Systems

[2] Alginate

[3] Brushite

Biocompatibility, low toxicity, and low price of Alg have made it a proper material to investigate and use for numerous biomedical applications [1].

1.1.1 Chemical structure

Alg was first discovered by Edward Stanford, a Scottish chemist, in 1883, but it was only with the work of Fischer and Dörfel in the 1950s that its structure became fully known. Alg is an anionic biopolymer composed of α-L-guluronicacid (G) and the β-D-mannuronic acid (M) (Figure. 1) which glycosidic bonds link guluronicacid (G) and mannuronic acid (β-(1–4) and α-(1–4)) together. Although there is a possibility to obtain Alg from bacterial sources, commercially available Alg is only extracted from algal sources. Different characteristic such as copolymer sequence and molecular weight are totally depending on the source of copolymers [2].

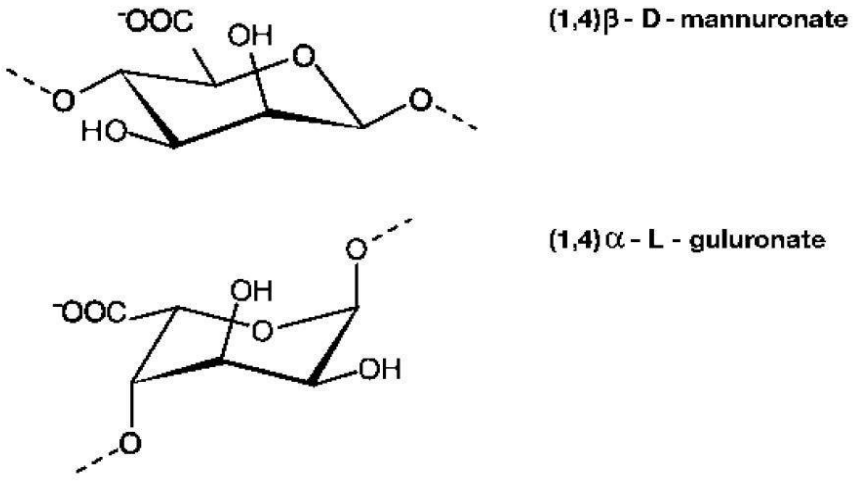

Figure 1. Chemical structure of mannuronate and guluronate, the 'building blocks' of Alg [2].

Consecutive guluronic residues (GGG), mannuronic residues (MMM) and blocks made of random or alternating residues (MGM) as shown by Figure. 2 are three types of block which form Alg structure. Alg structural properties is influenced by the type of blocks. In addition, properties like solubility and hydrophobicity in Alg derivatives can be modified through controlling the monosaccharide sequence and nature, location and quantity of substituents, as well [1]. For instance, chains made by the alternating MG units are more flexible and soluble at lower pH than the other kinds, while G-blocks give stiffer chains. Thus, the distribution and proportion of the two residues in the structure are critical factors affecting the chemical and physical properties of Alg. Noteworthy that the relative amount of guluronate and mannuronate may significantly vary in different Alg depending on the source extraction [3].

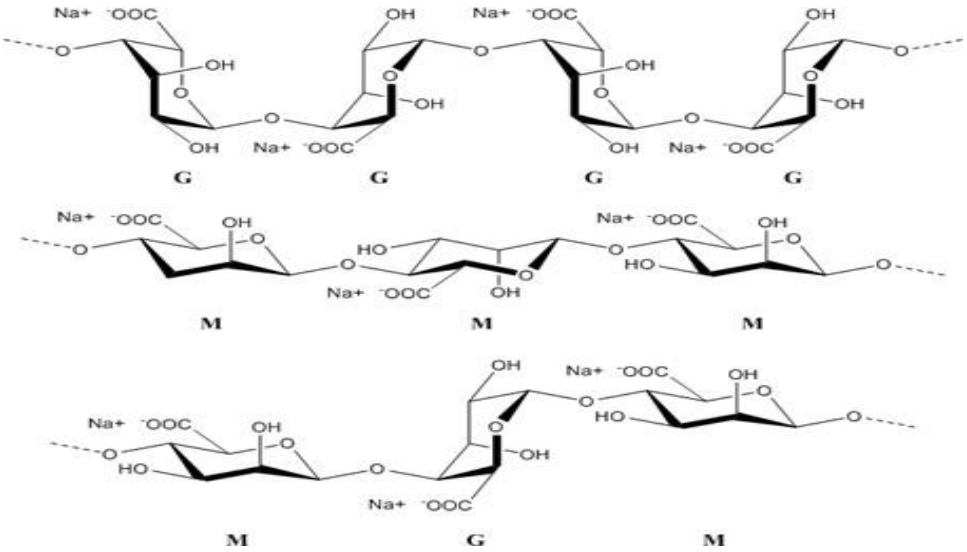

Figure 2. Structure of G-blocks, M-blocks and alternating blocks in Alg

Ionically cross-linked Alg hydrogels are obtained in the presence of divalent cations, such as Ca^{2+}. It has been reported that structure of Alg and type of cations are dominant parameter in bonding strength. For instance, Alg with high content of G-blocks form stronger gels than the high-M or high-MG due to the fact that bonding with G blocks is more favorable for divalent. Besides, it has been reported that the boning strength has descending trend within the following order of divalent: Pb > Cu > Cd > Ba > Sr > Ca >Co, Ni, and Zn > Mn [2, 4, 5]. Figure. 3 shows three possible types of junction in Ca-Alg hydrogels.

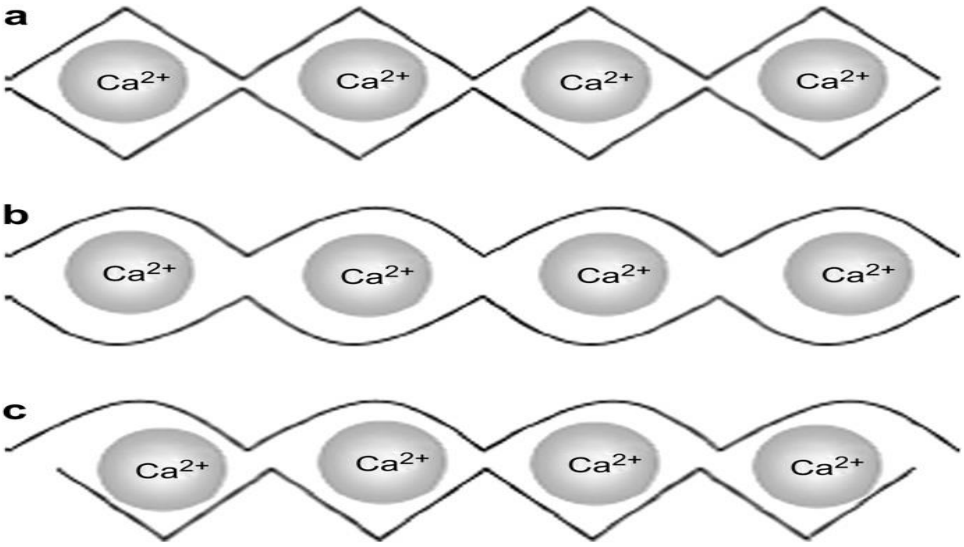

Figure 3. a) GG/GG b) MG/MG and c) GG/MG junction points in Alg [6]

1.1.2 Physical properties

Physical properties of Alg and its hydrogels intensively depend on structural factors such as sequence of M and G block, length of G blocks, and molecular weight. Moreover, these factors have a direct impact on the mechanical properties of Alg

hydrogels as well as their stability so that increase in the length of G blocks and molecular weight will result in mechanical properties and stability enhancement [3].

Also, there is a direct relationship between the viscosity of Alg solution and molecular weight of Alg so that Alg with higher molecular weight will yield to more viscose solution. However, sever viscose solutions are not desirable due to the hard processing of that. In addition, the pH of solution is another significant factor which has an important role in the viscosity of Alg. Protonation of carboxylate group in the Alg backbone as pH decrees will cause an increase in the viscosity. Furthermore, pH of solvent, ionic strength of the medium, and presence of gelling ions determined Alg solubility in water. It has been suggested that pH of solution should be above pKa of Alg to deprotonate the carboxyl acid group of Alg and subsequently increase water solubility. Noteworthy that physical properties of Alg and its gels can be modified by selecting primary compound structure (high-G, high-M, and poly MG) and gelling agents [7-9].

1.1.3 Hydrogel formation: the ‘egg-box’ model

The most common method to form Alg hydrogel is chelating with divalent cations such as Ca, Sr, and Mn through an ionic bonding. The Gel is obtained through participation of G blocks to form a tight held junction. This is due to the fact that G blocks structure is able to highly coordinate with divalent cations. Therefore, at least two polymeric chain will be aliened so that G blocks of one will form the junction with the adjacent G block through entrapping cations [4]. Also, this is associated with weak junction arising from participation of MG blocks [6]. This gelling mechanism was first described in 1973 and called as ‘egg-box’ model owing to its appearance [10]. As be seen

in Figure. 4, four G blocks (two from one polymeric chain) are surrounding divalent cations to form the junction. Among all the divalent cations, Ca is the most frequently used in formation of hydrogels. However, the stability of Ca-Alg in physiological conditions is poor because of fast integration resulting from ion exchange reaction with monovalent cations [1].

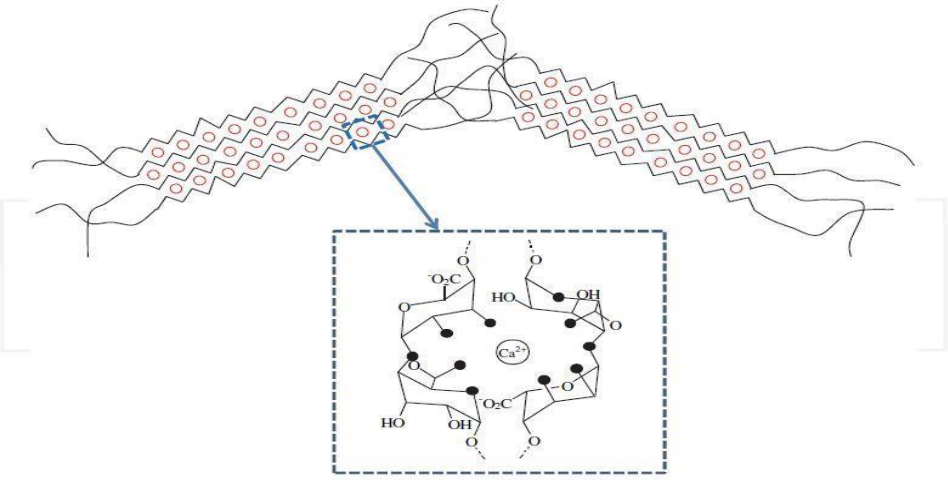

Figure 4. Ionotropic gelation of Alg according to the egg-box model

1.1.4 Biomedical applications

Alg have been widely used in biomedical applications ranging from tissue engineering to wound dressing and cell culturing.

- *Wound dressing*

The traditional wound dressing materials act as a barrier to prevent bleeding and maintain the wound area dry by evaporating wound exudate and hindering

pathogens inclusion to the wound area. The next generation of wound dressings like, Alg dressing, contain moisture to assist wound healing process [11]. Alg freeze-dried sheets and nonwoven fibers are extensively using in this regard, since they adsorb wound area blood and regel. Therefore, they can provide the desire physiological moisture to the wound area and decline the risk of bacterial infection at there. Subsequently, enhance in formation of granulated tissue, epithelialization rate which facilitate healing are listed as the result of using Alg wound dressing. Noteworthy that various kind of Alg wound dressing are commercially available. Further investigation yielded to fabrication of bioactive Alg wound dressing through incorporation of therapeutic agents such as dibutyryl cyclic adenosine monophosphate, stromal cell-derived factor-1, silver nanoparticle, and zinc ions. Completing re-epithelization, accelerating wound closure, minimizing scar formation, increasing antimicrobial activity and antioxidant capacity, promoting keratinocyte migration, and enhancing the level of endogenous growth factors at the wound microenvironment are listed as the advantageous of these kind of Alg wound dressing over the previous ones [12-15].

- *Cell culture*

Another significant application of Alg hydrogels are fabricating scaffold for culturing cells and being used as ideal blank slate. This is derived from poor protein adsorption capacity of Alg along with the lack of mammalian cell receptors for Alg. In this regard, Alg hydrogels are being used as 2D or 3D culture system for specific cell adhering demands through coupling synthetic peptides. Moreover, biocompatibility as

well as simplicity of Alg to be introduced into body have made the result obtained in in-vitro condition extensible to in-vivo conditions. One remarkable example is entrapping neural cells stem cells in 3D Alg platform in in-vitro conditions to evaluate impact of Alg hydrogel and mechanical properties on the neural cells differentiation and proliferation. The results confirmed the positive effect of Alg 3D scaffold on promoting differentiation, growth and extension of neurite [3].

- *Drug delivery*

The main role of Alg in delivering pharmaceutical agents are stabilizing and hindering it to have a controlled release. Alg hydrogels have been extensively used as drug carriers in oral uptake form. In addition, usage of Alg hydrogels as local delivery carriers have gain attentions. It has been stated that Alg hydrogels have nonoporous structure (pore size ~ 5 nm) [16] which let the drug molecules, especially low molecular weight drug, diffuse to the surrounding media. Therefore, drug diffusion is the primary mechanism for the drug release followed by gel gradual disintegration. Besides, water solubility of the drug plays an important role in determination of release mechanism so that drug diffusion and gel degradation are dominant mechanism for water soluble and non-soluble drugs, respectively. The content of Alg influences the size of pore which is significant factor for the diffusion of the drug. In general, the pore size increases parallel with increase in Alg content which facilitate migration of water inside the matrix and faster release. Furthermore, the pores are affected by the chemical structure of Alg so that high G Alg possess higher open pores than high M ones and yield to superior drug

diffusion rate. Nonetheless, burst release associated with Alg hydrogels is not ignorable [17].

The interactions between drug and Alg matrix effects on the release kinetic, as well. Drugs that stablish primary or secondary bonding (combination of ionic and covalent cross-linking) with Alg will cause restricting swelling of Alg which subsequently prolong the release profile. Another approach is entrapping several drug into Alg based hydrogels for simultaneous or sequential delivery and altering releasing each drug through chemical and structural changes. For instance, co delivery of methotrexate and doxorubicin is carrying out through fast diffusion for methotrexate (no interaction with Alg and chemical hydrolysis of cross-linker for doxorubicin (covalently bonded to Alg), respectively [18, 19]. Also, prolonging release profile through combination of Alg with poly cationic polymers has been extensively studied for smart delivery demands. Electrostatic adsorption in certain pH range restricts swelling behavior in off-state of release followed by electrostatic repulsion in on-state of release which facilitate swelling of the carrier defines as the release mechanism [20]. Moreover, Alg derived hydrogels have high potential for protein delivery owing to the fact that proteins can be entrapped into the hydrogels through a relatively mild conditions and Alg gel prevent degradation of protein till release them. This application of Alg assists tissue engineering for regeneration of bones, blood vessels, and muscles. Yet, fast release of protein from intrinsic pores of Alg as well as hydrophilic nature of the network is listed as the limitation of Alg as carrier of proteins [3].

- *Tissue engineering*

Alg hydrogels capability in cell and protein delivery along with Alg cell adhesion properties and degradable nature have made it a suitable materials for tissue engineering and regeneration of various organs. However, the pore size of Alg hydrogel is the main barrier for the releasing regenerative agents from Alg. It has been reported that most protein are able to release from Alg through diffusion mechanism and degradation of Alg would accelerate the release [21]. It should be noted that large molecules such as DNA and antibodies are released by degradation of Alg gels [22, 23]. The most frequently used tissue engineering application of Alg is explained bellow:

a) Blood vessels

Neovascularization which is referred to new blood vessel formation is a novel treatment for those patient suffering from blood flow obstruction and restriction. Transplantation of different cell types such as angiogenic molecules, heparin binding growth factors into the patient body help neovascularization. The local delivery of these therapeutic agents can be achieved via carrying them by Alg hydrogels [24-27]. It has been shown that direct injection of Alg gel loaded with VEGF[4] into ischemic muscle tissue yielded to a long term release of VEGF in the ischemic area and assisted formation of new capillary[28]. Also, sequential delivery of growth factor from Alg gels for different stages of treatment has been investigated to enhance maturation of new tissue

[4] **vascular endothelial growth factor**

and functionality. In vivo results on mice showed that sequentional delivery of VEGF and PDGF-BB[5], two growth factor, by Alg resulted in promoting blood vessels formation and maturation [29, 30]. Further investigations were carried out on the co-delivery of VEGF, MCP-1[6] and endothelial cells from Alg gels improved blood vessels formation [31, 32].

b) Bone tissue engineering

The main role of Alg in bone tissue engineering is delivering osteoinductive factors and bone forming cells. The main merits of Alg usage are minimally invasive introduction, filling irregular damaged area, simple chemical modifications, and controlled releasing of osteoinduction agents. What we should take into condiseration is that Alg gels are not suitable for load bearing tissue without fixation due to the fact that they possess weak mechanical properties. Alg gels have successfully used in bone growth factor delivery in animal model which directly impacted on bone regeneration [33]. In addition, sequential delivery of BMPs[7] (BMP-2 and BMP-7) as well as co-delivery of BMP-2 and VEGF resulted by Alg gels assisted bone marrow stem cell differentiation and improved new bone tissue formation [34-37]. Another approach is incorporating Alg with bioactive materials such as HA[8] to promote bone formation. In this approach

---

[5] **platelet-derived growth factor-BB**

[6] **Monocyte chemotactic protein-1**

[7] **Bone morphogenetic proteins**

[8] **Hydroxyapatite**

osteosarcoma cells are capable of adhering to the surface of scaffold and proliferate through interconnected pores of it which is useful for load bearing demands [38, 39]. Bone marrow stromal cells attachment and proliferation can be further improved by combining Alg with collagen type 1 and β-TCP [40].

c) Cartilage repair

One of the most challenging area of tissue engineering is cartilage repair owing to lack of proper concentration of chondrocyte and blood supply in the damaged area. In addition, poor mechanical properties of the damaged cartilage limits in-situ treatment of the damaged area by. One decent solution is fabricating mechanically stable cartilage in ex-vivo conditions followed by implanting in the damaged site. Alg gels have shown a promising potential for delivering chondrogenic cells in in-vivo conditions to repair damaged cartilage. The primary attempts was carried out by suspending chondrocyte in a solution containing Alg and calcium sulfate followed by molding and shaping cartilage implant [41, 42]. Application of stem cell to restore cartilage functionality has drawn attentions. It has been reported that using Alg modulate stem cell differentiation which resulted in chondrogenesis improvement. In addition, cell morphology regulation of chondrogeninc stem cells toward favorable round shape is facilitated in presence of Alg gels [43-45].

1.2 Brushite

Bru is a kind of calcium phosphate materials which have been widely used as bone cement owing to its osteocunductive properties and superior biodegradability respect to other calcium phosphate materials. It was discovered by Mirtchi and Lemaître

in 1989 . Generally, it is synthetized through an exothermic reaction between acidic and basic calcium phosphate sources. It has been reported that Bru is biocompatible and metastable under physiological conditions. However, fast setting and pour mechanical properties is listed as the main drawbacks of Bru materials [46].

1.2.1 Composition

Bru is constituting from a basic calcium source, an acidic phosphate source, water, and additive for prolonging setting time or enhancing mechanical properties.

- *Basic calcium sources*

Since Bru has the calcium to phosphate ratio of one, the main calcium source is other calcium phosphate materials which have high Ca/P ratio such as TTCP[9] [47]. The most frequently used calcium phosphate as calcium source is β-TCP[10] which have low energy requirement in this regard. Calcium oxide and calcium hydroxide have been used as calcium source, as well [48].

- *Acidic phosphate source*

MCPM[11] is the only calcium phosphate which can be used as phosphate source due to the fact that its Ca/P ratio is lower than one. In addition, MCPM donates one of its

---

[9] **tetracalcium phosphate**

[10] **β-Tricalcium phosphate**

[11] **Monocalcium phosphate monohydrate**

structural water and facilitate precipitation of Bru. Another phosphate source is phosphoric acid [48, 49].

- *Additive*

In order to tune the properties of Bru cements for a specific demand, additive incorporate into fabrication process. Some compounds such as pyrophosphate, sulfates, carbohydrates and carboxylic acid have been added to raw materials to prolong the setting reaction [50]. Also, hydrophilic polymers particularly hydrogels such as silica gel [51], hyaluronic acid [52], and albumin [53] are added at low concentration to improve injectability and cohesion of Bru cement. On the other hand, polymers such collagen type 1 and poly (lactic acid–co-glycolic acid) improve mechanical performance of the cement [48]. Moreover, incorporation of ionic metals such as Mg [54] and Sr [55] through metallic salt or doping cement precursors is another kind of additive which hinder setting time and modify final properties .

1.2.2 Setting reaction

Four phenomena are occurred within the setting reaction including dissolution of precursor in a solvent, formation of super-saturated gel, nucleation and growth inside the gel, formation of a solid of interlocked crystals. For example, the following equations will occurs to form Bru, if MCPM/β-TCP use as cement powder constituents [48]:

I. $Ca(H_2PO_{4)2}.H_2O \longrightarrow Ca^{2+} + 2H_2PO_4^- + H_2O$

II. $\beta\text{-}Ca_3(PO_4)_2 + 4H^+ \longrightarrow 3Ca^{2+} + 2H_2PO_4^-$

III. $Ca^{2+} + H_2PO_4^- + 2H_2O \longrightarrow CaHPO_4.2H_2O + H^+$

IV. $Ca(H_2PO_4)_2.H_2O + \beta\text{-}Ca_3(PO_4)_2 \longrightarrow 4CaHPO_4.2H_2O$

1.2.3 Biomedical applications

Orthopedics and dental applications are the main area of Bru usage which successfully passed in-vitro and in-vivo examination and are clinically available. In addition, this material is involved in area of biotechnology such as cancer therapy, drug delivery, and biosensors development. A brief overview about biomedical application of this materials is discussed in the following part of introduction chapter.

- *Orthopedics*

The main area of Bru applications in orthopedic fields relate to Restoration of metaphyseal defects, ligament anchor, reinforcement of osteosynthesis screws, and vertebroplasty. One of the most challenging area for orthopedics is in proximity of joints particularly in old people where typical treatment are associated with side effects [56]. Injectable Bru cement have successfully been used to treat defects in proximity of joint such as tibial plateau distal radial with high success rate. Although leakage of Bru cement to the adjacent tissue was observed, the cement finally adsorbed without showing siginificant side effect [56, 57]. Also, it has been showed that 3D printed Bru cement are capable of anchoring ligament to bone with a proper mechanical interface [58, 59]. One crucial factor in treatment of complicated bone defects is stability of osteosynthesis screws especially in the case of patient suffering from osteoporosis. Previously PMMA[12]

[12] **poly(methyl methacrylate)**

bone cement was used to stabilize these screws, but undeniable side effects such as exotermic setting reaction, non-degradability, and cytotoxic monomer have limited the usage of PMMA. Biodegradable Bru is a promising candidate to fix the screw, as it increases the pull-out force by 3-folds [60]. Finally, injectable Bru has shown a good capability to fill and fix damaged osteoporotic vertebrae. The results indicated that Bru improved mineral density of osteoporotic vertebrae by up to 20–50 % yielded to improve stiffness and maximum force before failure [61].

- *Craniofacial surgery*

Bru is a possible candidate for treatment of craniotomy defects, as it was observed in animal models that it induced osteogeneration and formation of fibrous tissue [62]. Preventing temporal depression in parietal craniotomies after craniotomy is another application of Bru in this area with superior outcomes respect to simple repair [63]. Custom made 3D printed craniofacial implant of Bru ceramic have been testing in tested for bone defects in cadavers. However, there is no record of clinical usage [64]. Vertical bone augmentation and bone defect healing are significant applications of Bru in maxillofacial surgeries. In this regard, Bru is using in the form of injectable cement or ceramic granules [65, 66]. Bru cement is injecting under the periosteum and set on the bone surface which will support bone growth in vertical direction [65]. Bru granules has the same impact on the vertical bone augmentation and the results was more promising respect to commercial bovine HA [67].

- *Drug delivery*

Bru cement has a good potential to act as a carrier of therapeutic agents such as drug, bioactive molecules and cells owing to its intrinsic porosity. The setting of Bru cement takes place at room or body temperature which prevent thermal denaturalization and activity loss during fabrication and implantation. These factors help Bru to have dual applications of osteoconductive bone grafts and local DDS. Method of drug loading is a very important factor which have a significant influence on the drug distribution and interactions with Bru. Figure. 5 shows different path to load drug or biomolecules on calcium phosphate cements [68].

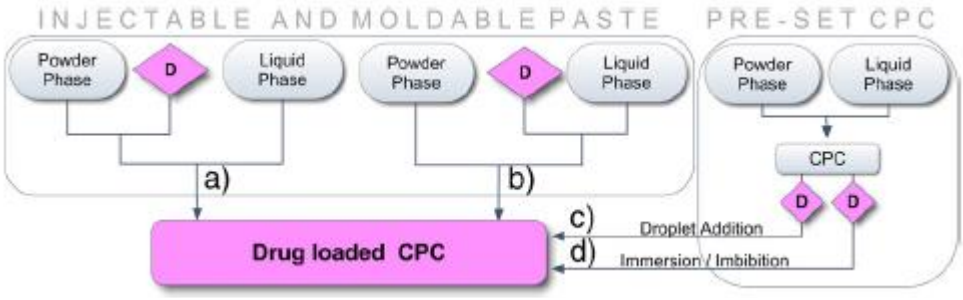

Figure 5. Different drug loading procedure in calcium phosphate materials [68]

In majority of studies drug was either incorporated in powder phase or dissolved in liquid phase which result to drug distribution within the whole cement volume. Noteworthy that a more uniform drug distribution will obtained by dissolving drug in liquid phase. Another path is to immerse preset cement inside drug solution which minimize the structural changes induced by active loading. However, injectability of cement will be reduced by this method. Entrapping drug inside polymeric microspheres and blending them with the cement will avoid initial burst release associated with drug

loaded Bru cement. In addition, degredation of these machrophers create pores and support higher level of bone growth capability [68].

Incorporation of drug has a significant effect on the setting time and final features of Bru cements. Drugs can prolong setting time of Bru which result in less porous structure and subsequently slower release kinetics. Selecting a proper drug to load on the Bru cement is crucial owing and should remain stable versus variations in pH and temperature during setting reactions. Bru has shown a good potential for releasing antibiotics and antiseptics such as vancomycin, doxycycline, tetracycline, ciprofloxacin, gentamicin and chlorhexidine and growth factors like PDGF, VEGF, RANKL[13], BMP-2 and heparin [48].

- *Other applications*

Bru have been used to fill the cancer related bone defects which supports bone formation more than PMMA and collagen gels [69]. Also, coprecipitation of Bru with magnetic nanoparticles such as ferrous chloride support the targeting and destroying cancer cells [70]. Ability of Bru in conducting protons as well as adsorbin proteins gives it the possibility to use as biosensors. For instance, detection of phenol using Bru combined with the enzyme tyrosinase resulted in faster signaling and higher sensivity respect to typical polymer and clays biosensors [71].

---

[13] **receptor activator of nuclear factor kB ligand**

CHAPTER 2

Synthetization and Characterization of alginate-brushite in-situ hydrogel composites

2.1 Introduction

Hydrogels, 3D cross-linked networks of water-soluble polymers, due to their well-known biocompatibility, and microporous structure, with tunable porosity and pore size, have emerged as versatile and viable platforms for several biomedical applications, such as sustained drug release, targeted drug delivery, tissue engineering and regenerative medicine [72, 73]. Among natural hydrogels, Alg has been widely studied due to its biocompatibility, biodegradability, and low cost [3]. Structural similarity of Alg hydrogels with the ECM[14] has made Alg a promising scaffold biomaterial [1, 74]. Moreover, Alg has been widely used as a carrier for the controlled release of drugs due to its low immunogenicity and its mucoadhesive properties [75]. However, hydrogels, including Alg, present several limitations, such as low tensile strength, high water content and large pore size, which could finally result in low drug loading efficiency of water soluble drugs and relatively rapid drug release [76].

Several studies have been focused on enhancing hydrogel properties in terms of drug release for extended periods of time with controllable release kinetics or self-regulated release [77-80]. In order to reduce drug release rates, different strategies can be adopted based on promoting the interaction between drug molecules and hydrogel matrix, increasing the number of cross-links which will result in decreasing the swelling ratio, and/or increasing the diffusive barrier through the hydrogel matrix via the development

[14] **extra-cellular matrix**

of composite matrices [16, 76, 81, 82]. An Alg-CNT[15] composite hydrogel has been proposed to this purpose [83]. However, the composite matrix should not affect the structure and morphology of the Alg and also must not result in cytotoxic behavior. In this respect, the development of Alg composite hydrogels based on the inclusion of calcium phosphate is interesting. Calcium phosphates have been widely used in bone tissue engineering, since they provide a preferred substrate for cell attachment and expression of osteoblast phenotype [84]. Moreover, calcium phosphates have been proposed for their use as implantable drug delivery systems for local antibiotic treatment of bone infections [68, 85-87].

There are few published work on Alg -calcium phosphate materials, to our knowledge, mainly focusing on Alg -hydroxyapatite composites [88, 89]. Recently Amer et al [90]have proposed a new hybrid material based on Alg -Bru and Alg -monetite.

Bru (dicalcium phosphate dihydrate) and Mon[16] (dicalcium phosphate) are two calcium phosphate materials can be resorbed under physiological conditions. However, their mechanical properties seem to be weak [91, 92]. Dicalcium Phosphate materials have been deeply studied for applications in bone tissue engineering, cancer therapy, and drug delivery [48]. Monetite can be precipitated by dehydration of Bru [93] or by modifying the precipitation conditions of Bru cements. This occurs when the cement is

---

[15] **carbon nanotubes**

[16] **Monetite**

prepared in a condition that available water is limited [94], in presence of metallic ions like Sr [95], and when the pH is maintained at very low values [96]. Despite the fact that monetite is more resorbable than Bru and does not convert easily to apatite, calcium phosphate cements usually set to form Bru for kinetic reasons, as the precipitation of Bru is an exothermic reaction, while the monetite formation is endothermic [97]. Also, mechanical properties of Bru phase is generally better than the monetite [98].

2.2 Materials and methods

2.2.1 Raw Materials

Sodium alginate from brown algae, having a viscosity of 15-20 cps at the concentration of 1% in water (w/v), calcium nitrate tetra hydrate [$Ca(NO_3)_2.4H_2O$, 99%], diammonium hydrogen phosphate [$(NH_4)_2HPO_4$, 98%], hydrochloric acid (HCl), sodium hydroxide (NaOH), Dulbecco Modified Eagle's Medium (DMEM), fetal bovine serum (FBS), phosphate buffered saline (PBS), [3-(4,5-dimethylthiazol-2-yl)-2,5-diphenyltetrazolium bromide] (MTT) were purchased from Sigma-Aldrich. MG-63 (human osteosarcoma) was obtained from the National Cell Bank of Iran (NCBI), Pasteur Institute of Iran. In addition, 96-well microtiter plates for cell culture were supplied by Nunc, Denmark. All reagents were used without any purification. Water, used in the experiments for the solutions preparation and washing, was purified by Milli-Q system and had resistance of 18.2 MΩ cm.

2.2.2 In-situ synthesis of Alg-Bru composites

Alg was added slowly to di-ammonium hydrogen phosphate solution, having a concentration 0.1 M in pure water, under stirring rate of 600 rpm to a final concentration of 1% (w/v) in water. The obtained solution stirred for 2 h at room temperature. Then, the Alg solution was added drop-wise using a syringe equipped with a 0.800 mm needle to 0.25 M $Ca(NO_3)_2$.4H2O cross-linking solution . The pH values of both solutions were set at different values ranging from 3 to 9, using HCl and NaOH (0.1 M), in order to evaluate the effect of the pH on the in-situ synthesis of the composite hydrogel. Cross-linked Alg-Bru beads were formed instantly. The beads were kept in the crosslinking solution for 24 hours to complete the crosslinking process and facilitate the growth of di-calcium phosphate into the beads. In order to remove excess Ca^{2+} ions and other impurities, the beads were subjected to centrifugation at 1000 rpm for 5 minutes and washed in distilled water. The rinsing process was repeated four times. Finally, the beads were dried at room temperature for 24 h and then heated at 50 ˚C overnight. Samples are referred as Alg-0.1-X, where 0.1 is the molar concentration of the phosphate solution and X is the pH value.

The next step was to evaluate the effect of phosphate concentration on the synthesis of the composite hydrogels. To this aim, different concentrations of di-ammonium hydrogen phosphate (0.1, 0.25, 0.5 and 1 M) were tested while the pH value of Alg solution and cross-linking one were set at 7. Samples are referred as Alg-Y-7, where 7 is the fixed pH value and Y is the concentration of the phosphate solution. Table.1 summarizes the different preparation conditions of composite hydrogels.

2.2.3 Characterization

In order to determine the phase composition of the prepared beads, a Philips PW 1800 X-ray diffractometer with Cu-k_α radiation source was used. The spectra were collected over the 2Θ range of 3˚ to 90˚ at 30 mA and 40 kV. The resultant spectra were compared with ICDD (JCPDS) standards number 9-0077 to characterize the phases. Fourier transform infrared spectroscopy was used to investigate the compounds and functional groups of beads using a Nicolet 380 Fourier transform infrared spectrometer (Thermo Fisher Scientific Inc, USA) by KBr pellet technique. A weighted amount of powders has been accurately mixed with KBr matrix at the concentration of 1% for each sample in order to obtain a standardized homogeneous mixtures. Besides, spectra were reported in common scale. The spectra were obtained within the range of 400 to 4000 cm^{-1} at room temperature. The surface morphology investigation was carried out via scanning electron microscopy with Hitachi S-2500 model. Thermogravimetric analysis, as well as differential thermal analysis, were performed using TG-DTA Netzsch Gerätebau STA 409 (Germany) in nitrogen atmosphere at the heating rate of 10 $K.min^{-1}$ in the range of 25 ˚C to 450 ˚C.

2.2.4 In-vitro cell culture and MTT assay

The cells were cultured in DMEM medium supplemented with 10% (v/v) fetal bovine serum (FBS), 100 U/ml penicillin and 100 μg/ml streptomycin. The cells were incubated at 37˚C in humidified air with 5% CO_2. Cells were plated in a multi-well (96) flat-bottomed plate with a density of 10^4 cells/well in 100 μl of culture medium. The sample sterilization process was carried out using UV light for 90 minutes. The rate of

proliferation was calculated using extracted samples based on ISO 10993-5 protocol. The sterilized samples were soaked into DMEM media at concentration of 0.1 g/ml and incubated at 37ºC for predetermined time intervals. Namely, after 3, 7 and 14 days, the medium was gathered for using in MTT assay. Pure culture medium, maintained under similar conditions was used as negative control. Cell viability was assessed using the cell viability assay kit MTT.

This method is based on the principle that viable cells change yellowish MTT into an insoluble purple formazan crystal. The absorbance of each solution is quantified using scanning multiwall spectrophotometer (ELISA reader). After 24 hours, the culture medium in each well was removed and replaced by 90µl sample (culture medium kept in contact with composite hydrogels) plus 10µl FBS. The medium was removed after 24 hours and then 100 µl of MTT solution ($0.5 mg.ml^{-1}$) was added into each well and incubated for 4 hours at 37˚C. In order to dissolve the formed formazan crystals, 100 µl of isopropanol was added to each well. The plate was placed in incubator for 15-20 minutes to completely dissolve formazan crystals. Finally, the optical density of formazan was recorded at 545 nm using a multiwell microplate reader.

Table 1. Preparation conditions of different samples, the concentration of sodium Alg and calcium nitrate in all samples were 1(w/v) %and 0.25 M, respectively

Item	Name	$(NH_4)_2HPO_4$ (M)	pH of solutions
1	Ca-Alg	0	7
2	Alg-0.1-3	0.1	3
3	Alg-0.1-4	0.1	4
4	Alg-0.1-5	0.1	5
5	Alg-0.1-6	0.1	6
6	Alg-0.1-7	0.1	7
7	Alg-0.1-8	0.1	8
8	Alg-0.1-9	0.1	9
9	Alg-0.25-7	0.25	7
10	Alg-0.5-7	0.5	7
11	Alg-1-7	1	7

2.3 Results and discussion

2.3.1 Preparation of composite beads

The in-situ process was employed to prepare different formulations of Alg -Bru hydrogel composites. The term in-situ refers to simultaneous occurrence of Bru nucleation and growth, and crosslinking of sodium Alg. The Alg crosslinking process started immediately when Alg solution was dipped into calcium nitrate solution and nucleation and growth of Bru crystals was carried out via following equation:

$$Ca(NO_3)_2 + (NH_4)_2HPO_4 + 2\ H_2O \longrightarrow CaHPO_4{\cdot}2H_2O + 2\ NH_4NO_3$$

The Ca^{2+} infiltrated into hydrogel network where it would react with HPO_4^{2-} which was dispersed homogeneously within Alg network. As a result Bru crystals started to grow in the polymeric network (Figure. 6). On one hand, dissolution of precursors resulted in formation of Ca^{2+} and HPO_4^{2-} ions in the media which caused pH variation in both solutions. On the other hand, the formation of Bru is highly dependent on the initial pH. Hence, we investigate the impact of initial pH on the formation of Alg-Bru hydrogel composites and later we evaluated the impact of initial phosphate concentration at pH 7 which is favorable for Bru formation.

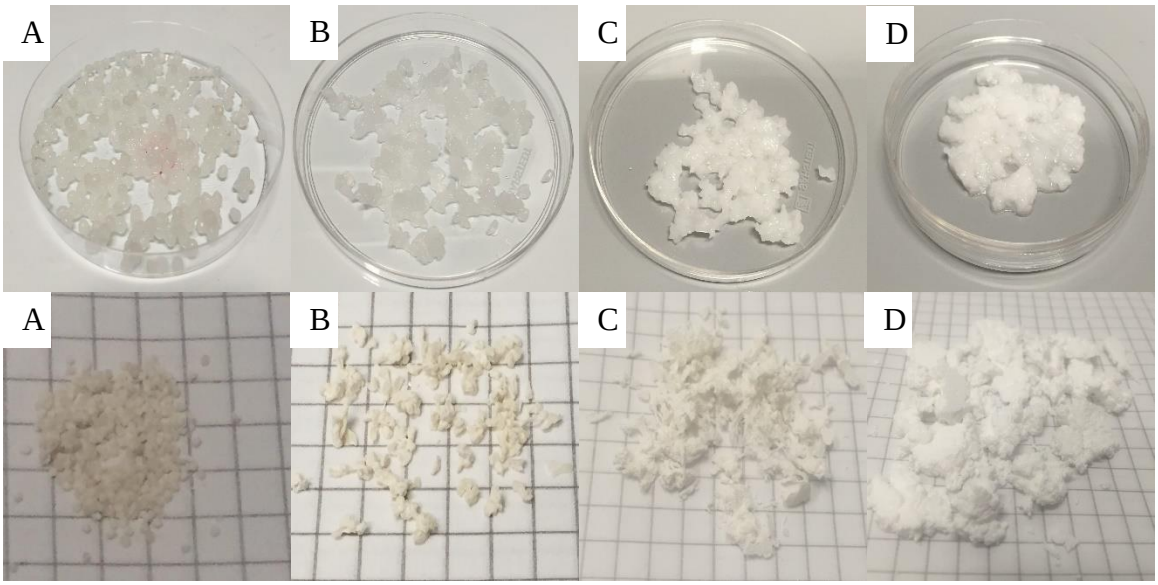

Figure 6. Water content and dried digital images of A)Alg-0.1-7, B) Alg-0.25-7, C)Alg-0.5-7, D) Alg-1-7

2.3.2 FT-IR analysis

Figure.7 shows FT-IR spectra of the different composite samples together with the spectrum of reference Ca- Alg. As for Alg spectrum, the main bands are detected at 1620 and 1425 cm^{-1} corresponding to the asymmetric and symmetric stretching mode of the carboxyl group [99]. At lower frequencies, a complex envelop of bands in the range 1200-1000 cm-1 is due to the C-O and C-C stretching modes of the carbohydrate chain. The very weak peak at 2930 cm^{-1} is assigned to C-H stretching mode [99]. Bru phase is characterized by two doublet of peaks at 3165, 3277 cm^{-1} and 3491, 3543 cm^{-1} assigned to O-H stretching modes of crystallization water molecules [100]. Correspondingly, the absorption peak at 1651 cm^{-1} relates to the H-O-H bending mode [101]. The bands of phosphate group PO4, i.e. P-O stretching modes, were detected at 1136, 1061 and 987 cm^{-1} [90, 100]. The P-O-H stretching mode and P-OH bending mode peaks can be

detected at 1221 and 874 cm^{-1}, respectively [101]. Finally, peaks at 667, 579 and 528 cm^{-1} are due to P-O deformation mode of phosphate group [100].

The impact of pH on the Alg has been studied extensively by researchers and they reported that the pKa of Alg is around 3.5 [102]. Hence, Alg mostly negatively charged in the pH range of 3-9. Besides, we have spectroscopic evidences of deprotonated carboxyl group (bands at 1425 and 1620 cm^{-1}) in the all pH value used in this experiment. As we can see in Figure. 7A pH value has a significant impact on the formation of Bru into Alg matrix. The characteristics peaks of brushite are detected in the spectra corresponding to composites from pH value of 6 to 8. It is clear that at the pH value of less than 6, regardless of some weak phosphate peaks (Figure. 8), the FT-IR spectra are pretty similar to that of Ca-Alg. As we increased the pH value from 7 to 8, the relative intensities of diagnostic Bru peaks (namely band at 1650 cm^{-1}) evaluated in comparison with Alg peaks (namely band at 1425 cm^{-1}) slightly increased while width of peaks decreased. This can attributed to strengthening of phosphate bonds at the pH value of 8 (for instance by increasing crystallinity of phosphate phase which was confirmed by XRD results) [103]. On the other hand, the characteristic O-H stretching bands of water at 3163, 3321, 3479, and 3549 cm^{-1} almost disappeared at the pH value of 9. Increasing pH values by adding NaOH can also affect the Alg component, for instance by forming Na- Alg, thus explaining some changes in the region of 1650-1400 cm^{-1} of the spectrum [102].

Figure. 7B represents the effect of Phosphate concentration on the in-situ formation of Alg-Bru composites at constant pH value of 7. All the spectra showed the

characteristics peaks of Bru and have very similar shape and width. Moreover, the best results in terms of sharpness of Bru IR peaks have been obtained at the concentration of 0.25M of phosphate. As expected, increasing the relative concentration of phosphate (from 0.25M to 1 M), results in decreasing the relative intensities of the carboxylate bands at 1620 and 1425 cm^{-1} in comparison to Bru characteristics bands.

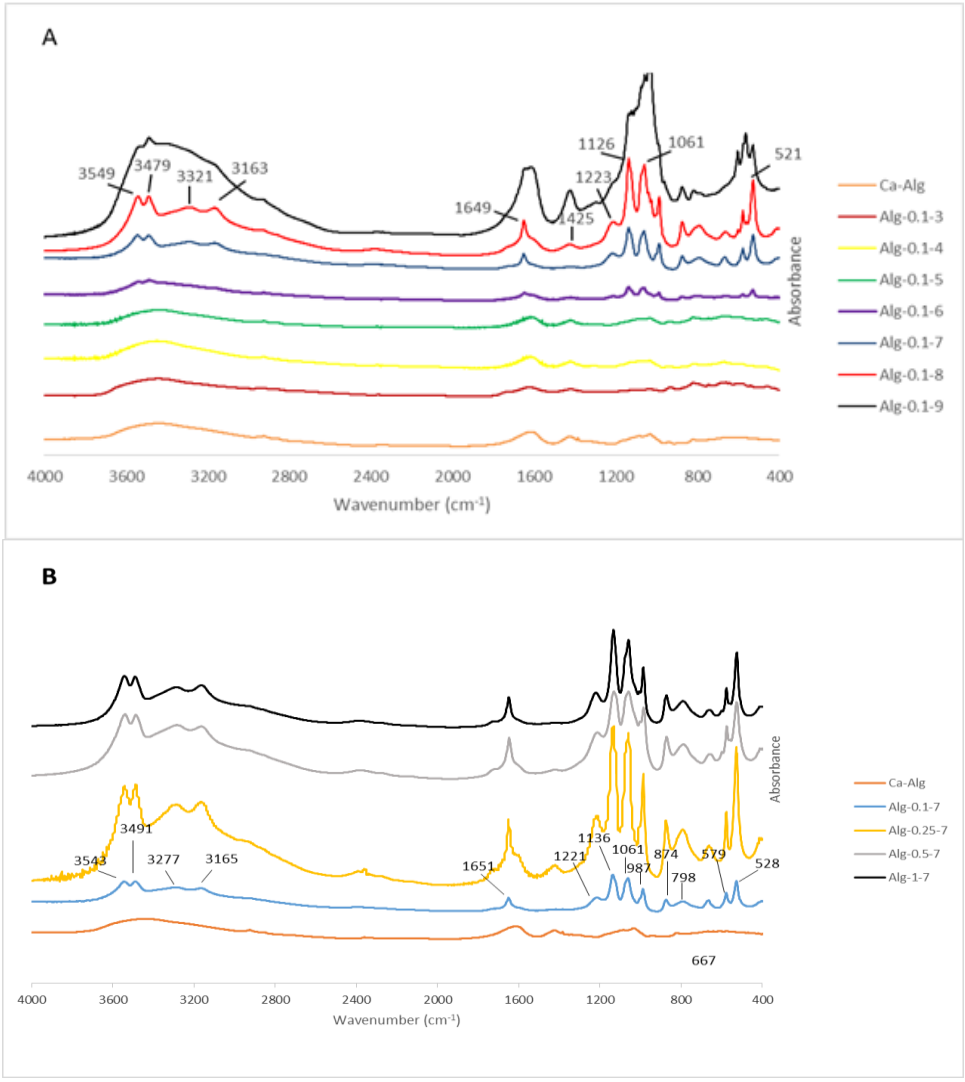

Figure 7. FT-IR spectra of fabricated samples A) different pH value, B) different phosphate concentration

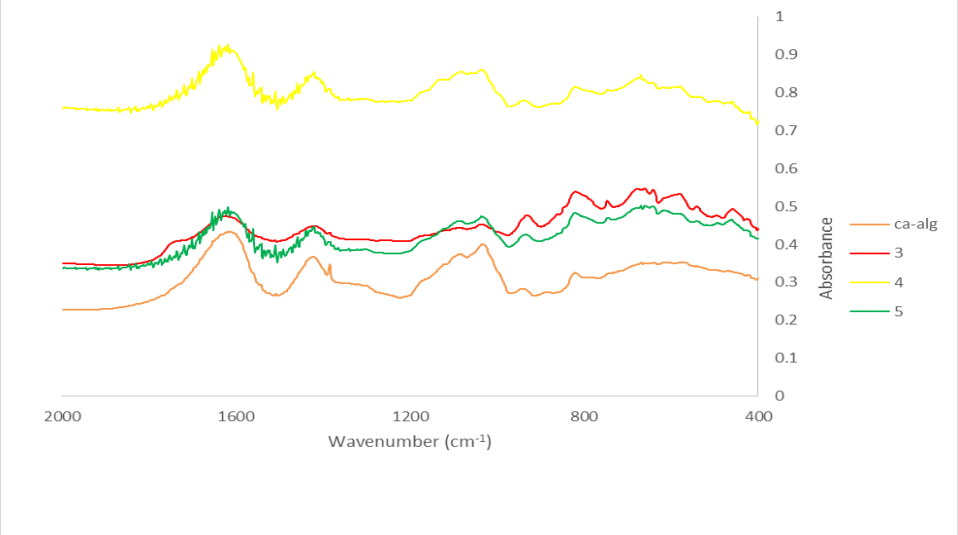

Figure 8. FT-IR spectra of Ca-Alg and samples prepared at pH values of 3-5 in the range of 400-2000 cm^{-1}

The comparison of the composite spectrum Alg-0.25-7 with spectra of pure Bru and Ca- Alg has been reported in Figure. 9 in order to study the interactions of these components. Corresponding bands of Alg carboxylate groups at 1620 and 1430 cm^{-1} are detected at the same wavenumbers in both the composite spectrum and the pure Alg spectrum, showing that there are no changes in the coordination of the COO^- group following Bru formation. C-H stretching bands at about 2930 cm^{-1} are indeed weakened in the spectrum of the composite, and this effect can be due to the lowering amount of organic compound.

On the other hand, bands due to Bru phosphate groups in the range of 1200-900 cm^{-1} are not affected by the co-presence of Alg, maintaining the same shape and

wavenumbers in both reference Bru and composite spectra. These data suggest that the interaction of Alg with Bru phase is weak.

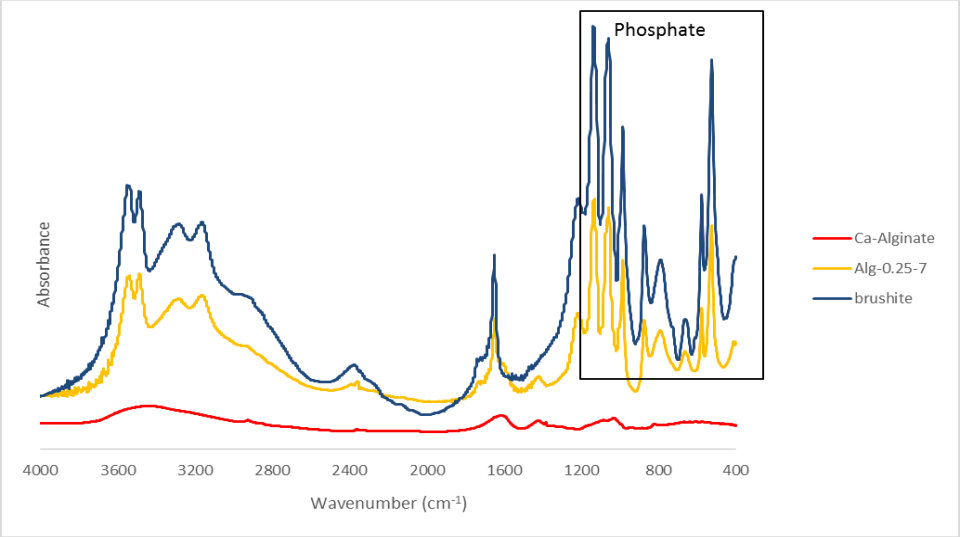

Figure 9. FT-IR spectra of: Ca- Alg, Bru, and Alg-0.25-7 composite

2.3.3 XRD analysis

The resultant XRD spectra are illustrated in Figure. 10. These spectra were compared with that of standard Bru JCPDS card (9-0077). It is clear that the samples were completely amorphous at the pH values lower than 6. At pH value of 6 the Bru crystals started forming and the best conditions for their formation are obtained at the pH value of 7 and 8 (Figure. 10A). Bru in these preparation conditions had monoclinic crystalline structure with the following crystallographic parameters: a= 6.363 Å, b= 15.190 Å, c= 5.815 Å, α= γ= 90˚, and β= 118.5˚. In addition, as the pH value exceed 8, reductions in the intensity of characteristics peaks, especially at 2Θ of 20.9˚, 29.25˚, and 34.16˚, and increases in the width of them were noticeable. This showed us that the degree of crystallinity would be lower if the pH value exceeded 8.

Figure. 10B demonstrates the effect of phosphate variation on the XRD spectrum of the samples. All the spectrum are quite in a good accordance with JCPDS card (9-0077). Besides, it is worth to notice that as the concentration of phosphate increased the intensity of characteristics peaks increased while the width decreased. We can say that these samples were more crystalline. The main reason for this compounds to be more crystalline seems to be the fact that the relative concentration of amorphous phase, Alg, significantly decreased as the concentration of phosphate increased.

The (020), (021), (040), (041), (-221), (220), (022), (151), (-260), and (241) diffractions were used to calculate mean crystallite size, t, according to Scherrer‘s equation [104]:

$$t = \frac{k\lambda}{\beta cos\theta}$$

Where k refers to a dimensionless shape factor ,the Scherrer constant, (generally assumed to be 0.9), λ is the wavelength of X-ray radiation, β is the line broadening at half the maximum intensity in radians, and θ is the Bragg angle. The calculated mean crystallite size for the sample prepared at pH 7 and 0.1 M of phosphate was 31.7 nm.

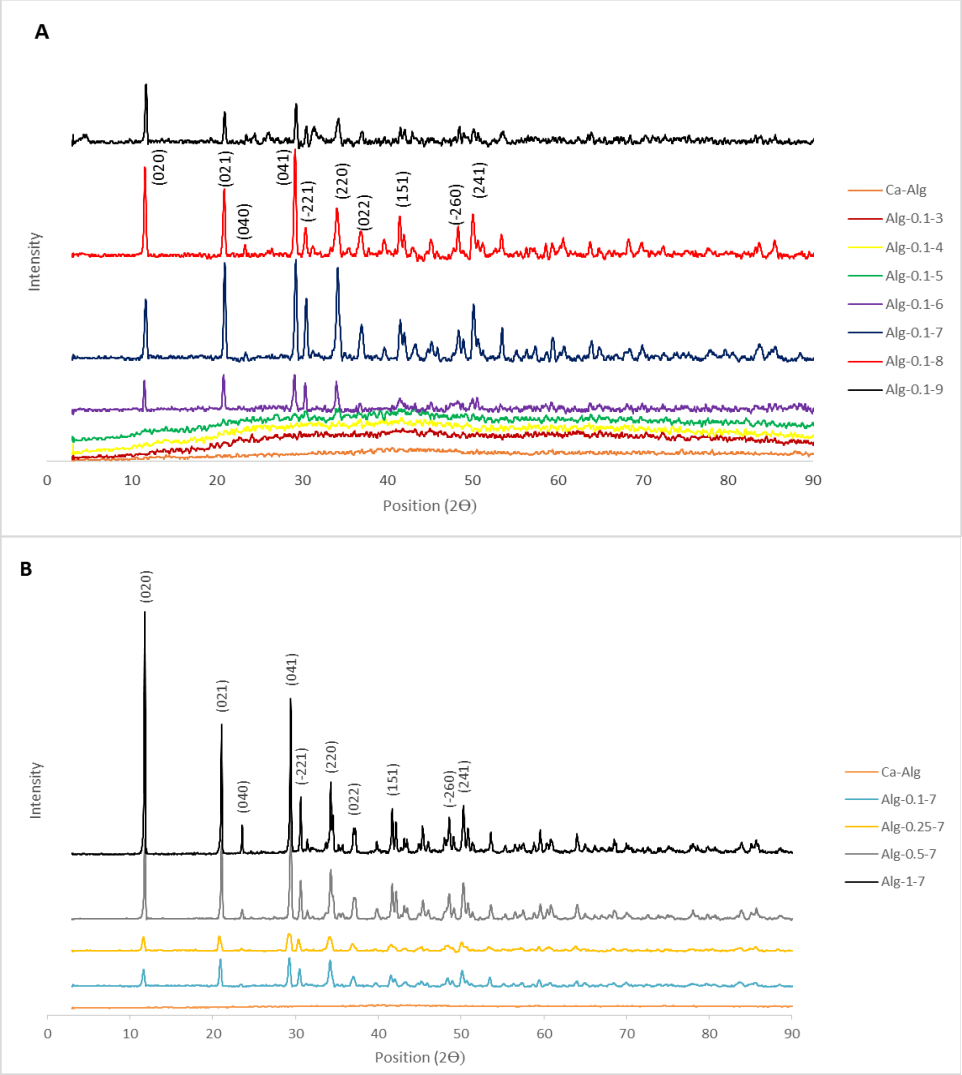

Figure 10. XRD spectra of fabricated beads A) different pH value, B) different phosphate concentration

2.3.4 Thermal behavior

Thermal behavior of two dried composite samples, prepared at pH 7 and 8, were studied performing TGA and DTA. The TGA results revealed a continuous weight loss in the range of 30 to 700 ˚C for both samples. The accurate amount of total weight loss for the samples prepared at pH of 7 and 8 were 49.3% and 46.2, respectively (Figure. 11A).

We can see that around 10% of weight loss from 60 ˚C to 180 ˚C corresponds to water loss in the transformation of DCPD to DCP [90, 105]:

$$CaHPO_4.2H_2O \longrightarrow CaHPO_4 + 2H_2O$$

The rest of weight loss can be assign to the decomposition of the organic moieties [106] and to the transformation of DCP to calcium pyrophosphate through the following reaction [105]:

$$2CaHPO_4 \longrightarrow Ca_2P_2O_7 + H_2O$$

Forest et al [107] have investigated on thermal decomposition of Bru and they concluded that 21.97 % of Bru weight had been lost due to complete transformation of DCPD to DCP and DCP to calcium pyrophosphate at the temperature range of 56-514˚C. Besides, other studies conducted on evaluating thermal behavior of sodium Alg and calcium Alg mentioned that about 55% mass loss was due to dehydration and decomposition of Alg in this temperature range [108, 109].

In addition, the DTA results indicated two endothermic and three exothermic phenomena in the heating range. As we can see in the Figure. 11B in the case of Alg-0.1-8 the endothermic peak at 124 ºC can be assigned to evaporation of water molecules trapped into small structural pores. Besides, endothermic reaction at 189 ºC corresponded to dehydration of Bru. The very small endothermic peak around 319 ºC is related to formation of calcium pyrophosphate. Finally, degradation and decomposition of Alg matrix to carbonate materials like $CaCO_3$ is responsible for the sharp exothermic peak at 227 ºC and wide exothermic peak at 572 ºC [108].

The phenomena discussed above occurred in both Alg-0.1-7 and Alg-0.1-8 samples although, slightly shifted toward higher temperatures in the former sample. This effect suggests that the samples Alg-0.1-8 had more stable crystalline structure than the other samples and these results are in a good accordance with the XRD results.

Figure. 12 presents derivate thermogravimetric (DTG) spectra of pure Alg, Bru, and Alg -Bru composite prepared at pH 8. The comparison DTG pattern of Alg-Bru composite with reference materials showed that the main weight loss can be detected in the range of 150-300˚C. Neither thermal degradation of pure Alg nor Bru demonstrated this kind of phenomena at this temperature range. The complexity of this peak suggests that several decomposition steps occured simultaneously, such as the degradation of the organic component through the extensive breaking of glycosidic bonds which resulted in the formation of small molecules and carbonaceous material, and the Bru dehydration. Therefore, the overall decomposition of the composite material seems to be more complex and since it shifted to a lower temperature, in comparison with pure Alg, we can conclude that there is a catalytic effect of the Bru materials on this phenomena. These results confirm the existence of specific interaction (however it is weak) between the organic and inorganic components of Alg-Bru hydrogel composite.

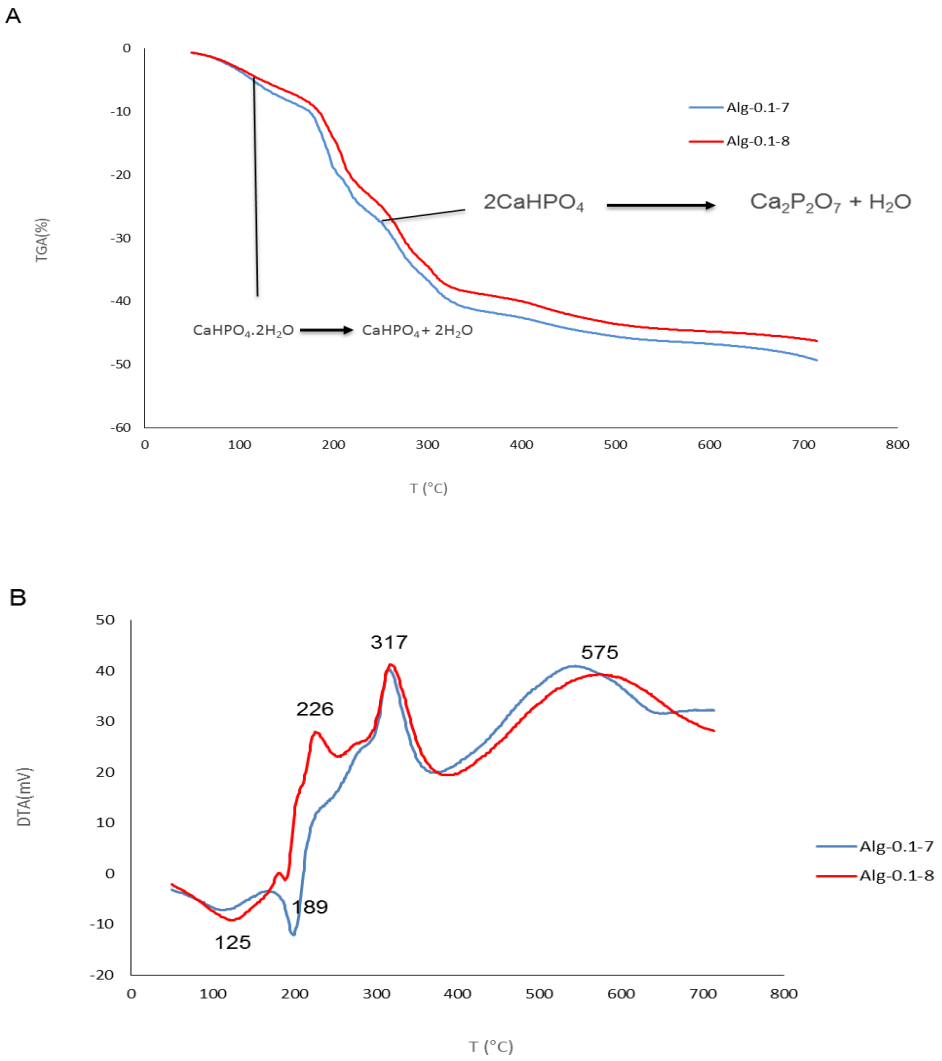

Figure 11. Effect of pH value on thermal analysis of Alg -Bru samples A) TGA B) DTA

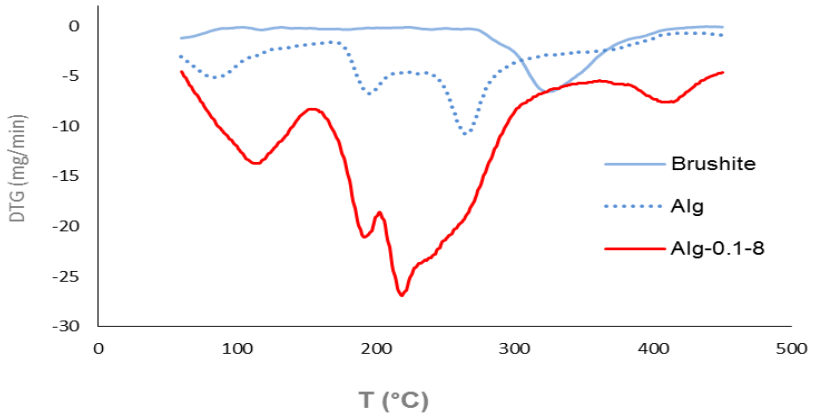

Figure 12. DTG spectra of Bru, Alg, Alg -Bru composite

2.3.5 Morphological study

Figure. 13 represents the effect of phosphate concentration on the morphology of formed Bru crystals within the Alg matrix. The pictures were taken at three different magnifications of 500x, 1000x, and 2000x. The morphology of Bru crystals in both samples was plate-like aggregates in multilayers. The morphology of formed Bru was in a good agreement with previous reports [110, 111]. The dimensions of the crystals were almost the same in both samples, 50 μm in length and 20 μm in width. Furthermore, the thickness of the plate-like particles was around 100 to 200 nm (Fig. 14).

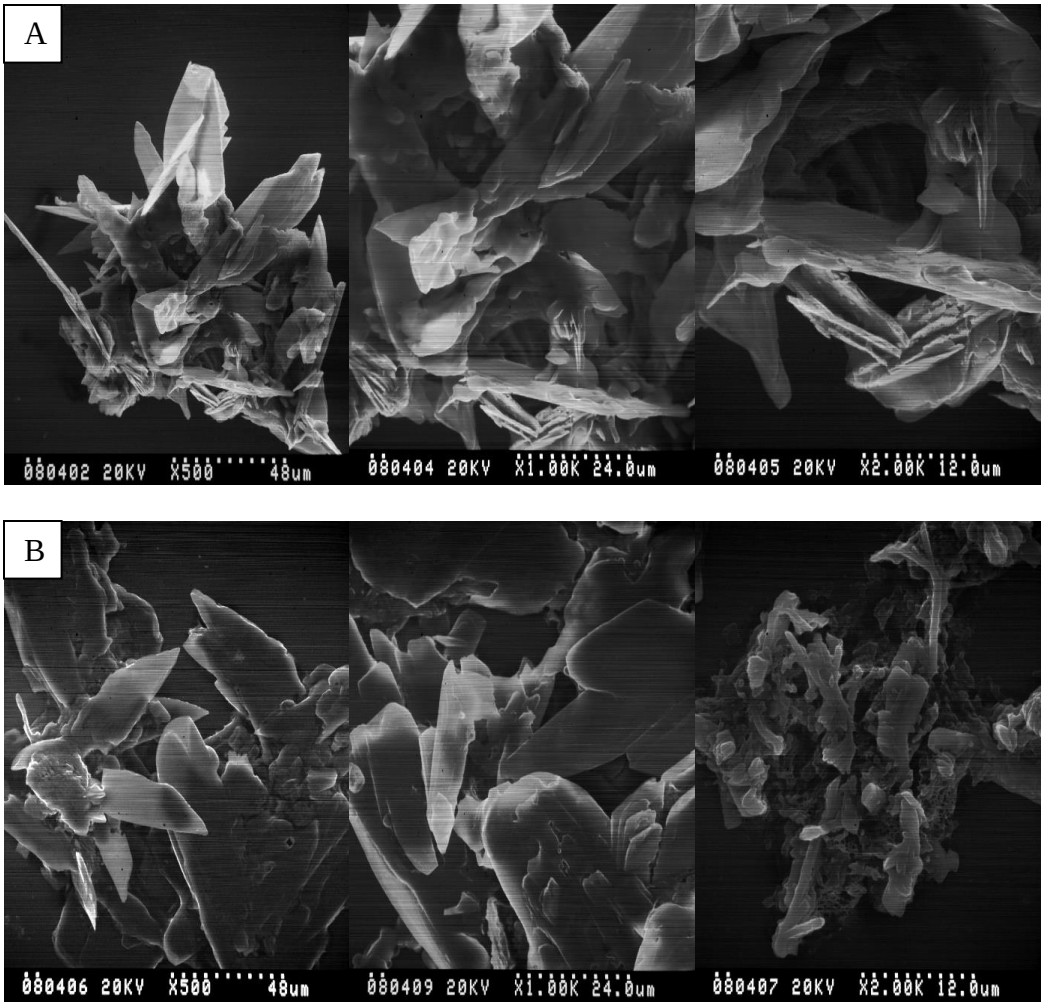

Figure 13. SEM micrograph of Alg-0.1-7 (A), and Alg-0.25-7 (B) at three different magnification of 500x, 1000x, and 2000x

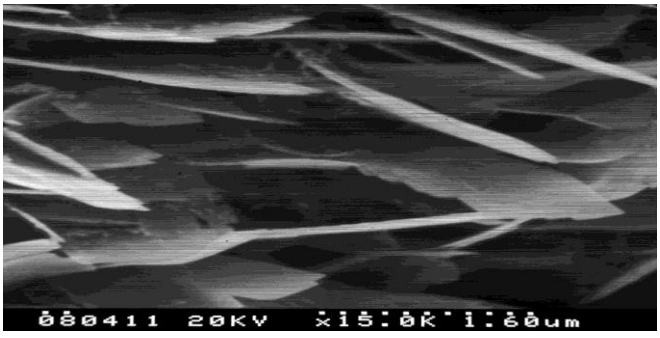

Figure 14. SEM image of the Bru crystals thickness in Alg-0.25-7 sample

2.3.6 In-vitro characterization

As shown in Figure. 15A, and Table. 2, cell viability was observed to grow smoothly throughout the incubation period of 3 to 7 days. All samples except those prepared at pH 7, 8, and Ca-Alg were toxic. According to XRD and MTT results we observed that samples with the crystalline structures ended up in biocompatible response. In other words, the residual phosphate in samples prepared at the pH value of 3-6 reacted with H^+, Figure. 8, in culture media and consequently decrease the pH value of culture media. Therefore, the main reason for this samples being toxic was inappropriate pH value of culture media and lack of favorable conditions for cells to be proliferated. On the 7^{th} day the calculated growth for the biocompatible samples were higher than negative control and Ca-Alg ($p<0.05$). Although these samples showed a downward viability trend from day 7 to 14, the rate of viability was almost equal ,higher than 90%, to negative control and higher than that of Ca-Alg ($p<0.1$).

Figure. 15B, and Table. 3, demonstrates the effect of phosphate concentration on the biological responses of Alg -Bru composite samples. The proliferation rate showed an upward trend from day 3 to 7. However, this was followed by a smooth decrease in proliferation rate at the end of day 14^{th}. All the samples were biocompatible and they supported almost equal value of negative control after 14 days. The cell viability for all Alg-Bru hydrogel composites were higher than that of Ca-Alg sample.

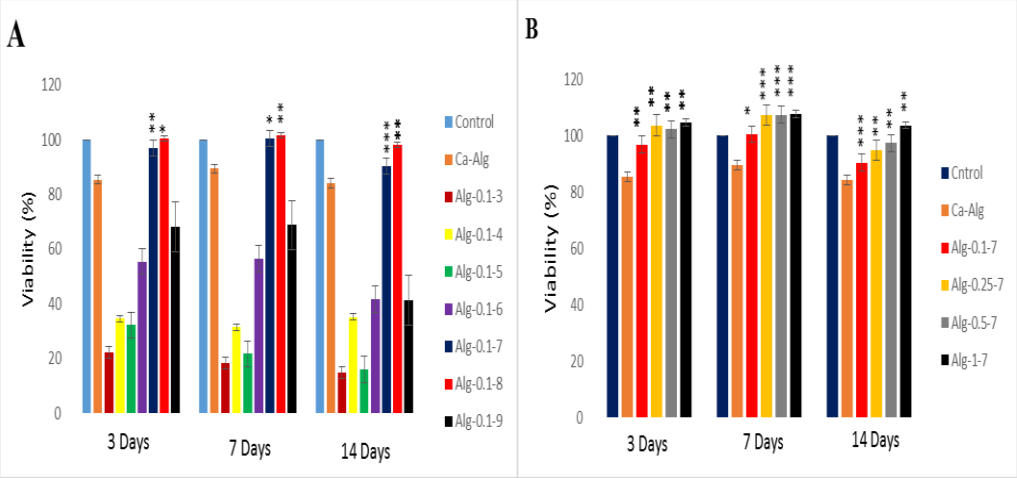

Figure 15. Cell viability of the extracted samples at three different time intervals A) different pH value, B) different phosphate concentration. ***p<0.01, ****p<0.05, and *****p<0.1 compared to control***

Table 2. Statiscla results of Cell viability of samples prepared at different pH value after 3, 7, and 14 days

Item	Name	Viability (%)		
		3 days	**7 days**	**14 days**
1	**Control**	**100**	**100**	**100**
2	**Ca-Alg**	**85.36 ± 10.12**	**89.45 ± 5.23**	**84.14 ± 7.45**
3	**Alg-0.1-3**	**22.21 ± 3.82**	**18.34 ± 0.61**	**14.84 ± 0.91**
4	**Alg-0.1-4**	**34.53 ± 2.63**	**31.36 ± 3.83**	**35.10 ± 9.78**
5	**Alg-0.1-5**	**32.15 ± 4.44**	**21.66 ± 4.64**	**15.87 ± 3.99**
6	**Alg-0.1-6**	**55.47 ± 3.59**	**56.46 ± 4.90**	**41.74 ± 8.44**
7	**Alg-0.1-7**	**96.85 ± 4.19**	**100.51 ± 6.51**	**90.39 ± 3.49**
8	**Alg-0.1-8**	**100.38 ± 4.53**	**101.74 ± 8.98**	**98.24 ± 6.89**
9	**Alg-0.1-9**	**68.14 ± 3.37**	**68.76 ± 9.99**	**41.17 ± 7.31**

Table 3. Statistical results of Cell viability of samples prepared at different pH value after 3, 7, and 14 days

Item	Name	Viability (%)		
		3 days	**7 days**	**14 days**
1	**Control**	**100**	**100**	**100**
2	**Ca-Alg**	**85.36 ± 10.12**	**89.45 ± 5.23**	**84.14 ± 7.45**
3	**Alg-0.1-7**	**96.85 ± 4.19**	**100.51 ± 6.51**	**90.39 ± 3.49**
4	**Alg-0.25-7**	**103.59 ± 1.61**	**107.32 ± 6.08**	**94.87 ± 10.53**
5	**Alg-0.5-7**	**102.22 ± 2.58**	**107.43 ± 4.04**	**97.34 ± 8.58**
6	**Alg-1-7**	**104.71 ± 2.53**	**107.71 ± 9.05**	**103.62 ± 5.78**

2.4 Conclusions

In this study a deep characterization of process parameters for the in-situ synthesis of Alg -brushite composite hydrogel was carried out. This hydrogel composite has a potential to use in different biomedical applications including drug delivery and bone cements due to excellent biocompatibility. The Bru crystals can act as a barrier to avoid leaking of drugs from Alg network and also burst release of drug by improving swelling behavior of this compound. In addition, since the synthetize process was carried out at the room temperature, it will be a good method to capsulate temperature sensitive drugs. The composite hydrogels were successfully prepared via complexation of Alg -Phosphate by calcium ions at room temperature. The Bru crystals were successfully formed inside the Alg matrix at pH ranging from 6-8 as evidenced by FT-IR and XRD. In addition, according to TGA, DTA, XRD, and FT-IR it was revealed that the optimum conditions and more stable structure were obtained at pH range of 7-8. XRD and FT-IR results indicated the presence of Bru crystals inside the Alg matrix as the concentration of phosphate increased. The in-situ formed Bru crystals had plate like structure with the thickness of 100-200 nm. Finally, MTT results, over the incubation time period of two

weeks, revealed that just the crystalline samples were non-toxic and all of them had a higher proliferation rate in comparison with Ca- Alg. The applications of this material are under investigation in our lab.

CHAPTER 3 In-situ synthetized hydrogel composite based on alginate and brushite as a potential pH sensitive drug delivery system

3.1 Introduction

In the past decade, DDS have attracted tremendous attentions as an optimized therapeutic method of drug administration. In fact, DDSs seek to control the release profile of drugs in order to have a sustained therapeutic level and to minimize adverse side effects [112]. Of all materials proposed for the fabrication of DDS, hydrogels are seem to have piqued more interest mainly because of their biodegradability, biocompatibility, and stimuli responsive characteristics [113]. Several polymers such as Alg [114], chitosan [115], gelatin [116], PVA[17] [117], and PEG[18] [118] have been widely used as carriers for drugs, cells and proteins. However, such applications of pure hydrogels have experienced burst release since hydrogels contain high amount of water and possess weak mechanical properties[119].

Alg is a promising biopolymer which has numerous biomedical applications ranging from wound healing and drug delivery to cell transplantation in tissue engineering. Alg exhibits pH sensitive swelling behavior, thereby making it a potential candidate for oral administration of drug, .This is mainly due to the fact that it protects the entrapped drug in the gastric fluid and releases it in intestine fluid [120]. Noteworthy, though, that Alg has been reported to possess a low encapsulation efficiency of water-soluble drug caused by drug leakage during the crosslinking procedure. Two additional

---

[17] **polyvinyl alcohol**

[18] **poly (ethylene glycol)**

factors that restrict the use of this polysaccharide are its quality of rapid integration in intestine fluid and its highly porous structure.

To bypass these limitations, increasing the number of cross-links may be advisable [16, 81, 82, 121]. One more solution is improving the mechanical properties via introducing other phases into the hydrogel matrix. This far, most studies have sought to improve the mechanical properties by fabricating biopolymer-inorganic reinforcement hydrogel composites as a result of restricting polymeric chain movements [83, 122-124]. It also seems that further improvements are achievable by changing the type of reinforcement and also, the content of polymer, and inorganic compound. Noteworthy that such incorporation must neither affect the structure of the Alg nor result in cytotoxic behavior [83].

To prolong the release profile, Calcium phosphate materials, mainly hydroxyapatite, have been incorporated into Alg. Previously Zhang et al [89] showed that in-situ synthetized hydroxyapatite micro particle within Alg restricted the polymer chain movement and consequently decreased the swelling ratio. It was also demonstrated that the incorporating of hydroxyapatite augmented the entrapment efficiency and prevented burst release. Along the same line, Ilie et al [125] also studied the release of ascorbic acid, Vitamin C, from Alg-hydroxyapatite composite and demonstrated the significant impact of hydroxyapatite on gradual release of ascorbic acid. In another study, hydroxyapatite nanoparticles were introduced into Alg-poly (vinyl pyrrolidone) blends and diclofenac sodium release was investigated from several compositions of these carriers [126]. The release profile indicated that the presence of nanohydroxiapatite

particles not only did improved the loading efficiency, but it also remarkably decreased the amount of released drug.

Previously, we investigated the in situ synthetization of Alg- Bru composite hydrogel and optimized the fabrication method. Moreover, we evaluated the biocompatibility of these materials respect to osteoblastic cell and observed a significant improvement in cell proliferation with respect to calcium Alg [127, 128].

3.2 Materials and methods

3.2.1 Raw materials

All the chemical reagents: sodium Alg from brown algae with a viscosity of 15-20 cps at the concentration of 1 wt%, calcium nitrate tetrahydrate [$Ca(NO_3).4H_2O$, 99%], diammonium hydrogen phosphate [$(NH_4)_2HPO_4$, 98%], hydrochloric acid (HCl), sodium hydroxide (NaOH), potassium dihydrogen phosphate (KH_2PO_4), phosphate buffered saline (PBS) tablets, and Ibu[19] sodium salt were supplied by Sigma-Aldrich. All reagents were used without any purification. A Milli-Q system with the resistance of 18.2 MΩ cm was used to purify the water which was eventually used for preparing solutions and washing steps.

[19] **Ibuprofen**

3.2.2 Beads preparation

A series of Alg-Bru beads were prepared according to the following procedure. First, a predetermined amount of di-ammonium hydrogen phosphate was dissolved in 10 ml of purified water at room temperature and 600rpm. Then, accurately weighted amounts of sodium Alg were added slowly to the above solution at a stirring rate of 600rpm. This solution was subsequently stirred for two hours to ensure the complete dissolution of Alg. After that, the solution was dripped into the crosslinking solution (0.2 M of calcium nitrate) at room temperature at a gentle stirring rate (50 rpm) through a syringe equipped with a 0.8 mm needle. The initial pH of the solutions was maintained at 7.5 using HCl and NaOH (0.1M). White beads were formed immediately and maintained in the crosslinking solution to ensure that the Bru crystal growth and crosslinking process were properly accomplished. Thereupon, the samples were centrifuged at 1000rpm for 5 minutes and rinsed 4 times to remove excess Ca^{2+} and other impurities. Finally, the samples were kept for 24 h at room temperature followed by placing them in the oven at 45˚C for 12 hours.

In order to prepare Ibu loaded beads, predetermined amounts of Ibu were added to the aqueous solutions composed of di-ammonium hydrogen phosphate and sodium Alg. The solutions were stirred for 1h to ensure that Ibu completely dissolved in the media. The rest of the procedure, including crosslinking and washing steps, were done as described above. In addition, calcium Alg samples were also prepared following the above procedure with the exception of adding no $(NH_4)_2HPO_4$ to the Alg solution. There were some factors which had significant impacts on the swelling behavior, drug loading,

and drug release behavior. These factors included the initial concentration of Alg, and primary concentration of phosphate precursor. The varying preparation conditions were summarized in table 4.

Table 4. Preparation conditions of Alg-Bru composite beads and their influence on swelling ratio and storage modulus

Item	Sample	Sodium alginate (wt %)	(NH4)2HPO4 (M)	Ca(NO3).4H2O (M)	Storage modulus at 85 Hz (kPa)
1	Alg 1.5	1.5	---	0.2	30.5±3.17
2	Alg 1- P 0.1	1	0.1	0.2	35.2±3.54
3	Alg 1.5- P 0.1	1.5	0.1	0.2	58.83±3.42
4	Alg 2- P 0.1	2	0.1	0.2	78.86±6.53
5	Alg 2-P 0.2	2	0.2	0.2	119.47±6.35
6	Alg 2-P 0.4	2	0.4	0.2	73.93±14.84
7	Alg 2	2	0.2	0.2	70±8.21

3.2.3 Characterization

A Nicolet 380 Fourier transform infrared spectrometer (Thermo Fisher scientific Inc, USA) was used to obtain FT-IR spectra through the KBr technique and to evaluate the formation of composite and the interactions between Ibu and composite materials. The spectra were collected within the range of 400 to 4000 cm^{-1}. In order to identify the inorganic phase of beads as well as presence of the entrapped drug, beads were subjected to X-ray diffraction (XRD) test. Therefore, A PANalytical Empyrean x-ray

diffractometer with irradiation source of Cu-Kα was used to collect the spectra over the Brag angle, 2Θ, range of 5-60 at a scan rate of 2˚ per minute. The obtained spectra were compared with those of standard JCPDS numbers for Bru (9-0077) and Ibu (32-1723). A JSM-6490LA scanning electron microscopy (SEM- JEOL Ltd, Japan) was used to investigate the dispersion of Bru crystals in Alg matrix and morphology of Bru crystals.

3.2.4 Dynamic mechanical analysis (DMA)

A typical test to gather information about mechanical properties of hydrogels is dynamic mechanical analysis (DMA). The mechanical properties of different hydrogel samples were obtained using a custom-made device, Figure. 16 of supporting information, developed at DICCA laboratory of University of Genova.

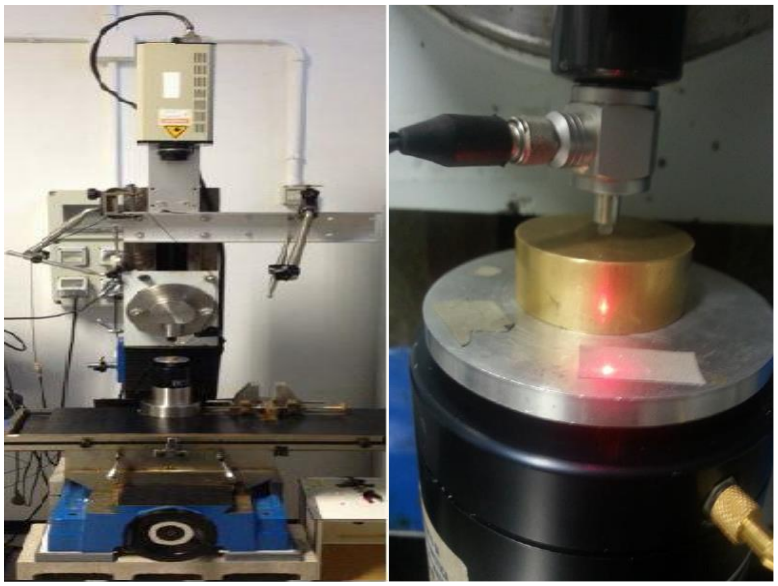

Figure 16. Schematic of the DMA test equipment to obtain storage and loss modulus

The experimental set-up posses following items:

- Fixed head movable by a screw, so that the distance between the two plates can be adjusted accordingly with the sample dimensions.
- Electrodynamic mini-shaker (Brüel & Kjær type 4810): it is provided with a permanent field magnet and it applies oscillating stimuli to the implant.
- Power amplifier (Brüel & Kjær type 2706): it controls the mini-shaker and the amplification magnitude of the sinusoidal vibrations can be set through a potentiometer.
- Force transducer: it consists of a piezoelectric load cell, which generates a charge signal (proportional to the applied force) as a response to the mechanical stimulus applied by the shaker.
- Laser vibrometer (Complete Polytec Laser Vibrometer System OFV 3000/302 with Nikon Lens Sensor Head Version): it's located above the experimental set-up and it measures the displacement. This component works on the principle of optical interference: a laser
- Beam is aimed towards a target plate, leading to light scattering. The light that has been scattered is then collected and it interferes with a reference beam.
- Metal plate placed over the mini-shaker and used as a reflecting surface for the laser beam.
- Sensor signal conditioning (482C series, PCB Piezotronics): it amplifies and converts the signal acquired by the force transducer into an electrical one.

- Labview software responsible for the functioning of the instrument, and for storing, displaying and processing measurement data. The instrument is isolated from vibration by blocks of cement and rubber supports.

All the tests were performed in compression within the range of 5-100 Hz with an initial pre-deformation of 20% of the sample diameter. The test consists in a sinusoidal vertical oscillation obtained with a shaker (Brüel & Kjær, Mini-shaker, type 4810). This sinusoidal oscillation causes deformation of the samples as a result of the cylindrical indenter action. The corresponding sinusoidal oscillating force (dynamic oscillating stimulus) is measured with a force transducer (*PCB Piezotronic, Load cell, model 208 M116*) with the accuracy of 10^{-3} N. Also, the displacement with a resolution of 0.01 µm is measured through a laser vibrometer (*Polytec OFV 3000 vibrometer controller*) focused on the oscillating plate. Table. 5 of supporting information summerized the set-up parameters of the device.

Table 5. set up parameter for the DMA tests

Initial deformation	**20% of initial diameter**
Amplitude	**5.00 V**
Start frequency	**5.00 Hz**
Stop frequency	**100.00 Hz**
Stimulus	**9.73 N/V**

The dynamic complex modulus, E^*, defines as the stress to strain ratio of the materials placed in the vibration conditions.

$$E^* = \frac{\sigma}{\varepsilon} \quad (1)$$

The complex modulus can be split in two parts according to the Equ.1:

$$E^* = E' + iE'' \quad (2)$$

where

$$E' = E^* \cos\delta = \frac{\sigma}{\varepsilon} \cos\delta \quad (3)$$

is the storage (or elastic) modulus

$$E'' = E^* \sin\delta = \frac{\sigma}{\varepsilon} \sin\delta \quad (4)$$

is the loss (or damping) modulus.

The Storage Modulus represents the elastic component of the material and it indicates the amount of energy stored during a loading cycle, while the Loss Modulus represents the viscous component and it is proportional to the energy dissipated during the same loading cycle. Both E' and E'' are dynamic material-specific characteristics that depend on the frequency. The loss factor (Q^{-1}) is the ratio of E''/E' ($\tan\delta$) and represents the mechanical damping in a viscoelastic system. The phase angle δ is the phase difference between the dynamic stress and the dynamic strain in a sample subjected to a sinusoidal oscillation. For a viscoelastic material δ falls into the following range:

$0 < \delta < \pi/2$

The behavior of a material is conventionally called solid-like when $\tan\delta < 1$ at a given frequency, otherwise it is defined as liquid-like.

3.2.5 Swelling ratio

The swelling ratio of the micro beads was calculated gravimetrically by measuring their weight gain in phosphate buffer saline (PBS) at pH 7.4. Accurately weighted (W_0) of dried micro beads were immersed in PBS at 37˚ C. After predetermined time intervals (30, 60, 90, 120, 180, 240, 300, and 360 minutes), the beads were filtered from the solution through a Millipore 0.22 μ filter equipped with a pump to remove extra liquid and weight immediately (W_t). The following equation will give us swelling ratio (SR) of micro beads at different time.

$$SR = \left(\frac{Wt - W0}{W0}\right)$$

3.2.6 Drug content

In order to estimate drug encapsulation efficiency, 10 mg of dried beads was placed and shaken in 10 ml of PBS for 24 h at 37˚ C, and then sonicated (FALC-HK2200, Italy) for 30 minutes in order to ensure a complete Ibu release. After that, the solution was centrifuged and filtered using Minisart 5.00 μ filter. The actual amount of Ibu was determined using a UV visible spectrophotometer (Jasco V-570) at the wavelength of 264 nm and a calibration curve in PBS. Then, the entrapment efficacy (% EE) for Ibu was calculated according to the following equation:

$$\% EE = \left(\frac{Acctual\ drug\ loading}{Theoretical\ drug\ loading}\right) \times 100$$

3.2.7 In-vitro drug release experiment

In vitro drug release of Ibu from the different formulation of Alg-Bru samples was carried out at 37 ˚C using Heraeus incubator equipped with an IKALABORTECHNIK shaker at the rotation speed of 100 rpm in PBS. The first two hours of experiment was carried out in a PBS solution at pH 1.5 (prepared by dissolving 0.05M of KH_2PO_4 and adding HCl to adjust the pH) and followed by 8 hours in PBS solution at pH 7.4 to simulate the behavior of the carrier in the gastric fluid and intestine fluid, respectively. 10 mg of dried hydrogel samples were immersed in a 10 ml of release media. After predetermined time intervals, 5 ml of solution was withdrawn and replaced with equal amount of fresh media. These withdrawn samples were subject to UV visible spectrophotometer at 264 nm. The IBP release percentage was calculated according to following equation:

IBP release percentage = $(R_t / R_0) \times 100$

Where R_t is the released amount of IBP at time t and R_0 is initial amount of Ibu encapsulated in the beads.

3.3 Result and Discussion

Previously we investigated the mechanism of in-situ fabrication of these hydrogel composites [127, 128]. Briefly, two simultaneous phenomena occurred as a result of in-situ synthetized method which was used to fabricate the hydrogel composites. First, the nucleation and growth of Bru crystals inside the Alg matrix occurred followed by crosslinking of the polymeric network and formation of the beads 3D structure. Ibu was loaded into the beads by dissolving it in the solution containing sodium Alg and

$(NH_4)_2HPO_4$. The loading procedure started as soon as the polymeric solution was introduced to the crosslinking solution in a dropwise manner. The homogeneous dispersion of Ca^{2+} and PO_4^{3-} ions in both solutions yield to uniform dispersion of Bru crystals within the Alg matrix. As reported before [89] the concentration of $(NH_4)_2HPO_4$ and sodium Alg have a significantly impacts on the mechanical properties, swelling ratio, entrapment efficiency, and in–vitro release behavior. Therefore, we investigated the influence of these factors on the mentioned characteristics. In addition, the initial drug content is another significant factor owing to its interaction with the carrier in the molecular scale. Hence, we studied the loading efficiency and its subsequent in-vitro release for three different concentrations of drugs. To our knowledge, no study was conducted on using the in-situ synthetized Alg-Bru hydrogel composite as a drug carrier. Therefore, structural and mechanical characterizations of these hydrogel composite and investigation of drug-carriers interactions are of crucial importance.

3.3.1 Characterization

- *FT-IR analysis*

Figure. 17 shows the IR spectra of Alg -Bru hydrogel composite and Ibu loaded Alg-Bru hydrogel composite in comparison to spectra of pure reference materials, i.e. calcium Alg, Bru and, Ibu. In the spectrum of the Ibu-loaded composite several bands are detected characterizing both the hydrogel matrix and the drug molecule. In the high frequency region, the two doublets are diagnostic peaks of Bru which corresponds to O-H stretching peaks of the two structural water molecules [100]. These peaks in our spectrum

were detected at 3164, 3278 cm^{-1} and 3496, 3546 cm^{-1}. Furthermore, the corresponding sharp peak to the H-O-H bending mode was observed at 1640 cm^{-1} [101]. The peaks at 1133, 1056 and 985 cm^{-1} represent the specific peaks of PO_4 [90, 100]. Besides, the bands at 1226 and 869 cm^{-1} indicate stretching and bending mode of P-OH, respectively [101]. P-O deformation mode of phosphate group were observed at 659, 574 and 526 cm^{-1} [100]. On the other side, the broad bands centered at 1640 and 1425 cm^{-1} represent the asymmetric and symmetric stretching mode of the carboxyl group in Alg spectrum [99]. These peaks appeared as very weak absorption peaks due to partial masking by the Bru strong features. Also, the complex peaks in the range of 1000-1200 cm^{-1} relate to C-O and C-C stretching modes of Alg chain [99] are overlapped with bands of the phosphate group.

As for the Ibu molecules loaded in the complex matrix, the band at 1720 cm^{-1} is assigned to C=O stretching vibration of the undissociated (acidic) COOH group. In addition, weak and sharp bands at 1508, 1461, and 1384 cm^{-1} can be attributed to C-C vibrational modes in phenyl ring and vibration of C-H bond in the Ibu structure [129, 130]. In the same figure, the spectrum of Ibue in form of Na-salt is reported for comparison. This spectrum is characterized by two strong bands at 1550 and 1412 cm^{-1} assigned to the asymmetric and symmetric vibrational modes of the $–COO^-$ group.

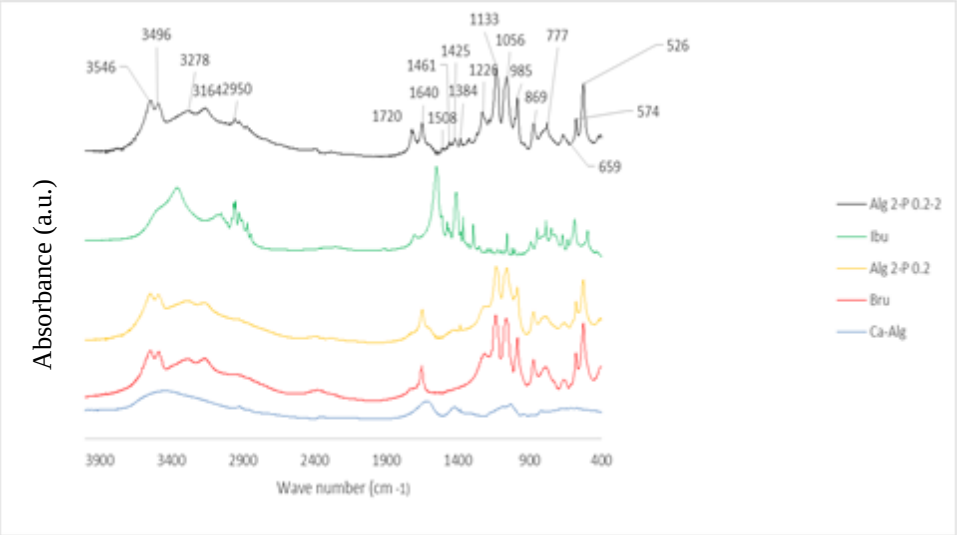

Figure 17. FT-IR spectra of calcium alginate (Ca-Alg), brushite (Bru), alginate-brushite (Alg 2-P 0.2), ibuprofen (Ibu), and ibuprofen loaded alginate-brushite (Alg 2-P 0.2-2)

The subtraction spectrum of [Alg 2-P 0.2-2] – [Alg 2-P 0.2] is reported in Figure. 18 of supporting information evidenced two main effects arising from the drug entrapment. i) the two strong bands appearing in the spectrum of the pure Na-Ibu due to asymmetric and symmetric stretching modes of the salt are not detected anymore and replaced by a sharp band at 1720 cm^{-1} (νC=O of the –COOH group). ii) Other bands of the drug molecules, for instance bands due to alkyl chain and aromatic ring, are clearly detectable and only very slightly affected by the interaction with the composite. A likely explanation is the pH decrease during Bru formation in the matrix [131] which leads to the formation of free COOH groups in the acidic form of Ibu. Loading acidic form of the drug on the beads might be more favorable than anionic form due to reduction in the electrostatic repulsion with negatively charged Alg chains.

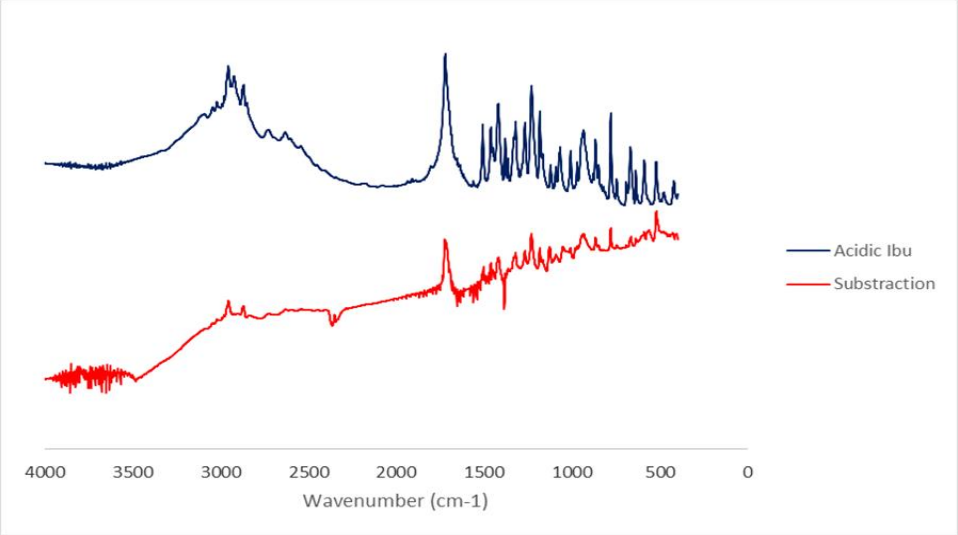

Figure 18. FT-IR spectrum of acidic Ibu and subtraction spectrum of [Alg 2-P 0.2-2] – [Alg 2-P 0.2]

- *X-Ray diffraction*

Figure. 19 shows the XRD patterns of Alg-Bru hydrogel composite, Ibu, and Ibu loaded Alg-Bru hydrogel composite. The standard Bru JCPDS card (9—0077) and the standard Ibu JCPDS card (32-1723) were used to analyze the resultant spectra. As we can see in Figure. 19, those peaks marked by red * are characteristic peaks of Ibu. In addition, those peaks with blue * are mutual peaks of Bru and Ibu. Rest of the peaks relate to characteristic peaks of Bru component. Hence, the FT-IR results along with those of XRD confirmed that the drug successfully was entrapped by Alg-Bru beads.

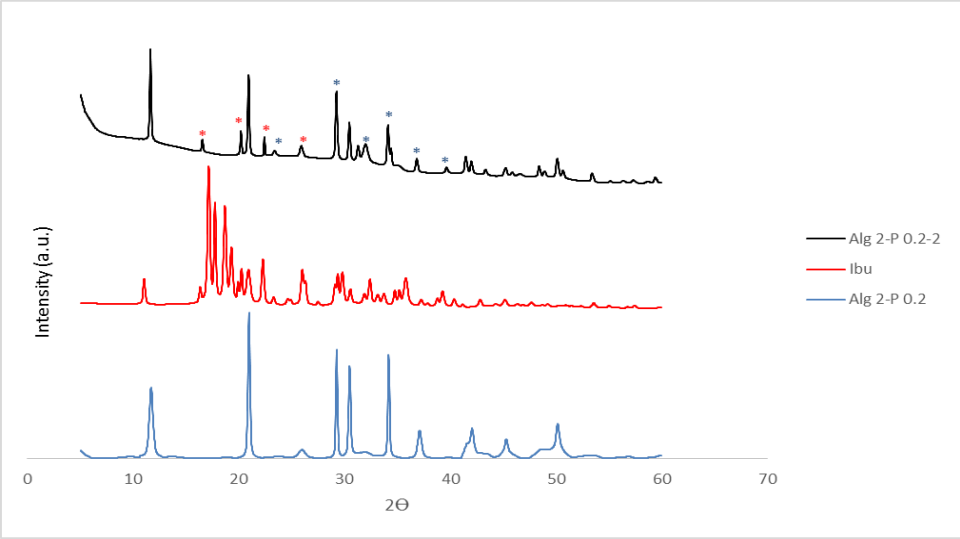

Figure 19. XRD patterns of Alg 2-P 0.2, Ibu, and Alg-P 0.2-2

- *Scanning electron microscopy (SEM)*

The SEM micrograph of calcium Alg and Alg-Bru dried beads at different magnification are presented in Figure. 20A, 20B, 20C, 20D, 20E and 20F to investigate the impact of phosphate group incorporation on the surface morphology of beads. In addition, Figure. 20G presents the EDS spectra of the beads to have an elemental analysis of the dried beads. It has been reported [89] that the dried beads of calcium Alg have a round, tight, and soft surface, whilstthe Alg-Bru beads present an irregular shape and rough surface with considerable wrinkles. Angadi et al [132] claimed that quick drying processes as well as heterogeneous structures were mainly responsible for irregular shapes of Alg composite dried beads. Higher magnification images demonstrated the accumulation of Bru plate-like crystals with various dimensions in the Alg matrix. Furthermore, the elemental analysis of the dried beads from EDS showed the presence of Ca, P, Na, C, and O. The calcium content relates to both calcium Alg and Bru, while the

phosphorous content can be attributed only to the Bru. In addition, Na is also detected due to presence of small amount of residual sodium Alg.

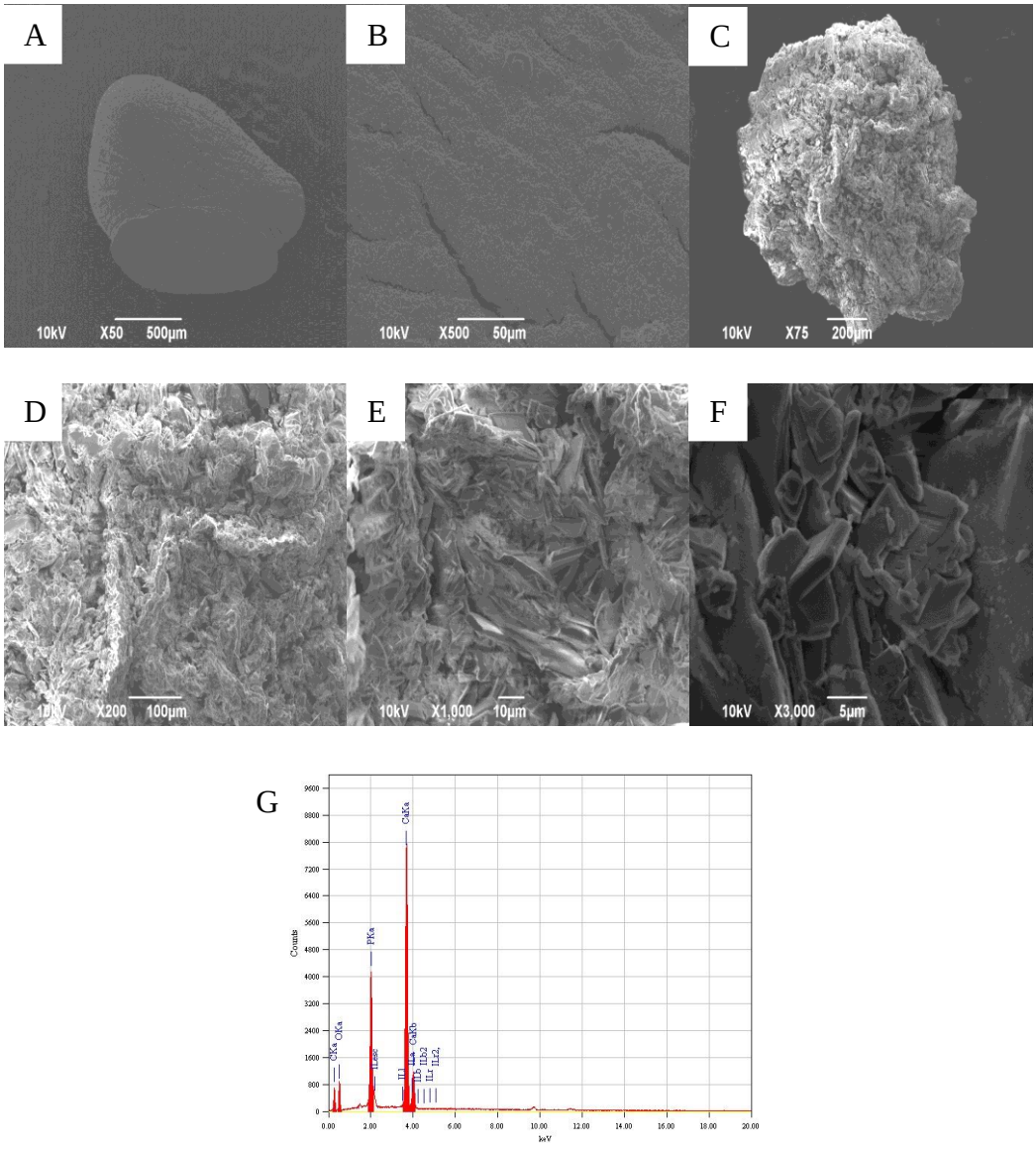

Figure 20. SEM micrographs of Alg 1.5 at magnifications of (A) 50x, (B) 500x and Alg 2-P 0.2 sample at magnifications of (C) 75x, (D) 200x, (E) 1000, and (F) 3000x. (G) EDS spectra of Alg 2-P 0.2

3.3.2 Dynamic mechanical analysis (DMA)

Figure. 21A, 21B, Figure. 22 and table. 4 present DMA results of different composite and reference samples versus frequency. As can be seen, the loss factor $Q^{-1} < 1$ in all samples is indicating that all the hydrogel samples presented a solid like behavior. Besides, as the concentration of Alg increased, the storage modulus showed an upward trend (Figure. 22). An approximate of 35 kPa enhancement in the storage modulus of composite samples seemed to be considerable when the concentration of Alg increased from 1% to 2%. This improvement can be attributed to the fact that an increase in the concentration of Alg led to a denser polymeric chain. In addition, higher crosslinking density resulting from an increase in the electrostatic attraction between carboxylate groups of Alg and calcium ions can explain this improvement [133]. The comparison between the Alg 1.5 and Alg 1.5-P 0.1 samples, which were composed of equal Alg concentration, revealed more than 20 kPa improvement in the storage modulus. This relates to the fact that Bru component has higher mechanical properties than Alg and the polymeric chains movements are restricted by the crystalline component.

The impact of Bru content on the storage modulus at different frequency can be seen in the Figure. 21 and Figure. 22. Obviously, storage modulus at different frequency, i.e. 10 and 85 Hz, was significantly enhanced by an increase in the content of Bru. However, this improvement was followed by a remarkable decrease when higher content of Bru (Alg 2-P 0.4) was introduced into the sample. This can be explained by the fact that the higher amount of PO_4^{3-} in the Alg 2-P 0.4 sample is acting as a barrier in the crosslinking process. As a result, the sample Alg 2-P 0.4 is less crosslinked than the other

two as evidenced by storage modulus results. As can be seen in Figure. 21B, that increase in the content of Bru led to reduction in the mobility of polymeric chain and subsequently decrease the loss factor (increase in solid like status).

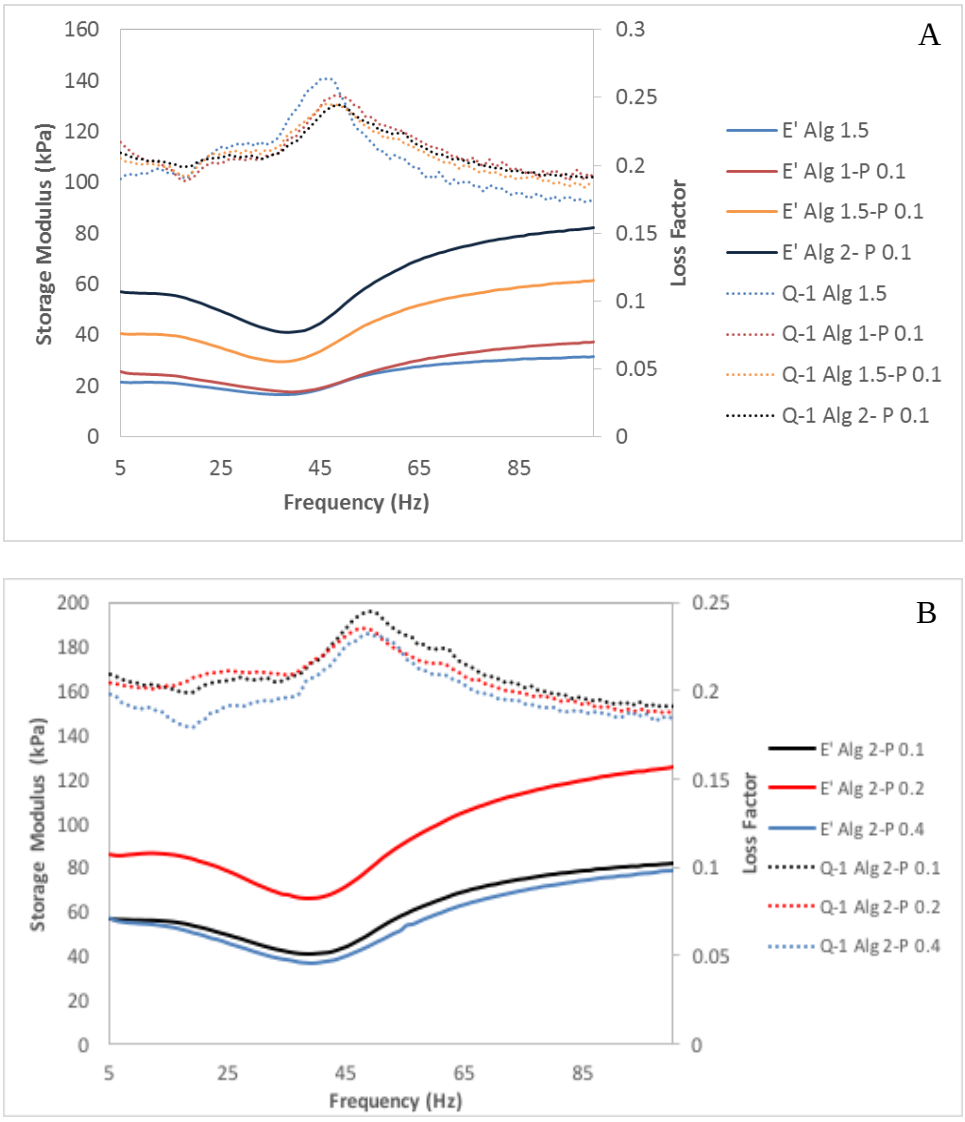

Figure 21. Effect of the content of Alg (A) and Bru (B) on the storage modulus and loss factor at different

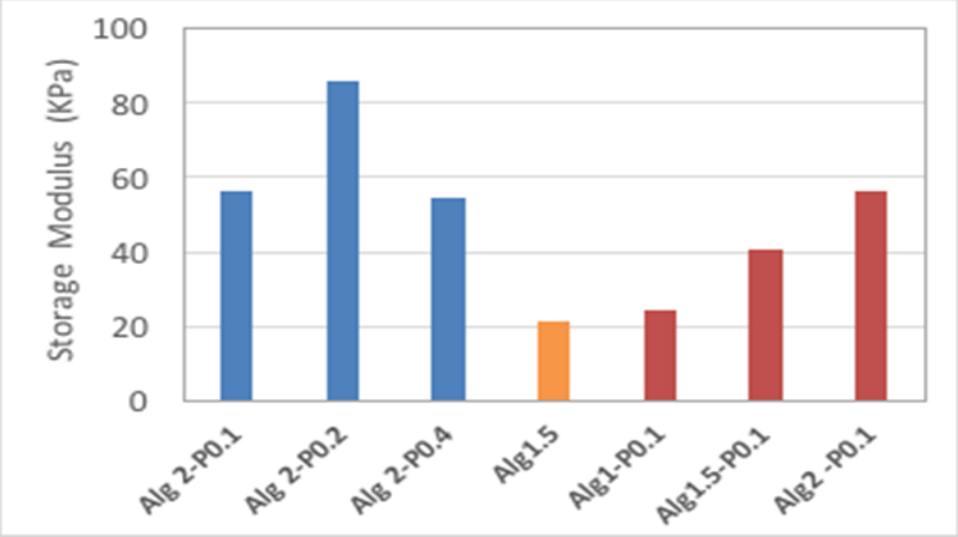

Figure 22. Effect of changes in the Bru content and Alg concentration on the storage modulus at 10 Hz

3.3.3 Swelling ratio

The release behavior of Alg and its composites is highly dependent upon the swelling ratio and swelling kinetics. In fact, the main release mechanism is based on the swelling behavior. As we can see in the Figure. 23, the presence of Bru had a favorable effect on the swelling behavior of the hydrogel so that at the same concentration of Alg, the swelling ratio decreased from 12.72 to 10.29. On the other hand, the swelling behaviors of samples were significantly influenced by variation of Alg concentration. The swelling ratio showed an upward trend as the concentration of Alg increased and the relative content of Bru crystals decreased. We can see that the swelling ratio grew from 7 to 10.29 with a 0.5% increase in the concentration of Alg. This was followed by 1.09 further growth in the sample prepared with 2% of Alg. In addition, the sample Alg 1- P 0.1 had the lowest swelling ratio because in-situ formed Bru crystals restricted the Alg

polymer chain movement, thus hindering penetration of water into the network. Besides, as the content of Bru increased in the Alg matrix due to an increase in the primary concentration of $(NH_4)_2HPO_4$, a slight decrease was detected in swelling ratio of Alg 2-P 0.2 and Alg 2-P 0.4 samples.

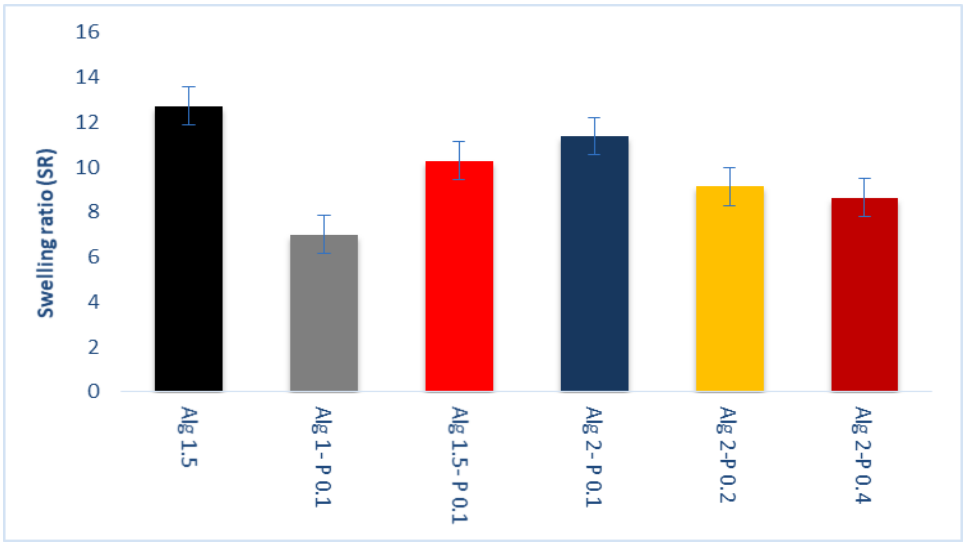

Figure 23. Effect of changes in the Bru content and Alg concentration on the swelling ratio

Figure. 24 shows the swelling kinetics of different samples in PBS media at 37˚C. As can be seen, the swelling ratio of the samples increased significantly through swelling time passage to reach their maximum ratio. Then, it followed a sharp downward trend with further swelling time passage and even ALg-1.5 and Alg 1- P 0.1 samples experienced disintegration. Osmotic pressure is the core cause of water penetration into the polymeric network and consequently weight gain of the samples [134]. Since the strength of $–COO^{-\cdots+}Ca^{+\cdots-}OOC$ interactions were at its minimum in the swelling ratio peak due to the polymer chain expansion, the bonds were easily broken by PO_4^{3-} in the

surrounding PBS media. This resulted in disintegration of the Alg and leading to a burst release of the drug.

The significant impact of Bru is considerable in the kinetics of swelling so that the composite samples smoothly gain weight and the disintegration process prolonged further. This can be attribute to Bru crystals resistance against penetration of the PO_4^{3-} functional group and consequently postponing the breakage of $–COO^{-\cdots+}Ca^{+\cdots-}OOC$ interactions.

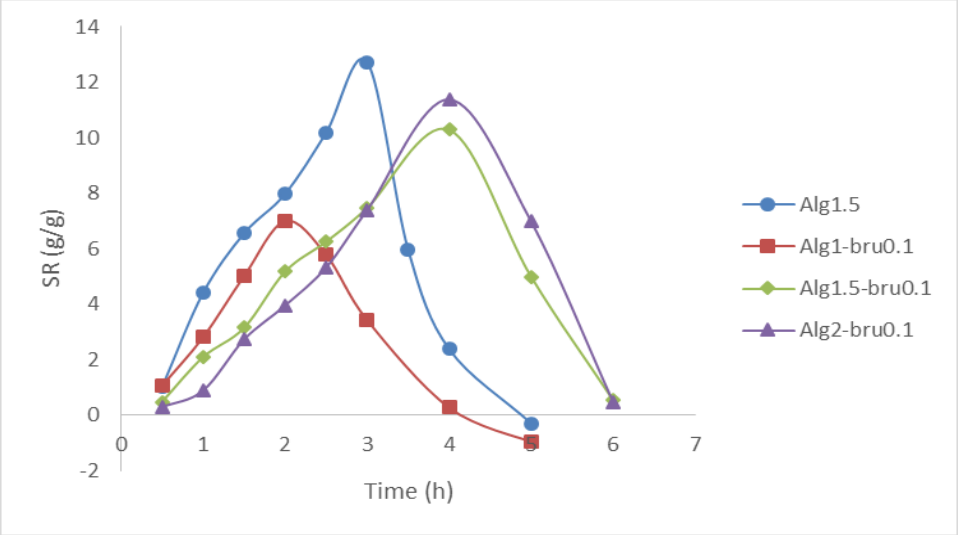

Figure 24. Variation of swelling ratio vs. time in Alg and Alg-Bru composites

3.3.4 Release behavior

- *Encapsulation efficiency*

The encapsulation efficiencies of the different samples are listed in Table. 6. Although we expected that incorporation of Bru into Alg matrix would increase the

encapsulation efficiency via retarding the drug leakage as a result of formation of a denser surface, the results were unexpected. This can be attributed to the fact that the presence of Bru has limited the sol-gel transition and made a delay in crosslinking process. This can also be down in part to the time consuming process of the composite formation and the leakage of the drug from surface pores. Therefore, more Ibu molecules leaked out from the composite samples during fabrication process. Besides, dissolving higher amount of drug in the initial polymeric solution resulted in composite beads carrying higher amount of drug. Noteworthy that the significant decreased in EE% does not seem to be ignorable.

Table 6. Compositions of loaded hydrogel beads and their encapsulation efficiency (EE)

Item	Sample	Sodium alginate (wt %)	[(NH4)2HPO4 (M)	Ca(NO3).4H2O (M)	Ibuprofen (%)	EE (%)
1	Alg 1.5-1	1.5	---	0.2	1	74.97±6.67
2	Alg 1- P 0.1-1	1	0.1	0.2	1	70.02±5.43
3	Alg 1.5- P 0.1-1	1.5	0.1	0.2	1	73.65±16.14
4	Alg 2- P 0.1-1	2	0.1	0.2	1	74.96 ± 2.81
5	Alg 2-P 0.2-1	2	0.2	0.2	1	79.91 ± 2.13
6	Alg 2-P 0.4-1	2	0.4	0.2	1	63.80 ± 2.23
7	Alg 2-P 0.2-1.5	2	0.2	0.2	1.5	67.68 ± 1.15
8	Alg 2-P 0.2-2	2	---	0.2	2	63.24 ± 3.29

- *Cumulative release*

As it is evident in Figure. 25, all the formulations demonstrated pH sensitive release behavior. It has been reported that pKa of Alg is almost 3.2 and the transformation of carboxylate group in the Alg chain into -COOH occurs at a pH lower

than 3 [135]. Therefore, this transformation established hydrogen bonding between –COOH and hydroxyl group in Alg which restricted the dried beads to swell in simulated gastric fluid. The impact of Alg concentration on cumulative release is illustrated in Figure. 25A. As we can see, the rate of release is not significant owing to low swelling ratio of the samples in acidic condition and all the sample release almost the same level of Ibu. Hence, these results suggest that the Ibu was released from the samples by diffusion mechanism. Also, low solubility of Ibu in acidic media (simulated gastric fluid) could be another reason for slow release of Ibu from the samples. As discussed before, the formation of Bru within Alg matrix resulted in loading acidic form of Ibu with –COOH carboxyl group into carriers. Therefore, formation of hydrogen bonds between –COOH of Ibu and -COOH of alg is another cause for slow release of Ibu from the carriers in acidic environment. This phenomena was also reported for Diclofenac release from a hydrogel based on methacrylated Alg [135]. On the other hand, samples in simulated intestine fluid (pH=7.4) exhibit a completely different behavior. All the samples showed a burst release of Ibu owing to extensive swelling in PBS 7.4 and consequently penetration of PO_4^{3-} into the polymer. Besides, all the –COOH groups in Alg and Ibu transformed into $-COO^-$ at pH 7.4 which not only increased the solubility of Ibu but also, caused electrostatic repulsion between $–COO^-$ groups and led to faster release of Ibu.

We can see that more than 85% of IBU was released from Ca-Alg samples after 4 hours in PBS 7.4 while, the Alg 2- P 0.1-1 sample release 62% of entrapped Ibu at the same time and further 4 hours was needed to release 81% of entrapped Ibu. Also, we can see that the presence of Bru in the Alg matrix resulted in more than 10% decrease in final

Ibu release in the Alg 1.5- P 0.1-1 sample. This suggested the positive effect of Bru on release behavior and controlled release of Ibu. Although the sample Alg1– P 0.1-1 had the highest relative content of Bru, the Ibu release behavior was almost similar to that of Ca-Alg. This behavior can be explained by the irregular shape of this sample. Unlike the other samples which had the spherical shape, Alg1-P0.1-1 shape tended to be less spherical due to platelet-like morphology of Bru. In other words, the beads of Alg1-P0.1-1 were less stable than the other composite samples. Hence, the disintegration process accelerated and a higher content of the drug was released.

Next step was evaluating the impact of Bru content on release behavior. Therefore, Alg2-P0.1-1 was chosen as the reference sample because it had the best release profile as well as the beads had sufficient stability so that the beads would remain stable following the increase in the content of $(NH_4)_2HPO_4$. As plotted in Figure. 25B the cumulative release decreased when the primary concentration of $(NH_4)_2HPO_4$ was 0.2 M. The Bru crystals resisted against swelling and following PO_4^{3-} penetration. Further increase in the concentration of $(NH_4)_2HPO_4$ had a negative impact on the release profile since the beads were less crosslinked than the other two samples and were unable to restrict release of Ibu. Furthermore, Figure. 25C demonstrates how initial drug content would change the release profile. It is clear that the Alg 2- P 0.2-1.5 sample follows almost the same pattern of release as Alg 2- P 0.2-1 sample when the incorporated drug increased up to 0.5%. Further increase in the content of drug possibly had reverse effect on the release profile owing to intermolecular interactions between sodium Ibu and sodium Alg, sodium Ibu and Bru. As a result, less stable beads were formed in a way that

the beads exhibit less resistance against release of Ibu to the surrounding media. Hence, these results indicate that an increasing in the initial drug content not only decreased the EE%, but also it had a reverse effect on release profile.

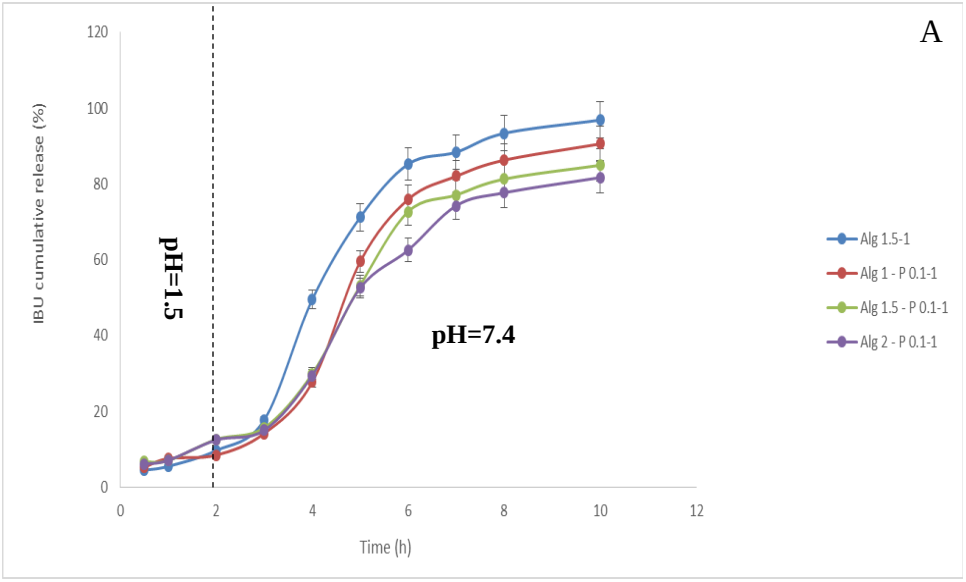

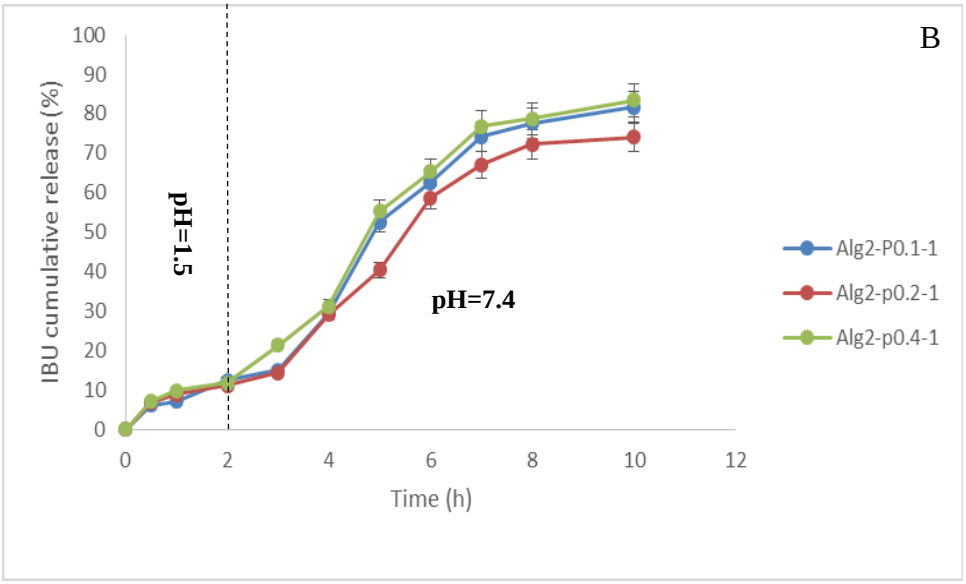

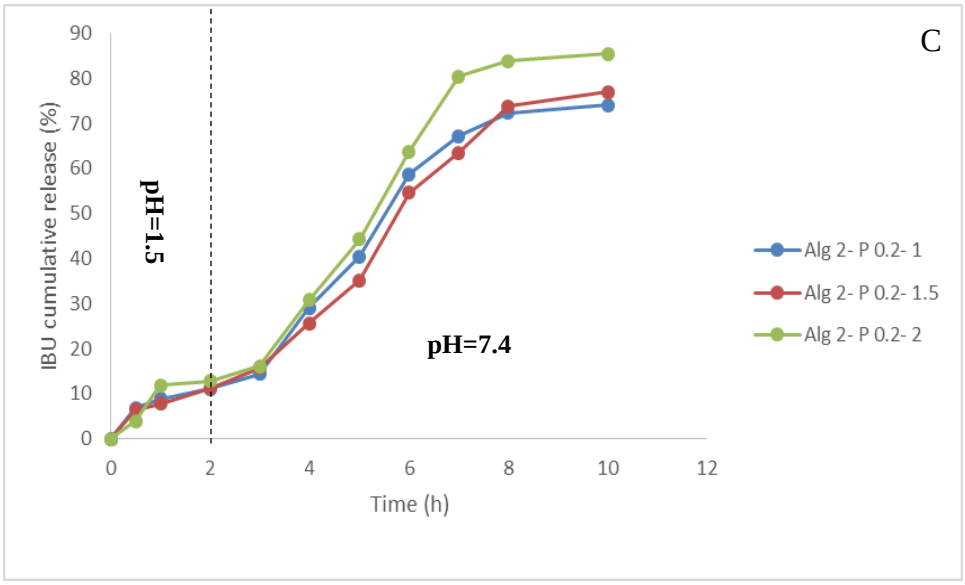

Figure 25. Effects of variations in (A) Alg concentration, (B) Bru content and (C) initial Ibu concentration on the release profile of Ibu from Alg and Alg-Bru composite beads at pH 1.5 PBS (first two hours) followed by pH 7.4 PBS

3.4 Conclusion

The current study was carried out to evaluate in-situ synthetized Alg-Bru as a new potentially reinforced carrier for delivering drug and other active biomolecules. To this aim, Ibu was actively loaded in the carriers during crosslinking and formation of Bru within Alg matrices. According to FT-IR and XRD results, the composite materials were successfully fabricated and the drug was loaded into the carriers. SEM images demonstrated the significant impact of Bru crystals on the morphology of the beads. In addition, the restriction of Alg chain movement by uniformly dispersed Bru crystals was the main cause of regulating swelling behavior and enhancing the mechanical behavior. Furthermore, improving the swelling behavior ultimately triggered the gradual release in composite samples and avoided burst release observed in calcium Alg beads. The

optimized formulation prolonged Ibu release for a period of 10 hours. These results seem to suggest that the in-situ synthetization of Bru within Alg sufficiently modified release behavior. However, the entrapment efficiency was not remarkably improved in comparison with that of calcium Alg. The simplicity and effectiveness of the method used in the present study to fabricate a pH sensitive DDS can be further improved to encapsulate bioactive molecules including other drugs, proteins, vitamins.

CHAPTER 4 : Controlled Gentamicin release by Brushite cement modified with Alginate

4.1 Introduction

The reconstruction of bone defects, due to trauma and disease, by bone grafting represents an important challenge owing to the fact that millions of people are annually dealing with it [136]. The gold standard in this respect is defined as autologous bone grafting which contains living cells and osteogenic growth factors in order to help the formation of new bone tissue. Limited bone sources, associated donor site pain and morbidity, possible cell and damaging during transplantation are listed as the main draw backs, which have limited autologous bone grafting so far [137-139]. Hence, there is a significant demand for synthetic materials which not only can overcome the above-mentioned disadvantages, but can also help the restoration of bone defects.

Calcium phosphate bone cements (CPC) and their modified formulations have been widely used for treating bone defects since the first time that Brown and Chow introduced them in 1980s [140]. Notable biocompatibility, bioactivity, and osteoconductivity, as well as similarity to the mineral component of bone, have made these materials a proper candidate for treating low or none load-bearing bone defects [141-143]. CPC are obtained via a chemical setting reaction between a solid and a liquid phase leading to the precipitation of Ca-salts in the form of apatite, hydroxyapatite, calcium-deficient hydroxyapatite and Bru [144]. The main advantage of Bru cements over apatite ones seems to be having up to two times higher solubility rate in physiological conditions [145]. Bru cements are formed as the result of an exothermic reaction between an acidic calcium phosphate (i.e. MCPM) and a basic calcium phosphate (i.e. β-TCP) according to the following reaction [91]:

$$\beta\text{-}Ca_3(PO_4)_2 + Ca(H_2PO_4)2.H_2O + 7H_2O \longrightarrow 4CaHPO_4.2H_2O$$

Several biopolymers including chondroitin sulfate [146], chitosan [147], gelatin [148], and Alg [149] have been incorporated in the cement as additives (less than 1 wt%) to modify CPC mechanical and anti-washout properties. Such biopolymers have a high potential to entrap biological active agents like stem cells [150, 151] and drug [152] for long term treatment of bone regeneration. Among them, Alg seems to be a suitable material, as an additive or carrier, to modify cement owing to its biocompatibility, biodegradability, and low price [153]. It has been reported that Alg can form Alg gel through a crosslinking reaction with release of calcium from CPC and protects the cement from primary disintegration on early contact with human body fluids [149].

Bone regeneration processes are often associated with complications such as bacterial infections, and inflammatory responses of the immune system. Thus, administration of different drugs, via intravenous injection or oral uptake, has been proposed to treat these complications. However, these administration routes may damage the non-targeted tissue. Moreover, the efficacy of treatment could be low due to insufficient bio-distribution and uncontrolled drug release [154, 155]. On the other hand, the intrinsic micro/submicro porous structure of Bru [156] cements has made them a highly interesting carrier for delivering of active therapeutic agents such as drugs [157], antioxidant [158], and stem cells [150, 151]. The local administration of Gen[20] is highly recommended for the treatment of bacterial infections owing to its antibacterial activity

[20] **Gentamicin sulfate**

against a wide range of microorganisms such as Pseudomonas aeruginosa, Staphylococcus aureus, Proteus species, and Enterobacteriaceae [159].

4.2 Materials and methods

4.2.1 Materials

Sodium alginate from brown algae, β-tricalcium phosphate (β-TCP), monocalcium phosphate monohydrate (MCPM), sodium citrate tribasic dihydrate, gentamicin sulfate, Dulbecco Modified Eagle's Medium (DMEM), fetal bovine serum (FBS), phosphate buffered saline (PBS), isopropanol, paraformaldehyde, glutaraldehyde and [3-(4,5-dimethylthiazol-2-yl)-2,5-diphenyltetrazolium bromide] (MTT) were obtained from Sigma-Aldrich. Human osteoblast cell line was obtained from the National Cell Bank of Iran (NCBI), Pasteur Institute of Iran. In addition, 96-well microtiter plates for cell culture were supplied by Nunc, Denmark. All reagents were used without any purification.

4.2.2 Cement preparation

Bru cement was prepared at room temperature through mixing equimolar amounts of β-TCP and MCP powders, solid phase, and distilled water, liquid phase, with the powder to liquid (P/L) ratio of 3. In addition, sodium citrate tribasic dihydrate with a concentration of 0.5 M was incorporated into the liquid phase as cement retardant agent. Predefined amounts of Alg, as listed in Table. 7, were added to the powder mixture in order to form the Bru-Alg composite cement. The resulting paste was poured into

cylindrical plastic molds for setting. The obtained samples were used for mechanical, biological and release experiments.

4.2.3 Mechanical tests

The mechanical behavior of Bru and Bru-Alg cements were examined using a universal testing machine (Zwick/Roell Z10) with a 10 KN load cell. For the standard compressive analysis, cylindrical samples having a diameter of 9 mm and a height of 18 mm were positioned vertically on a plate supported with a spherical joint to correct the non-planar imperfections of the cylindrical base samples. The tests were performed in displacement control at a rate of 1 mm/min, according to the ASTM standard F451. The same cylindrical geometry, having a diameter of 9 mm and a height of 5 mm, was used to perform diametrical tensile test, Brazilian tests, (DTS). For these tests the samples were positioned horizontally on the same tilt plate used for the compressive analysis and were compressed at a rate of 1 mm/min.

4.2.4 In-vitro biological assays

- *In-vitro cell culture*

The in vitro characterization was carried out using human osteoblast cell line from femoral bone according to the published protocol [160]. The cells were cultured in DMEM supplemented with 10% FBS (v/v), 100 U/ml penicillin and 100 µg/ml streptomycin followed by incubating them at 37 ˚C in humidified atmosphere containing 5% CO2.

- *Cement extraction*

The rates of proliferation and differentiation were calculated using extracted samples based on ISO 10993–5 protocol where 0.1 gr of different cement formulations were soaked into 1 ml of culture media. After 3, 7 and 14 days, the mediums were gathered to be used in different cellular tests. Pure culture medium, maintained under similar conditions, was used as the negative control.

- *Cell proliferation*

The proliferation rates of the cells over various cement samples were determined by dimethylthiazol diphenyl tetrazolium bromide (MTT) assay. Briefly, 1×104 cells/well with 100 µL culture mediums were cultured into 96- well microtiter plates (Nunc, Denmark). After 24 hours, the culture medium in each well was withdrawn and replaced by 90 µl cement extraction solutions (3, 7, and 14 days) and 10 µl FBS. The medium was removed after 24 hours and then 100 µl of MTT solution (0.5mg/ml) was added into each well and incubated for 4 hours at 37˚C. In order to dissolve the formed formazan crystals, 100 µL of isopropanol was added to each well. The plate was placed in a shaker at 37 ˚C for 15-20 minutes to dissolve the purple crystals. Finally, the optical density of formazan was recorded at 545 nm using a multiwall microplate reader (STAT FAX 2100, USA). In addition, the results were normalized respect to the negative control sample (tissue culture Polystyrene (TPS)).

- *Alkaline phosphatase activity (ALP)*

ALP enzyme activity, as an osteoblast cell marker, was measured to evaluate cell activity. In order to determined ALP activity the cells were trypsinized after reaching to appropriate concentration (5-7 days). About 5000 cells in 1000 µl of culture medium containing 10% FBS were poured into each well of sterile 6-well culture plates and the cements at the concentration of 30 µg/ml were exposed to the cells. After 7 and 14 days of culturing, cell supernatant (medium on the samples) was removed and examined by auto-analyzer (Hitachi Model 911, Germany, AUDIT Kit). The results were normalized similarly to those of MTT assay.

- *Alizarin red staining*

Evaluation of calcific deposition by osteoblastic cells was carried out by conducting alizarin red staining assay. This was done by culturing 5000 cells in a 6-well plate followed by adding the sample at the concentration of 30 µg/ml to each well. The medium was withdrawn after 10 days and cells rinsed twice with NaCl solution (0.9%). Then, cells were fixed by paraformaldehyde (1%) for 20 minutes and then they were stained using Alizarin red solution (2%) at pH 4.2 and room temperature for 45 minutes. Finally, cells were washed with NaCl solution prior to taking images by optical microscopy.

- *Cell attachment and morphology*

Cell adhesion assay was carried out in order to investigate the morphology and adhesion of isolated cells to the cement surface. Fist the sterilized samples were placed

into each well of 24-wells plate. Then, 4000 -5000 cells in 50 µL of culture medium were dropped on each sample surface and were placed in an incubator for 24 hours. Afterwards, the samples were washed four times with DMEM to remove unattached cells from the surface. Then, glutaraldehyde 2.5 % (v/v) was used to fix the cells at room temperature followed by rinsing them with graded alcohol of 50, 60, 70,80,90,95 and 100 %, respectively. Finally, adhesion of the cells to the sample was detected by secondary electron microscopy (SEM -TescanVegaï, Czech) at an accelerating voltage of 30 KV

4.2.5 Gentamicin loading

Gen was loaded only onto most promising samples, selected after compression and in vitro characterizations. Predetermined amounts of Gen, as reported in Table. 8, were incorporated in the liquid phase (Gen Solution, GL) or in the solid phase (Gen Powder, GS) in order to study the effect of Gen incorporation protocol on the release behavior.

- *Characterization*

Setting time measurements were conducted according to ASTM C 191-04a for hydraulic cements using a Vicat needle with the diameter of 1mm equipped with a 300 gr plunger. Periodic penetration of Vicat needle was performed after molding the cements paste into cylindrical shape having a diameter of 9 mm and height of 5 mm. The final setting time refers to the time when the Vicat needle penetrates less than 1 mm. 4 different positions in each sample were checked in terms of penetration depth to ensure that the cements were fully set and the test was repeated three times.

In order to characterize the main functional groups of the composite materials, FTIR was used. Samples in the form of powders were mixed with KBr and then pressed to prepare KBr disks. Spectra were collected in the range 400 - 4000 cm-1 using a Nicolet 380 Fourier transform infrared spectrometer (Thermo Fisher scientific Inc, USA).

The crystalline structure of different samples was examined using PANalytical Empyrean x-ray diffractometer operating with CuKα over the brag 2Θ range of 5-55˚. The resulting diffractograms were compared with ICDD (JCPDS) standards number 9-0077 for Bru. In addition, the crystalline size was measured following Scherrer's equation [161]:

$t=k\lambda/BCos\Theta$

where k assumed to be 0.9 and λ is the wavelength of X-Ray radiation, B represents full width at half maximum, and Θ is the brag angle.

A TG-DTA Netzsch Gerätebau STA 409 was used to carry out thermogravimetric analysis (TGA) along with differential thermal analysis (DTA). The thermal analysis was carried out in the range of 40-700 ˚C in nitrogen atmosphere with a heating rate of 10 K.min-1. In addition, morphological and microstructural investigations were carried out using JEOL SEM at an accelerating voltage of 10 KV.

4.2.6 Soaking properties in phosphate buffer saline

Cement behaviors in in-vitro conditions like (37 °C, PBS buffer) in terms of degradation, mechanical properties, chemical and structural stability are of vital importance. To this regard, 4 different samples namely Alg-Bru, Bru-Alg-GL 1, Alg-Bru-GL 2, and Alg-Bru-GL 5, having a diameter of 9 mm and height of 3 mm, were

immersed into 10 ml of PBS at 37 ˚C for predefined time intervals. At each time interval, samples were withdrawn from PBS solution and placed at 37 °C to completely dry. Then, the samples were subject to DTS to obtain strength of the samples after different soaking times. Finally, chemical stability and microstructure of fractured surface were examined by FTIR spectroscopy and SEM (Hitachi S-2500), respectively.

4.2.7 Drug release

Release of Gen from different cement formulations was evaluated at 37 ˚C in PBS at pH 7.4. Drug release was measured by placing ≈0.4 gr of different cement formulations in the form of disk in 10 ml of PBS. 5 ml of released medium for each sample was withdrawn at predefined period of time and replaced with 5 ml of fresh PBS. The content of Gen in each withdrawn medium aliquot was spectrophotometrically determined via a calibration curve on a UV-visible spectrophotometer (AGILENT-Cary 100, USA) at 248 nm. The related calibration curve equation was A=0.0866C, R2 = 0.96, where A represents adsorption at 248 nm and C indicates the concentration of Gen and Gen fractional release percentage was calculated as follows:

% Fractional Release =Rt/R0*100

where Rt is Gen release at time interval t and R0 is the initial amount of Gen loaded on the cements. In order to determine R0, an amount (≈0.4 gr) of each cement formulation was crushed into powders and then, immersed in 10 ml of PBS. The media were kept in the incubator at 37 ˚C for one week and subjected to rigorous shaking for 5 minutes followed by sonication for 30 minutes every day to ensure that all the Gen loaded on the cements was release. This step was followed by centrifuging the media at

3000 rpm for 5 minutes and the final determination of Gen concentration was carried out using UV visible spectrophotometer. The release for each formulation was measured in triplicate and the results were normalized respect to the weight of each sample.

4.2.8 Data analysis

The results presented as mean value and standard deviation of at least three repeats. In addition, one-way ANOVA with LSD post hoc test using SPSS (version 16.0 SPSS Inc. Chicago IL) was employed to analyze the data where probability value $p<0.05$ were defined as statistically significant.

4.3 Results and discussion

4.3.1 Compressive strength

Variation of compressive strength and elastic modulus of different cement formulations versus Alg percentage are reported in Table. 7. As we can see, both of these parameters followed a similar pattern in which they increased to a maximum value as 0.5% (w/w) of Alg added into Bru cement. Although the mechanical properties declined when Alg concentration further increased to 1%, these samples still possess higher mechanical properties in comparison to pure Bru cement. The compressive strength, as well as elastic modulu,s sharply decreased with another 1% increase in the content of alginate. It was reported that [149] Alg in the Bru cement acted like a water reducing agent which enhanced cement consistency, increasing mechanical properties through formation of a tighter packing. The decline in the mechanical properties as the

concentration exceed from 0.5% likely arose from agglomeration of Alg component as well as hindrance effect of Alg on Ca and P ions diffusion.

Mechanical properties of bone cements are highly dependent on the type of cement as well as fabrication technic. Therefore, the reported values in this criteria is different in each study. For instance, Fullana et al [152] reported that the compressive strength of calcium phosphate cement continuously decreased from 5.78 MPa to 2.4 MPa, as up to 6 wt% of pectin was added to the cement. Almost Similar results was obtained by Zhao et al [150] which Alg microspheres were incorporated into calcium phosphate cement. On the other hand, some studies reported compressive strength higher than 20 MPa for the same type of calcium phosphate cements [149, 162]. The compressive results of the cement fabricated in the present study exceeded the minimum level reported before.

Table 7. Mechanical properties of cements respect to Alg variations

Item	Name	Alginate content (wt %)	Elastic modulus (MPa)	Compressive strength (MPa)
1	Bru	0	783.62 ± 124.27	9.43 ± 1.49
2	Bru-Alg 0.5	0.5	1507.17 ± 267.74	10.36 ± 1.89
3	Bru-Alg 1	1	912.02 ± 109.41	9.8 ± 0.84
4	Bru-Alg 2	2	438.48 ± 115.21	9.05 ± 0.8

4.3.2 In-vitro biological assays

- *Cell proliferation*

Figure. 26A presents the viability of human osteoblast cells exposed to different cement extractions obtained after 3, 7 and 14 days. The results indicate that the proliferation rate of all the cement formulations were almost in the same level of control

group and Bru-Alg 1 cement supported higher proliferation rate ($p^* < 0.1$) than control and other cements within the considered time intervals. Moreover, a slight increase in proliferation rate, respect to pure Bru cement, was observed. Therefore, the results evidenced no negative effects of cements extraction on the cell viability.

- *ALP activity*

One of the conventional markers for determinating the osteoblastic phenotype expression is ALP [163]. Figure. 26B represents the relative activity of ALP for the cements with different concentration of Alg over the time period of two weeks. The results indicated that ALP activity after 7 days for all the cement was almost of the same level of control sample, and cement with 1% of Alg promoted higher ALP activity ($p^*<0.1$). In addition, further increase in culture time resulted in increase in the ALP activity for all the formulations, so that all the formulations promoted higher ALP activity respect to control samples. Besides, for both time intervals the cement with 1% Alg (Bru-Alg 1) possessed the highest ALP activity, which is quite in a good agreement with MTT assays, where this formulation had the highest cell viability for all of the time intervals. The primary mechanical properties results, along with cell proliferation and ALP outcomes, suggest that the cement with 1 % Alg (Bru-Alg 1) seems to be the best cement to carry Gen. So, hereafter further experiments, including alizarin red and cell adhesion assays, along with loading Gen and related tests were conducted on the Bru-Alg 1 cement, referred as Bru-Alg.

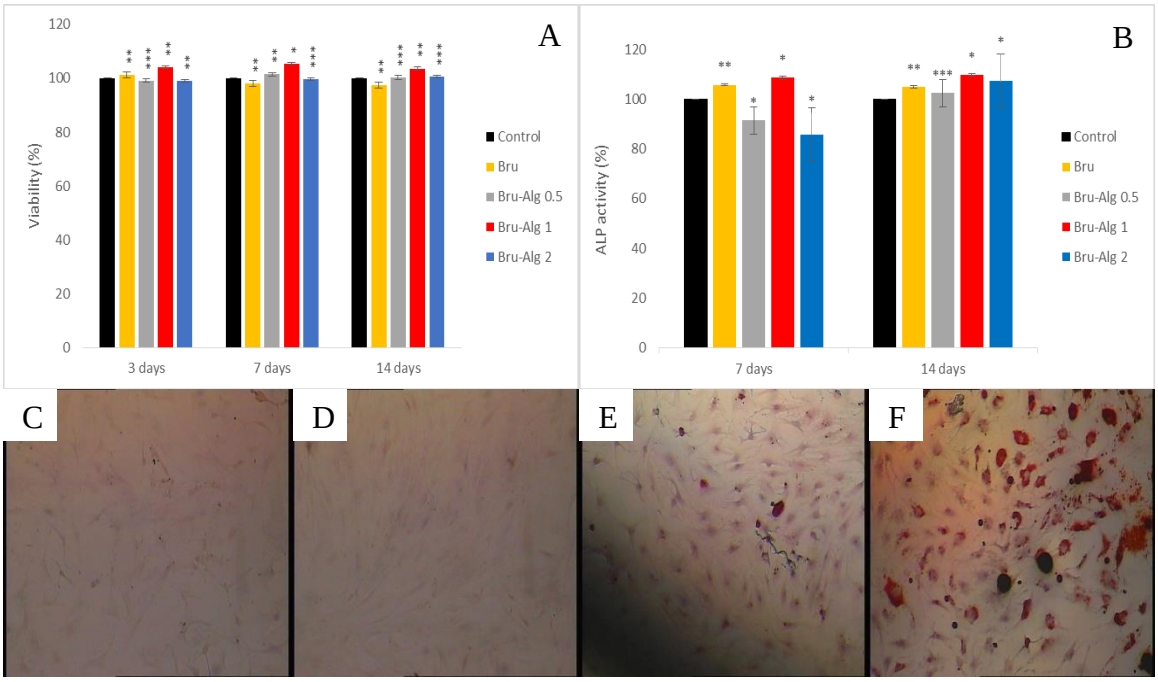

Figure 26. A) Viability of osteoblast cells on various cements after 3, 7 and 14 days. B) ALP activity of various cements after7 and 14 days. C -F) Optical microscopy images after alizarin red staining for control sample at 100×(C), 300× (D); and Bru-Alg cement at 100×(E), 300× (F).

- *Alizarin Red staining*

The calcium mineralization capacity of osteoblast cells exposed to the extracts of Bru-Alg and control samples are shown by Figure. 26C-F. A significant difference between the cement and control sample is quite observable. The results indicated clear positive staining and deposition of calcium by cells seeded on Bru-Alg. This can be attribute to the presence of calcium phosphate materials which progress the bone mineralization. Besides, ion exchange capability of Alg component possibly has a positive impact on the biomineralization process.

- *Cell attachment and Morphology*

Figure. 27 shows SEM micrograph of Bru-Alg cement seeded with osteoblast cells. It was found that the osteoblast cells are capable of attaching and proliferating on the surface of Bru-Alg cement. This result indicates that the surface of cement composite is osteoconductive and provides a suitable platform for the growth and the proliferation of osteoblast cells. Moreover, the osteoblast cells attached to the cement with a normal morphology which is flattened (Figure. 27 A and B). In addition, the cells were able to penetrating in the cement through the pores of Bru-Alg . (Figure. 27 C and D).

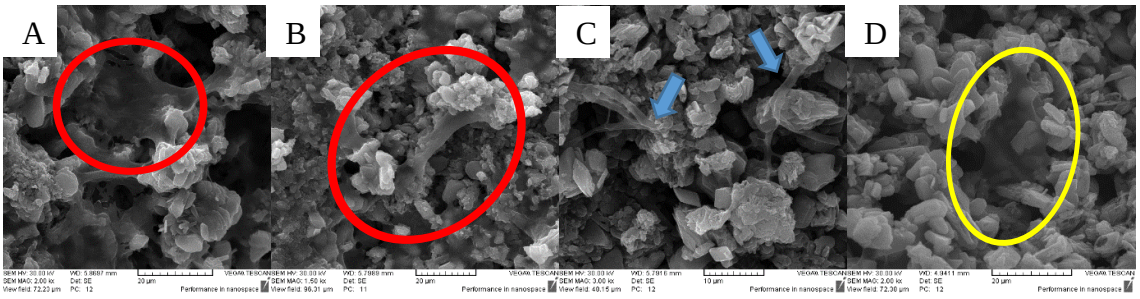

Figure 27. SEM micrograph of osteoblast cells seeded on Bru-Alg cement.

4.3.3 Characterization

- *Setting time*

One drawback of Bru cements is represented by the rapid setting time, which was reported to be 150 s [162], therefore sodium citrate tribasic monohydrate, in the concentration of 0.5 was introduced to the liquid phase as a setting retarding agent. This was based on the fact that citrate ions interacted with β-TCP component to restrict β-TCP dissolution and consequently postponed precipitation of Bru crystals [164]. In addition, P/L ratio is another important parameter for prolonging setting reaction so that lower P/L

would result in a slower setting reaction. The P/L ≈ 3 was proposed as the best ratio for Bru cement [162]. The final setting times of the different cement formulations are listed in Table. 8. As we can see, the retarding agent significantly increased the setting time of Bru, which is in a good agreement with a previous study [165]. Besides, incorporation of Alg in the solid phase yielded in a longer setting time which is due to the inhibition effect of Alg on Bru forming reaction, as reported by Chen et al [166]. Moreover, it was reported [167] that incorporation of Alg would cause a chemical reaction between Alg and the cement which possibly results in the Alg gelation, according to the below reaction, and in the postponed precipitation of Bru cement:

$$2C_5H_7O_4COONa + Ca^{2+} \longrightarrow (C_5H_7O_4COO)_2Ca + 2Na^{+}$$

Furthermore, it was demonstrated that [168] sulfate ions, arising from Gen, prolonged the setting of Bru crystals at least at low Gen percentage contents. This was also observed for our samples, so that the cement with 5% Gen in liquid phase was set after 38 minutes. However, the comparison between Nr-Bru-Alg-GL 5 and Bru-Alg-GL 5 revealed that sodium citrate was the main responsible for prolonging the setting time. Moreover, the results showed that incorporation of Gen in solid phase led to longer setting time than in liquid phase, except for Bru-Alg-GS 2, which had the highest Gen concentration considering P/L=3. This could be due to the formation of calcium sulfate dehydrated crystals, which acted as the nucleation sites for Bru formation [168].

Table 8. different formulation of loaded cements and their setting time

Item	Name	Alginate Concentration (wt %)	Gentamicin concentration (wt %)	Na_3C6H5O_7 (M)	Setting Time (min)
1	Bru	0	0	0.5	19.1±1.0
2	Bru-Alg	1	0	0.5	22.5±1.1
3	Bru-GL 2	0	2	0.5	22.3±0.9
4	Bru-Alg-GL* 1	1	1	0.5	24.3±0.8
5	Bru-Alg-GL 2	1	2	0.5	25.8±1.2
6	Bru-Alg-GL 5	1	5	0.5	37.5.1±1.2
6	Nr**-Bru-Alg-GL 5	1	5	0	3.3±0.4
8	Bru-GS*** 2	1	2	0.5	28.8±0.6
9	Bru-Alg-GS 1	1	1	0.5	31.3±0.9
10	Bru-Alg-GS 2	1	1	0.5	34.1±1.0

***Gen dissolved in liquid phase, ** no retardant was used, *** Gen powder incorporated in solid phase**

- *FTIR*

Figure. 28A presents FTIR spectra of Gen loaded cements Alg-bru-GS 2 and Alg-bru-GL 5 which were compared to the spectra of reference materials such as Alg-Bru and Gen. The spectra of the composite materials showed features typical of the main components, as the two doublet O-H stretching bands detected in the high frequency region (3116, 3288, 3489, and 3539 cm-1) due to two crystallization water molecules of Bru [100], whose corresponding H-O-H bending mode appeared at 1641 cm-1 [101]. The bands observed at 1134, 1061, and 985 cm-1 are due to P-O stretching mode of phosphate group [100, 169]. In addition, the corresponding peaks of P-O-H stretching mode and P-OH bending mode were detected at 1209 and 876 cm-1 [101]. The bands in the low frequency region, namely at 525, 577 and 661 cm-1, were arising from P-O deformation mode of phosphate group [169]. The spectra of Bru-Alg and pure Bru were almost identical. This was indeed due to overlapping the characteristics peaks of Alg in

the 1000-1200 cm-1 region [99] with those of phosphate group. Besides, the concentration of Alg in Bru matrix was negligible. The weak bands due to the Gen sulfate molecule can be better evidenced in the subtraction spectra [Bru-Alg-GL 5] – [Bru-Alg] and [Bru-Alg-GS 2] – [Bru-Alg] (Figure. 28B). Two broad bands centred at 3400 and above 3000 cm-1 are assigned to OH and NH stretching modes of the alcohol and amine groups in Gen, partially overlapped with band due to OH stretching modes of the adsorbed water vapor. The band at 1510 cm-1 is related to N-H bending mode. The sulfate group is characterized by a strong and complex absorption in the region 1100-1000 cm-1 together with a sharp band at 619 cm-1 which corresponds to vibrational bending mode of S-O [170, 171]. The complexity of the former absorption is due to the superimposition of sulfate absorption with CO/CC/CN stretching modes, too. Amine salts should give rise to multiple broad IR absorption in the region 2700-2300 cm-1 due to combination bands, which can also be detected in our spectra, suggesting that at least a fraction of Gen is present as cationic salt in the final cement formulation [172]. It is noteworthy that some shifts were observed specially at high frequency regions in loaded sample suggesting some specific interaction of Gem with such a complex matrix. The overall intensity of the bands was enhanced in the case of the sample prepared with the drug dissolved into liquid phase. This effect pointed out a better loading outcome for this preparation method (Figure. 28B).

3.3.3. XRD

Figure. 28C presents the XRD spectra of Bru, Bru-Alg, Gen, Bru-Alg-GS 2, and Bru-Alg-GL 5 which were compared to Bru standard JCPDS card (09-0077). The XRD

results confirmed the formation of Bru cement in all formulations. In addition, some residual β-TCP was observed in the unloaded cement formulation. The XRD spectra did not remarkably change as a result of Gen incorporation, except for the disappearance of β-TCP peak at 2Θ = 26.7. The main difference between Gen loaded cement spectra and the reference one is the increased relative intensity of several peaks within the 2Θ range of 30-50 in the case of solid incorporation. Moreover, it has been reported [168] that loading Gen into CPC may lead to the formation of gypsum (CaSO4.2H2O). Yet, it is not possible to assure that this compound was formed within the cement due to similar crystallographic structure between gypsum and Bru.

The mean crystalline size of loaded and unloaded cements was calculated using the diffraction pattern of (020), (021), (041), (-221), and (220) crystalline planes. The results showed that the calculated mean crystalline size for Bru, Bru-Alg, Bru-Alg-GL 5, Bru-Alg-GS 2 were 92.4 ± 29.2, 107.1 ± 35.8, 92.4 ± 30.8, and 61.2 ± 36.6 nm, respectively. As we can see incorporation of Alg yielded to increase the crystalline size of the cement while, addition of Gen decreased the crystalline size so that the smallest one belonged to Bru-Alg-GS 2 which had the highest content of Gen.

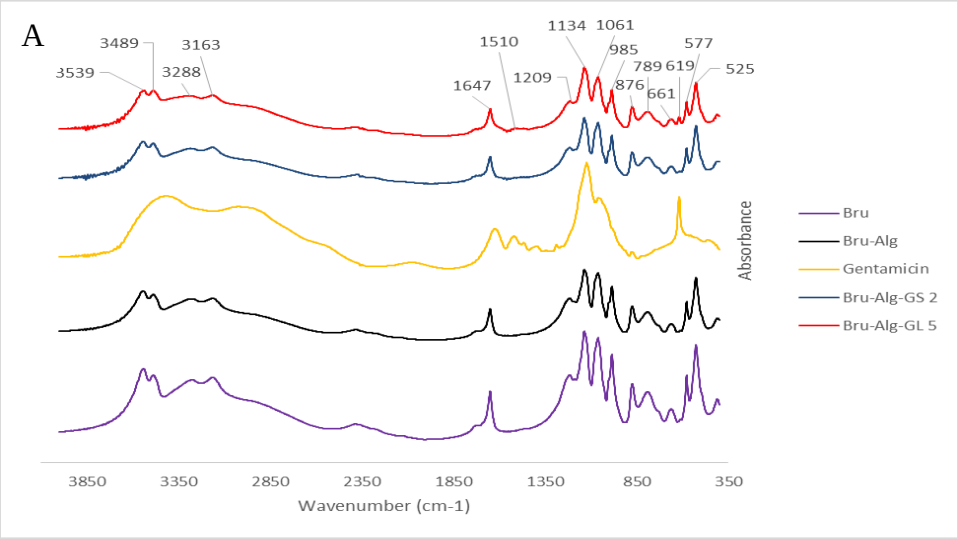
A
3539
3489
3288
3163
1647
1510
1209
1134
1061
985
876
789
661
619
577
525
Absorbance
Bru
Bru-Alg
Gentamicin
Bru-Alg-GS 2
Bru-Alg-GL 5
3850
3350
2850
2350
1850
1350
850
350
Wavenumber (cm-1)

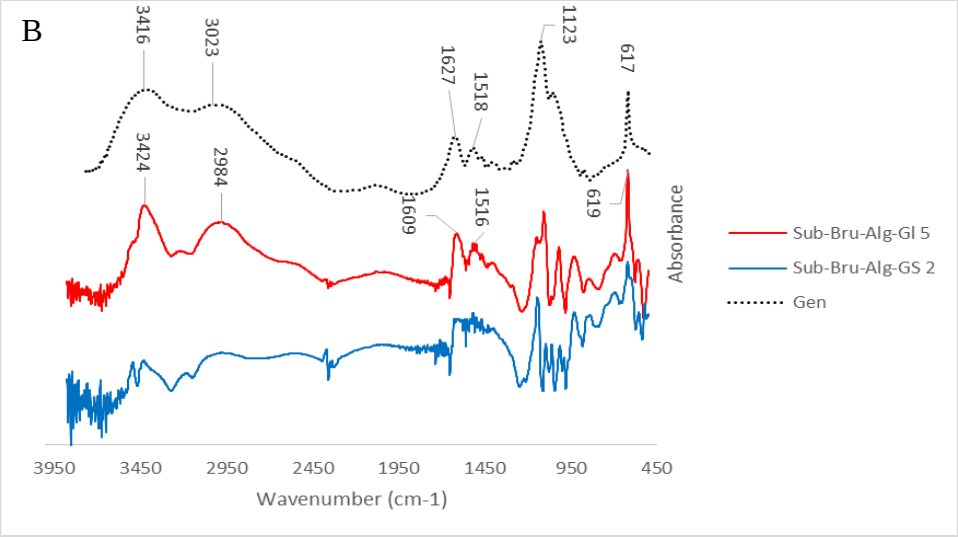
B
3416
3424
3023
2984
1627
1609
1518
1516
1123
619
617
Absorbance
Sub-Bru-Alg-Gl 5
Sub-Bru-Alg-GS 2
Gen
3950
3450
2950
2450
1950
1450
950
450
Wavenumber (cm-1)

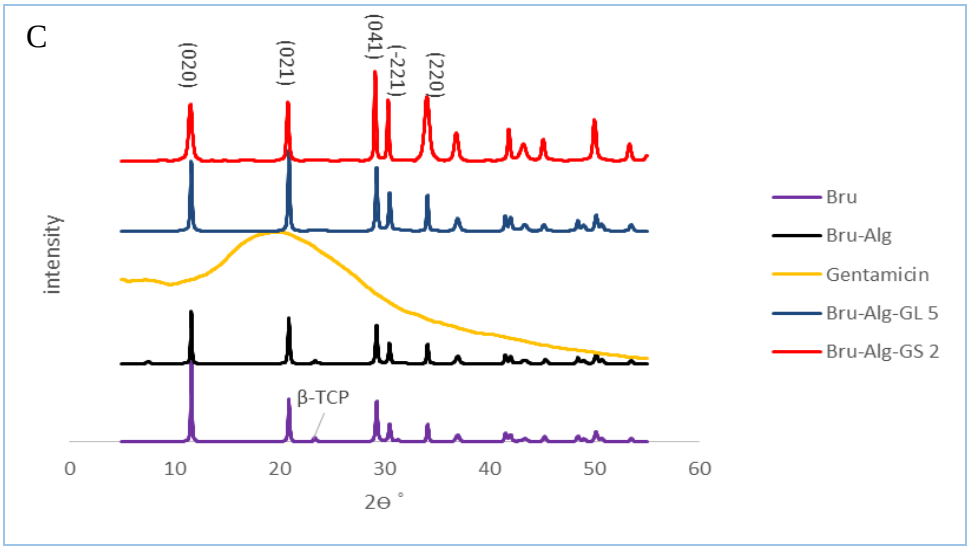

Figure 28. A) FTIR spectra of loaded cements along with the reference materials B) FT IR Subtraction spectra of loaded cements in comparison with spectrum of pure solid Gen. C) XRD spectra of loaded cements and the reference materials.

- *Thermal analysis*

Thermal behavior and stability of loaded and unloaded cement were evaluated by TGA, DTG, and DTA. A continuous weight loss was observed within the range of 50-650 ˚C for both loaded and unloaded cements, which were 24% and 23.5 %, respectively (Figure. 29A). The difference between the two curves is not significant and the main weight loss corresponds to transformation of Bru into monetite (90-140 ˚C, 16%) and monetite into calcium pyrophosphate (280-420 ˚C, 5.5%) [127, 128]. Therefore, the impact of Gen addition on the TGA results is not significant. As we can see in the Figure. 29B, the DTA results indicated two and three endothermic peaks for unloaded and loaded cements respectively. The first endothermic peaks related to dehydration of Bru and formation of monetite at 116 ˚C for both samples. The second endothermic peak for Bru-

Alg cements appeared at 310°C, which was due to calcium pyrophosphate formation. The Gen loaded cement possesses two small endothermic peaks at 312 and 401 ˚C, corresponding to transformation of monetite and melting of Gen respectively. Figure. 29C presents the DTG spectra of Alg-Bru, and Gen as reference materials and Gen loaded cement. It is observable that the range of 70-170°C is the main region in which both cements mainly lost their weight. The similarity between the DTG results of loaded cement with that of unloaded one suggests that similar decomposition steps occurred in both of them. Yet, it is logic to state that loaded cement presented more stable crystalline structure due to slight shift to a higher temperature in the obtained DTA and DTG spectra.

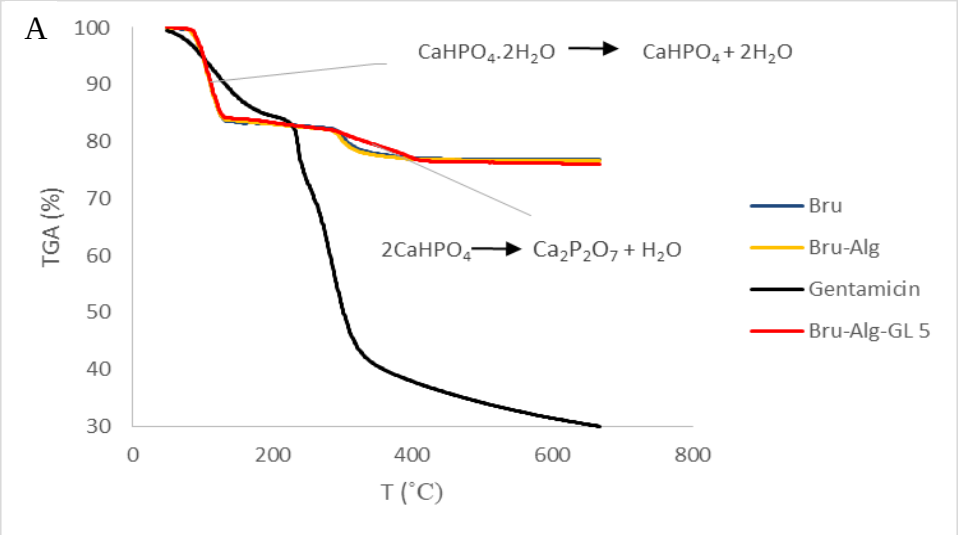

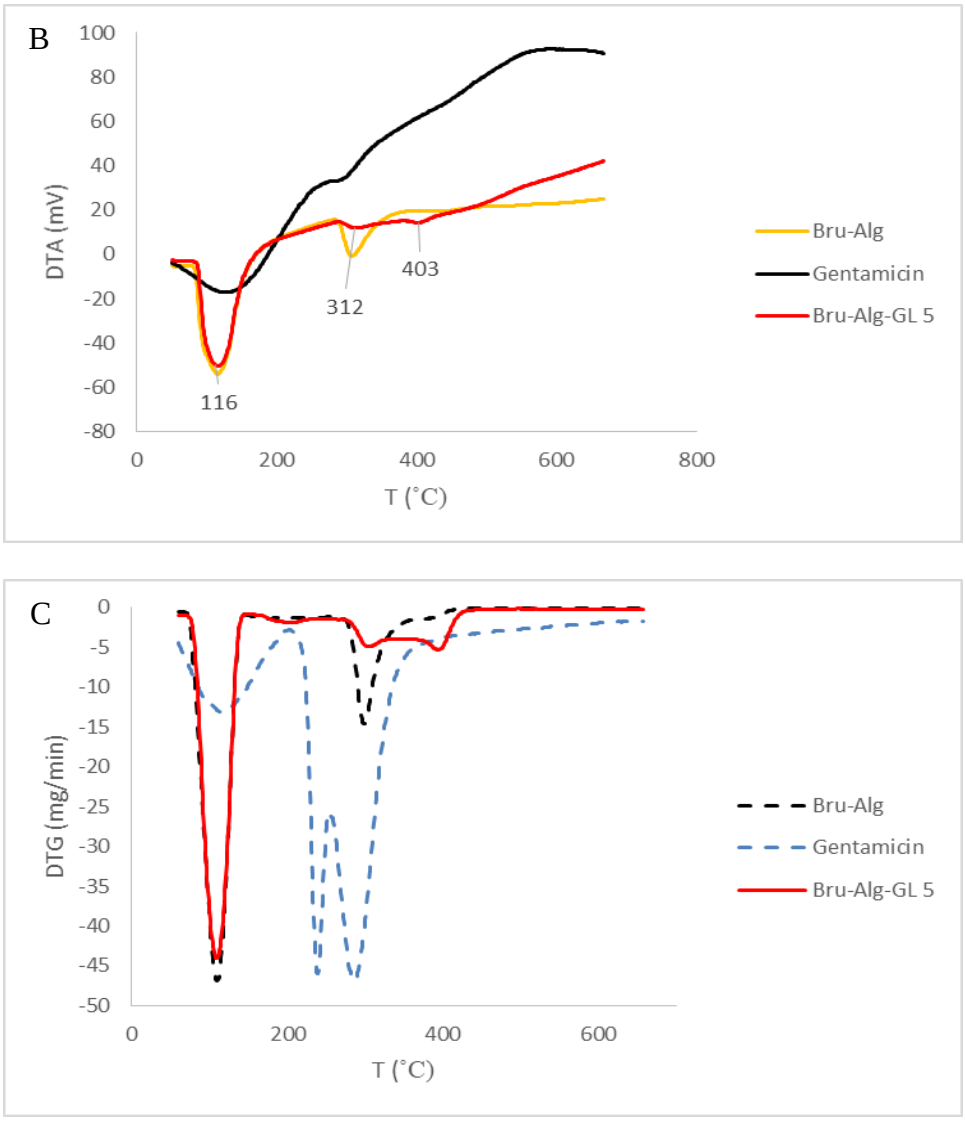

Figure 29. A)TG, B)DTA, and C)DTG spectra of Gen, Bru-Alg, and Bru-Alg-GL 5

- *Morphology study*

Fracture surface of Bru and Bru-Alg cements after compression test were used to take SEM images and conduct microstructure study. As shown in Figure. 30A, 30B, and 30C Bru cements had a heterogeneous structure composed of large plate and fine needle like crystals which were accumulated in multilayers. Similar results were obtained in a

previous work conducted by Cama et al. with the same fabrication technique [165]. In contrast, incorporation of Alg into the cement led to formation of petal like crystals along with fine plate like structures (Figure. 30D, 30E, and 30F).

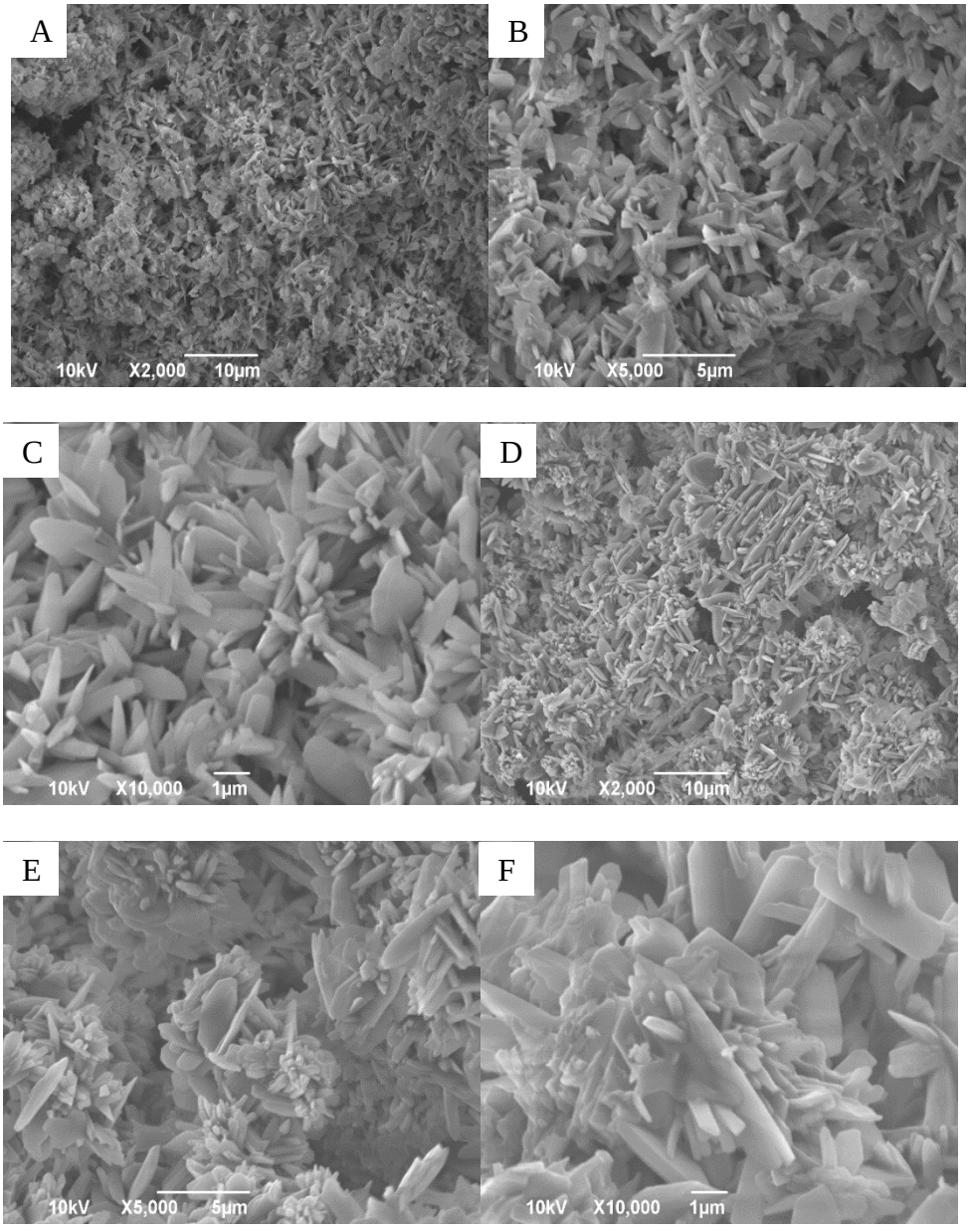

Figure 30. SEM images taken from fracture surface of A-C) Bru and E-F) Bru-Alg at the magnification of 2000, 5000, and 10000

4.3.4 Soaking in phosphate buffer saline

Figure. 31A shows the FTIR spectra of Bru-Alg-GL 5, recorded to investigate chemical changes following soaking in PBS. The obtained spectra contained all the characteristics peaks of Bru after different time intervals and no significant difference was observed in the typical bands of Bru matrix. The results indicated the chemical stability of the cements within the soaking time. The DTS results, after soaking the samples in PBS, are reported in Figure. 31B. As we can see incorporation of Gen resulted in DTS improvement which is related to decrease in crystalline size of Bru as stated by Bohner et al [168] and observed in XRD results. The results indicated that in all samples an increase in DTS, within the soaking time of 1 to 7 days, was followed by a sharp decrease for the remaining time of immersion. For instance, the primary strength of 1.66 MPa for Bru-ALg-GL 2 increased to 1.81 MPa within 7 days of soaking in PBS. This can be attributed to crystal growth, as evidenced by SEM, and further hardening of Bru by allowing setting reaction to continue. Therefore, the small pores were reduced and an interlocked crystal structure was achieved [165, 173, 174]. Then, 0.27 and 0.61 Mpa declines in DTS were noticeable after 14 and 30 days, respectively. Dissolution of Bru, as well as leaching of Alg and Gen, were the main reasons for the observed diminish in DTS results [166].

Figure. 31C-F illustrates the SEM images taken from fracture surface of the Bru-Alg-GL 5 cement after 1 and 30 days of in-vitro soaking. The comparison between

samples with different aging time revealed that heterogeneous crystals after one day (Figure. 31C and 31D) of soaking transformed to homogeneous plate like crystals at the end of 30 days. In addition, the results indicated that Bru crystal grew as a result of in-vitro soaking so that an increase was observable in the Bru crystals dimensions (Figure. 31E and 31F).

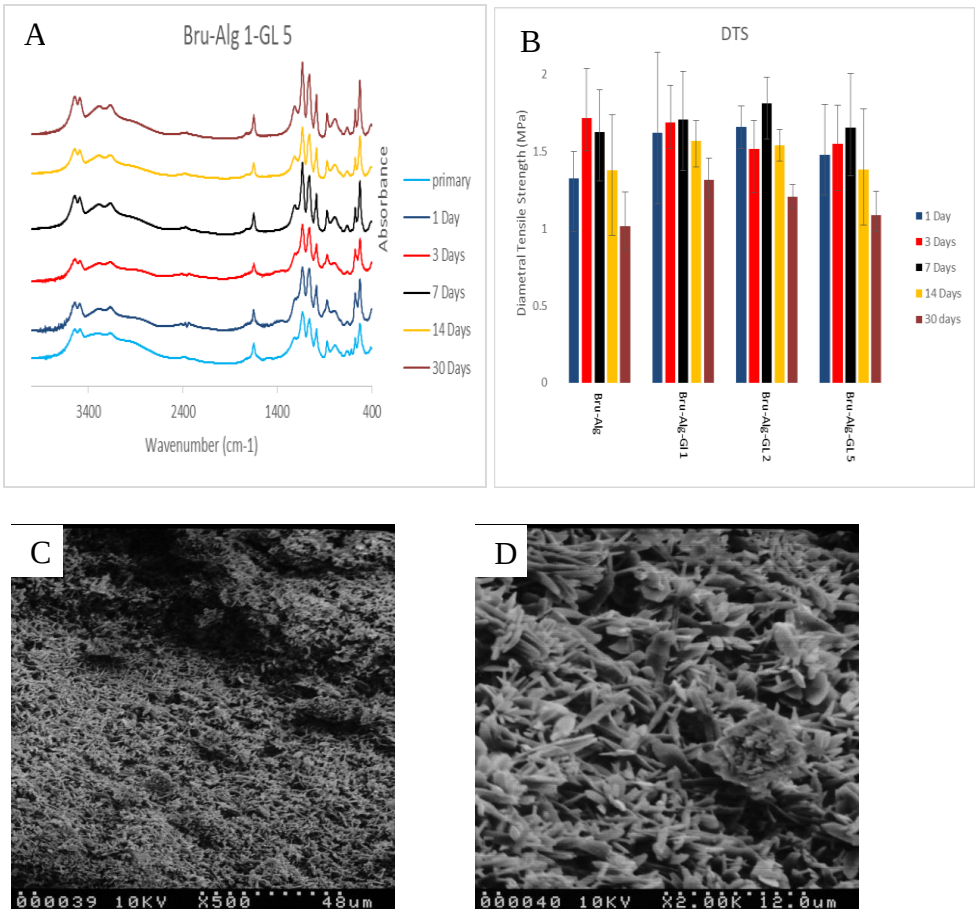

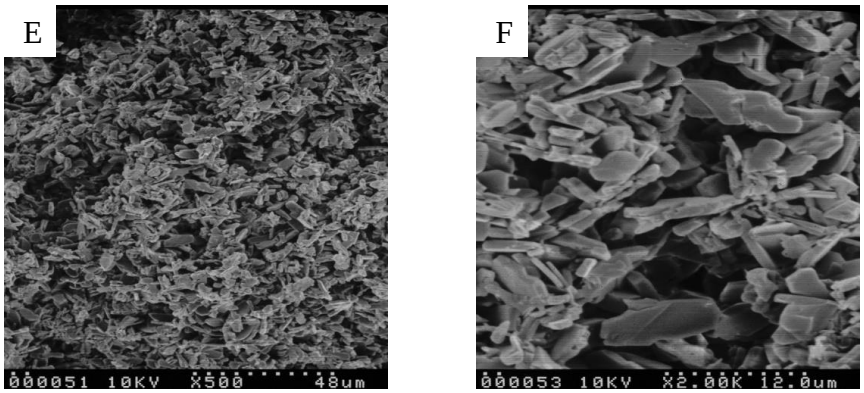

Figure 31. A) FTIR spectra of Bru-Alg-GL 2 cement different soaking time B) 9 Diametrical tensile strength (DTS) results of different cements after various soaking time in PBS C-F) SEM micrographs taken from fracture surface of Bru-Alg-GL 5 after 1 day at 500× (C) , 2000× (D) and 30 days at 500× (E) and 2000× (F)

4.3.5 Drug release

The in-vitro Gen release by the Bru cement was evaluated compared to: addition of Alg, content of drug, method of drug incorporation. The error bars are not presented in the figures to avoid overlapping: the obtained standard deviation of triplicate repeat was lower than 5%. Figure. 32A shows the Gen release profile from different cement formulation when the drug was dissolved in the liquid phase in the preparation step. The release profile can be summarized into three phases: primary release, secondary release, and plateau level over 14 days. The primary burst release falls into the range of 37.9 ± 2.2 to 58.5± 3.4% after 24 h for Bru-Alg-1GL and Bru-Alg-2GL, respectively. This significant initial increase in the released drug level was related to the part of drug that was physically entrapped by the cement. In addition, high solubility of Gen in PBS is another significant reason for the primary burst release [175]. Correspondingly, the band corresponding to the vibrational bending mode of S-O at 619 cm-1 almost disappeared

after 24 hours of incubation in PBS as shown by Figure. 31A confirming the initial burst of Gen after 24 h. This was followed by the secondary burst release with lower rate from 24h to 144h and it was noticeable that an increase in the initial concentration of Gen resulted in a greater drug release within this period of time. The third phase started after one week of release experiment where all the release profile almost followed a period of stability. The results indicated that Bru cement released almost 91.5% ± 4.9 % of the loaded Gen after 2 weeks, while Bru-Alg with similar concentration of drug reached to the level of 86.5 ± 4.5 % and further decrease to less than 80% of fractional released was observed in Bru-Alg-GL 1. The results revealed that addition of Alg had a positive effect on the release profile especially in the first and second phase of release, this can be due to selective interaction of Gen with mannuronic residues of Alg [176]. Singh et al [177] stated that Gen is a cationic drug with a positive net charge in physiological conditions which stablishes electrostatic interaction with COO- of Alg mannuronic blocks. Since Alg was incorporated at a low concentration (1%), the cement with the lowest concentration of drug had the strongest electrostatic interactions. Similar release profiles were obtained when Gen was incorporated into solid phase of the cement. Yet, for all the cement formulations, Gen release profiles showed an increase in the fractional release so that almost all of the loaded drug was released in PBS (Figure. 32B). This can be attribute to a less uniform distribution of drug and consequently a lowered interaction with the cement materials. Furthermore, addition of Alg to the cement negatively influenced the release profile in the way that the lowest release rate achieved in Bru-2GenS with 93.6 ± 3.9 %.

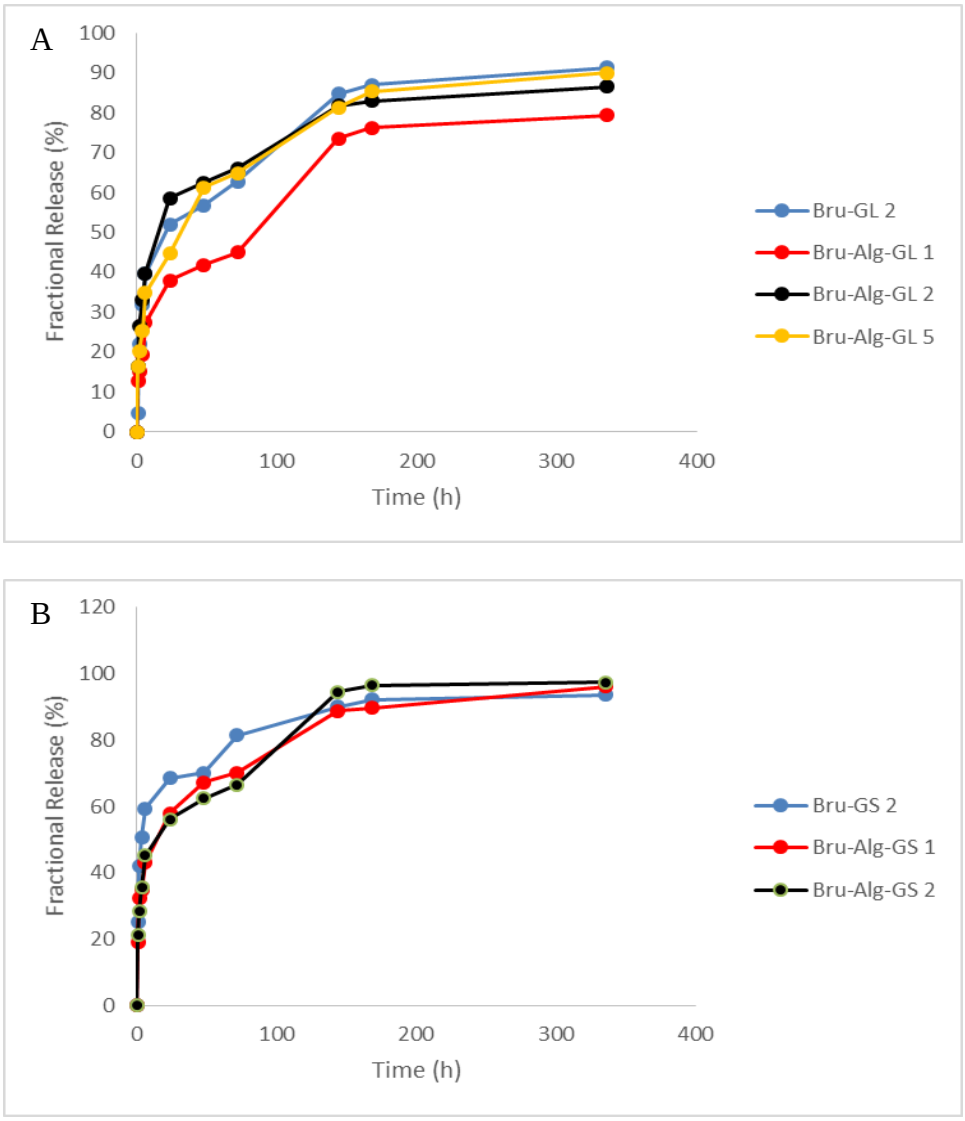

Figure 32. Cumulative Gen release by different cement formulations as Gen A) dissolved in liquid phase and B) incorporated in solid phase

4.4 Conclusion

The present study focused on functionalizing Bru cement through incorporation of Alg in order to improve mechanical and biological characteristics as well as to control

Gen release from this bone cement. The primary results indicated that adding 1 wt% Alg to the solid phase of cement improved both mechanical and biological performance. In addition, the cement is a viable platform for cells to attach with a normal morphology and penetrate inside the cement structure. Using Gen in the form of solution during the cement preparation step yielded to a more efficient drug loading than using Gen in form of powder. Moreover, addition of Gen to the Bru-Alg cement enhanced crystalline stability and mechanical properties as shown by thermal analysis and diametrical tensile test. Although both Gen and Alg prolonged the setting time, the retarding agent played the major role in extending setting time. The soaking experiment in PBS medium revealed that the cements chemically and mechanically remained almost stable during soaking time. Finally, Alg component exhibit a positive effect on the release behavior when Gen was dissolved in liquid phase at low concentrations so that more than 10% decrease was observed in the fractional release. These results indicate the positive effect of Alg on Bru cement mechanical, biological, structural and antibiotic release behaviors.

CHAPTER 5 : Conclusion

The first part of the present thesis discus about in-situ synthetization of Alginate-brushite hydrogel composite. Initial pH of solutions and primary concentration of phosphate precursors were chosen as the variables to obtain the optimum conditions and the following results were obtained:

- Alginate-brushite hydrogel composites were obtained through an in-situ process
- The brushite crystals started forming at initial pH value of 6
- The interaction between brushite crystals and alginate matrix was weak
- The increase in the initial concentration of phosphate precursor resulted in more crystalline structure
- Samples prepared at pH value of 8 had the most stable crystalline structure
- Brushite crystals promoted the biocompatibility of alginate

In the second part, the release of ibuprofen from the hydrogel composite fabricated in the first part was taken into consideration. The impact of brushite on the morphology, mechanical properties and swelling behavior along with drug-carrier interaction were deeply investigated. The bellow outcomes were concluded from this part:

- Ibuprofen was loaded on the in-situ synthetized alginate-brushite hydrogel beads.
- Transformation of Na-ibuprofen to its acidic form occurred within the loading procedure.
- The brushite within alginate matrix improved mechanical properties
- The brushite crystals restricted swelling behavior of alginate

- Less crosslinked beads obtained as the concentration of (NH4)2HPO4 reached to 0.4M.
- The hydrogel composite beads released ibuprofen in a controlled manner.

The final part was aimed to improve mechanical properties of brushite cement and modify gentamicin sulfate release from brushite cement by adding alginate to the matrix. Following outcomes were obtained at the end of this part:

- Addition of Alginate up to 1% improved mechanical and biological performance of the cement.
- Morphology of brushite changed from plate and needle like to petal like as Alginate was added to the cement.
- Alginate, gentamicin sulfate, and sodium citrate tribasic remarkably prolonged the setting time.
- Dissolving gentamicin sulfate in the liquid phase yielded to better loading conditions.
- The cement present adequate mechanical and chemical stability during soaking time
- Adding alginate significantly improved release profile of gentamicin sulfate when gentamicin sulfate was dissolved in liquid phase at low concentration

Bibliography

[1] S.N. Pawar, K.J. Edgar, Alginate derivatization: a review of chemistry, properties and applications, Biomaterials 33(11) (2012) 3279-3305.
[2] G.O. Phillips, P.A. Williams, Handbook of hydrocolloids, Elsevier2009.
[3] K.Y. Lee, D.J. Mooney, Alginate: properties and biomedical applications, Progress in polymer science 37(1) (2012) 106-126.
[4] P. Sikorski, F. Mo, G. Skjåk-Bræk, B.T. Stokke, Evidence for egg-box-compatible interactions in calcium− alginate gels from fiber X-ray diffraction, Biomacromolecules 8(7) (2007) 2098-2103.
[5] E. Torres, Y. Mata, M. Blazquez, J. Munoz, F. Gonzalez, A. Ballester, Gold and silver uptake and nanoprecipitation on calcium alginate beads, Langmuir 21(17) (2005) 7951-7958.
[6] I. Donati, S. Holtan, Y.A. Mørch, M. Borgogna, M. Dentini, G. Skjåk-Bræk, New hypothesis on the role of alternating sequences in calcium− alginate gels, Biomacromolecules 6(2) (2005) 1031-1040.
[7] Ý.A. Mørch, I. Donati, B.L. Strand, G. Skjåk-Bræk, Effect of Ca2+, Ba2+, and Sr2+ on alginate microbeads, Biomacromolecules 7(5) (2006) 1471-1480.
[8] S.N. Pawar, K.J. Edgar, Chemical modification of alginates in organic solvent systems, Biomacromolecules 12(11) (2011) 4095-4103.
[9] K. Draget, G.S. Bræk, O. Smidsrød, Alginic acid gels: the effect of alginate chemical composition and molecular weight, Carbohydrate Polymers 25(1) (1994) 31-38.
[10] G.T. Grant, E.R. Morris, D.A. Rees, P.J. Smith, D. Thom, Biological interactions between polysaccharides and divalent cations: the egg-box model, FEBS letters 32(1) (1973) 195-198.
[11] D. Queen, H. Orsted, H. Sanada, G. Sussman, A dressing history, International wound journal 1(1) (2004) 59-77.
[12] B. Balakrishnan, M. Mohanty, A.C. Fernandez, P.V. Mohanan, A. Jayakrishnan, Evaluation of the effect of incorporation of dibutyryl cyclic adenosine monophosphate in an in situ-forming hydrogel wound dressing based on oxidized alginate and gelatin, Biomaterials 27(8) (2006) 1355-1361.
[13] S.Y. Rabbany, J. Pastore, M. Yamamoto, T. Miller, S. Rafii, R. Aras, M. Penn, Continuous delivery of stromal cell-derived factor-1 from alginate scaffolds accelerates wound healing, Cell transplantation 19(4) (2010) 399-408.
[14] C. Wiegand, T. Heinze, U.C. Hipler, Comparative in vitro study on cytotoxicity, antimicrobial activity, and binding capacity for pathophysiological factors in chronic wounds of alginate and silver-containing alginate, Wound repair and regeneration 17(4) (2009) 511-521.
[15] A.B. Lansdown, U. Mirastschijski, N. Stubbs, E. Scanlon, M.S. Ågren, Zinc in wound healing: theoretical, experimental, and clinical aspects, Wound Repair and Regeneration 15(1) (2007) 2-16.
[16] T. Boontheekul, H.-J. Kong, D.J. Mooney, Controlling alginate gel degradation utilizing partial oxidation and bimodal molecular weight distribution, Biomaterials 26(15) (2005) 2455-2465.
[17] J. Wang, C. Liu, Y. Shuai, X. Cui, L. Nie, Controlled release of anticancer drug using graphene oxide as a drug-binding effector in konjac glucomannan/sodium alginate hydrogels, Colloids and Surfaces B: Biointerfaces 113 (2014) 223-229.
[18] A. Morelli, D. Puppi, F. Chiellini, Polymers from renewable resources, Journal of Renewable Materials 1(2) (2013) 83-112.
[19] K.H. Bouhadir, E. Alsberg, D.J. Mooney, Hydrogels for combination delivery of antineoplastic agents, Biomaterials 22(19) (2001) 2625-2633.

[20] R.M. Lucinda-Silva, H.R.N. Salgado, R.C. Evangelista, Alginate–chitosan systems: in vitro controlled release of triamcinolone and in vivo gastrointestinal transit, Carbohydrate polymers 81(2) (2010) 260-268.
[21] E.A. Silva, D.J. Mooney, Effects of VEGF temporal and spatial presentation on angiogenesis, Biomaterials 31(6) (2010) 1235-1241.
[22] H.J. Kong, E.S. Kim, Y.-C. Huang, D.J. Mooney, Design of biodegradable hydrogel for the local and sustained delivery of angiogenic plasmid DNA, Pharmaceutical research 25(5) (2008) 1230-1238.
[23] O.A. Ali, D.J. Mooney, Sustained GM-CSF and PEI condensed pDNA presentation increases the level and duration of gene expression in dendritic cells, Journal of Controlled Release 132(3) (2008) 273-278.
[24] C.-H. Chang, Y.-H. Lin, C.-L. Yeh, Y.-C. Chen, S.-F. Chiou, Y.-M. Hsu, Y.-S. Chen, C.-C. Wang, Nanoparticles incorporated in pH-sensitive hydrogels as amoxicillin delivery for eradication of Helicobacter pylori, Biomacromolecules 11(1) (2009) 133-142.
[25] F. Gu, B. Amsden, R. Neufeld, Sustained delivery of vascular endothelial growth factor with alginate beads, Journal of Controlled Release 96(3) (2004) 463-472.
[26] L. Cao, D.J. Mooney, Spatiotemporal control over growth factor signaling for therapeutic neovascularization, Advanced drug delivery reviews 59(13) (2007) 1340-1350.
[27] S.M. Jay, W.M. Saltzman, Controlled delivery of VEGF via modulation of alginate microparticle ionic crosslinking, Journal of Controlled Release 134(1) (2009) 26-34.
[28] K.Y. Lee, M.C. Peters, D.J. Mooney, Comparison of vascular endothelial growth factor and basic fibroblast growth factor on angiogenesis in SCID mice, Journal of controlled release 87(1) (2003) 49-56.
[29] Q. Sun, E.A. Silva, A. Wang, J.C. Fritton, D.J. Mooney, M.B. Schaffler, P.M. Grossman, S. Rajagopalan, Sustained release of multiple growth factors from injectable polymeric system as a novel therapeutic approach towards angiogenesis, Pharmaceutical research 27(2) (2010) 264-271.
[30] X. Hao, E.A. Silva, A. Månsson-Broberg, K.-H. Grinnemo, A.J. Siddiqui, G. Dellgren, E. Wärdell, L.Å. Brodin, D.J. Mooney, C. Sylvén, Angiogenic effects of sequential release of VEGF-A165 and PDGF-BB with alginate hydrogels after myocardial infarction, Cardiovascular research 75(1) (2007) 178-185.
[31] M.C. Peters, P.J. Polverini, D.J. Mooney, Engineering vascular networks in porous polymer matrices, Journal of Biomedical Materials Research Part A 60(4) (2002) 668-678.
[32] S.M. Jay, B.R. Shepherd, J.W. Andrejecsk, T.R. Kyriakides, J.S. Pober, W.M. Saltzman, Dual delivery of VEGF and MCP-1 to support endothelial cell transplantation for therapeutic vascularization, Biomaterials 31(11) (2010) 3054-3062.
[33] Y.M. Kolambkar, K.M. Dupont, J.D. Boerckel, N. Huebsch, D.J. Mooney, D.W. Hutmacher, R.E. Guldberg, An alginate-based hybrid system for growth factor delivery in the functional repair of large bone defects, Biomaterials 32(1) (2011) 65-74.
[34] Y. Lópiz-Morales, A. Abarrategi, V. Ramos, C. Moreno-Vicente, L. López-Durán, J.L. López-Lacomba, F. Marco, In vivo comparison of the effects of rhBMP-2 and rhBMP-4 in osteochondral tissue regeneration, Eur Cell Mater 20(367) (2010) e78.
[35] M.D. Krebs, E. Salter, E. Chen, K.A. Sutter, E. Alsberg, Calcium phosphate-DNA nanoparticle gene delivery from alginate hydrogels induces in vivo osteogenesis, Journal of Biomedical Materials Research Part A 92(3) (2010) 1131-1138.
[36] F.B. Basmanav, G.T. Kose, V. Hasirci, Sequential growth factor delivery from complexed microspheres for bone tissue engineering, Biomaterials 29(31) (2008) 4195-4204.
[37] J.M. Kanczler, P.J. Ginty, L. White, N.M. Clarke, S.M. Howdle, K.M. Shakesheff, R.O. Oreffo, The effect of the delivery of vascular endothelial growth factor and bone morphogenic

protein-2 to osteoprogenitor cell populations on bone formation, Biomaterials 31(6) (2010) 1242-1250.
[38] H.R. Lin, Y.J. Yeh, Porous alginate/hydroxyapatite composite scaffolds for bone tissue engineering: preparation, characterization, and in vitro studies, Journal of Biomedical Materials Research Part B: Applied Biomaterials 71(1) (2004) 52-65.
[39] M.D. Weir, H.H. Xu, C.G. Simon, Strong calcium phosphate cement-chitosan-mesh construct containing cell-encapsulating hydrogel beads for bone tissue engineering, Journal of Biomedical Materials Research Part A 77(3) (2006) 487-496.
[40] M. Lawson, J. Barralet, L. Wang, R. Shelton, J.T. Triffitt, Adhesion and growth of bone marrow stromal cells on modified alginate hydrogels, Tissue engineering 10(9-10) (2004) 1480-1491.
[41] S.C. Chang, J.A. Rowley, G. Tobias, N.G. Genes, A.K. Roy, D.J. Mooney, C.A. Vacanti, L.J. Bonassar, Injection molding of chondrocyte/alginate constructs in the shape of facial implants, Journal of Biomedical Materials Research Part A 55(4) (2001) 503-511.
[42] S.C. Chang, G. Tobias, A.K. Roy, C.A. Vacanti, L.J. Bonassar, Tissue engineering of autologous cartilage for craniofacial reconstruction by injection molding, Plastic and reconstructive surgery 112(3) (2003) 793-799.
[43] F. Guilak, D.M. Cohen, B.T. Estes, J.M. Gimble, W. Liedtke, C.S. Chen, Control of stem cell fate by physical interactions with the extracellular matrix, Cell stem cell 5(1) (2009) 17-26.
[44] H. Dashtdar, H.A. Rothan, T. Tay, R.E. Ahmad, R. Ali, L.X. Tay, P.P. Chong, T. Kamarul, A preliminary study comparing the use of allogenic chondrogenic pre-differentiated and undifferentiated mesenchymal stem cells for the repair of full thickness articular cartilage defects in rabbits, Journal of Orthopaedic Research 29(9) (2011) 1336-1342.
[45] R.S. Tuan, G. Boland, R. Tuli, Adult mesenchymal stem cells and cell-based tissue engineering, Arthritis Res Ther 5(1) (2002) 32.
[46] A.A. Mirtchi, J. Lemaître, E. Hunting, Calcium phosphate cements: action of setting regulators on the properties of the β-tricalcium phosphate-monocalcium phosphate cements, Biomaterials 10(9) (1989) 634-638.
[47] K. Lilley, U. Gbureck, A. Wright, D. Farrar, J. Barralet, Cement from nanocrystalline hydroxyapatite: effect of calcium phosphate ratio, Journal of Materials Science: materials in medicine 16(12) (2005) 1185-1190.
[48] F. Tamimi, Z. Sheikh, J. Barralet, Dicalcium phosphate cements: Brushite and monetite, Acta biomaterialia 8(2) (2012) 474-487.
[49] F.T. Mariño, J. Torres, M. Hamdan, C.R. Rodríguez, E.L. Cabarcos, Advantages of using glycolic acid as a retardant in a brushite forming cement, Journal of Biomedical Materials Research Part B: Applied Biomaterials 83(2) (2007) 571-579.
[50] M. Bohner, J. Lemaitre, T.A. Ring, Effects of sulfate, pyrophosphate, and citrate ions on the physicochemical properties of cements made of β-tricalcium phosphate-phosphoric acid-water mixtures, Journal of the American Ceramic Society 79(6) (1996) 1427-1434.
[51] M.H. Alkhraisat, C. Rueda, L.B. Jerez, F.T. Mariño, J. Torres, U. Gbureck, E.L. Cabarcos, Effect of silica gel on the cohesion, properties and biological performance of brushite cement, Acta biomaterialia 6(1) (2010) 257-265.
[52] M. Alkhraisat, C. Rueda, F. Marino, J. Torres, L. Jerez, U. Gbureck, E. Cabarcos, The effect of hyaluronic acid on brushite cement cohesion, Acta biomaterialia 5(8) (2009) 3150-3156.
[53] S. Chauhan, M. Hofmann, R. Shelton, Effect of protein addition on the setting behaviour of a calcium phosphate cement, Key Engineering Materials, Trans Tech Publ, 2006, pp. 841-844.
[54] M. Bohner, Calcium orthophosphates in medicine: from ceramics to calcium phosphate cements, Injury 31 (2000) D37-D47.

[55] M.H. Alkhraisat, F.T. Mariño, C.R. Rodríguez, L.B. Jerez, E.L. Cabarcos, Combined effect of strontium and pyrophosphate on the properties of brushite cements, Acta biomaterialia 4(3) (2008) 664-670.
[56] C. Ryf, S. Goldhahn, M. Radziejowski, M. Blauth, B. Hanson, A new injectable brushite cement: first results in distal radius and proximal tibia fractures, European Journal of Trauma and Emergency Surgery 35(4) (2009) 389-396.
[57] F. Theiss, D. Apelt, B. Brand, A. Kutter, K. Zlinszky, M. Bohner, S. Matter, C. Frei, J.A. Auer, B. Von Rechenberg, Biocompatibility and resorption of a brushite calcium phosphate cement, Biomaterials 26(21) (2005) 4383-4394.
[58] J.Z. Paxton, K. Donnelly, R.P. Keatch, K. Baar, L.M. Grover, Factors affecting the longevity and strength in an in vitro model of the bone–ligament interface, Annals of biomedical engineering 38(6) (2010) 2155-2166.
[59] N. Mehrban, J.Z. Paxton, J. Bowen, A. Bolarinwa, E. Vorndran, U. Gbureck, L.M. Grover, Comparing physicochemical properties of printed and hand cast biocements designed for ligament replacement, Advances in Applied Ceramics 110(3) (2011) 162-167.
[60] P. Van Landuyt, B. Peter, L. Beluze, J. Lemaitre, Reinforcement of osteosynthesis screws with brushite cement, Bone 25(2) (1999) 95S-98S.
[61] P.F. Heini, U. Berlemann, M. Kaufmann, K. Lippuner, C. Fankhauser, P. van Landuyt, Augmentation of mechanical properties in osteoporotic vertebral bones-a biomechanical investigation of vertebroplasty efficacy with different bone cements, European Spine Journal 10(2) (2001) 164-171.
[62] J.M. Kuemmerle, A. Oberle, C. Oechslin, M. Bohner, C. Frei, I. Boecken, B. von Rechenberg, Assessment of the suitability of a new brushite calcium phosphate cement for cranioplasty–an experimental study in sheep, Journal of Cranio-Maxillofacial Surgery 33(1) (2005) 37-44.
[63] C. Ji, J.-G. Ahn, Clinical experience of the brushite calcium phosphate cement for the repair and augmentation of surgically induced cranial defects following the pterional craniotomy, Journal of Korean Neurosurgical Society 47(3) (2010) 180-184.
[64] U. Klammert, U. Gbureck, E. Vorndran, J. Rödiger, P. Meyer-Marcotty, A.C. Kübler, 3D powder printed calcium phosphate implants for reconstruction of cranial and maxillofacial defects, Journal of Cranio-Maxillofacial Surgery 38(8) (2010) 565-570.
[65] F. Tamimi, J. Torres, E. Lopez-Cabarcos, D.C. Bassett, P. Habibovic, E. Luceron, J.E. Barralet, Minimally invasive maxillofacial vertical bone augmentation using brushite based cements, Biomaterials 30(2) (2009) 208-216.
[66] F.T. Mariño, J. Torres, I. Tresguerres, L.B. Jerez, E.L. Cabarcos, Vertical bone augmentation with granulated brushite cement set in glycolic acid, Journal of Biomedical Materials Research Part A 81(1) (2007) 93-102.
[67] F.M. Tamimi, J. Torres, I. Tresguerres, C. Clemente, E. López-Cabarcos, L.J. Blanco, Bone augmentation in rabbit calvariae: comparative study between Bio-Oss® and a novel β-TCP/DCPD granulate, Journal of clinical periodontology 33(12) (2006) 922-928.
[68] M.-P. Ginebra, C. Canal, M. Espanol, D. Pastorino, E.B. Montufar, Calcium phosphate cements as drug delivery materials, Advanced drug delivery reviews 64(12) (2012) 1090-1110.
[69] G. Pasquier, J. Lemaitre, B. Flautre, M. Ikenaga, P. Hardouin, Development of a model which makes it possible to test injectable bone substitutes and evaluation of a calcium phosphate cement, Bulletin de l'Academie nationale de medecine 182(9) (1998) 1851-64; discussion 1865.
[70] C.-h. Hou, C.-w. Chen, S.-m. Hou, Y.-t. Li, F.-h. Lin, The fabrication and characterization of dicalcium phosphate dihydrate-modified magnetic nanoparticles and their performance in hyperthermia processes in vitro, Biomaterials 30(27) (2009) 4700-4707.

[71] M.S.-P. López, F. Tamimi, E. López-Cabarcos, B. López-Ruiz, Highly sensitive amperometric biosensor based on a biocompatible calcium phosphate cement, Biosensors and Bioelectronics 24(8) (2009) 2574-2579.
[72] A.S. Hoffman, Hydrogels for biomedical applications, Advanced drug delivery reviews 64 (2012) 18-23.
[73] H. Kamata, X. Li, U.i. Chung, T. Sakai, Biomaterials: Design of Hydrogels for Biomedical Applications (Adv. Healthcare Mater. 16/2015), Advanced healthcare materials 4(16) (2015) 2598-2598.
[74] K.Y. Lee, D.J. Mooney, Hydrogels for tissue engineering, Chemical reviews 101(7) (2001) 1869-1880.
[75] D. Jain, D. Bar-Shalom, Alginate drug delivery systems: application in context of pharmaceutical and biomedical research, Drug development and industrial pharmacy 40(12) (2014) 1576-1584.
[76] T.R. Hoare, D.S. Kohane, Hydrogels in drug delivery: progress and challenges, Polymer 49(8) (2008) 1993-2007.
[77] C.L. Bayer, N.A. Peppas, Advances in recognitive, conductive and responsive delivery systems, Journal of Controlled Release 132(3) (2008) 216-221.
[78] C. He, S.W. Kim, D.S. Lee, In situ gelling stimuli-sensitive block copolymer hydrogels for drug delivery, Journal of controlled release 127(3) (2008) 189-207.
[79] R. Cheng, F. Feng, F. Meng, C. Deng, J. Feijen, Z. Zhong, Glutathione-responsive nano-vehicles as a promising platform for targeted intracellular drug and gene delivery, Journal of controlled release 152(1) (2011) 2-12.
[80] M. Delcea, H. Möhwald, A.G. Skirtach, Stimuli-responsive LbL capsules and nanoshells for drug delivery, Advanced drug delivery reviews 63(9) (2011) 730-747.
[81] S. Maiti, K. Singha, S. Ray, P. Dey, B. Sa, Adipic acid dihydrazide treated partially oxidized alginate beads for sustained oral delivery of flurbiprofen, Pharmaceutical development and technology 14(5) (2009) 461-470.
[82] Q. Wang, J. Zhang, A. Wang, Preparation and characterization of a novel pH-sensitive chitosan-g-poly (acrylic acid)/attapulgite/sodium alginate composite hydrogel bead for controlled release of diclofenac sodium, Carbohydrate Polymers 78(4) (2009) 731-737.
[83] X. Zhang, Z. Hui, D. Wan, H. Huang, J. Huang, H. Yuan, J. Yu, Alginate microsphere filled with carbon nanotube as drug carrier, International journal of biological macromolecules 47(3) (2010) 389-395.
[84] R. Pilliar, M. Filiaggi, J. Wells, M. Grynpas, R. Kandel, Porous calcium polyphosphate scaffolds for bone substitute applications—in vitro characterization, Biomaterials 22(9) (2001) 963-972.
[85] S. Nardecchia, M.C. Gutiérrez, M.C.n. Serrano, M. Dentini, A. Barbetta, M.L. Ferrer, F. del Monte, In situ precipitation of amorphous calcium phosphate and ciprofloxacin crystals during the formation of chitosan hydrogels and its application for drug delivery purposes, Langmuir 28(45) (2012) 15937-15946.
[86] M. D'este, D. Eglin, Hydrogels in calcium phosphate moldable and injectable bone substitutes: Sticky excipients or advanced 3-D carriers?, Acta biomaterialia 9(3) (2013) 5421-5430.
[87] S. Bose, S. Tarafder, Calcium phosphate ceramic systems in growth factor and drug delivery for bone tissue engineering: a review, Acta biomaterialia 8(4) (2012) 1401-1421.
[88] M. Rajkumar, N. Meenakshisundaram, V. Rajendran, Development of nanocomposites based on hydroxyapatite/sodium alginate: Synthesis and characterisation, Materials Characterization 62(5) (2011) 469-479.

[89] J. Zhang, Q. Wang, A. Wang, In situ generation of sodium alginate/hydroxyapatite nanocomposite beads as drug-controlled release matrices, Acta Biomaterialia 6(2) (2010) 445-454.
[90] W. Amer, K. Abdelouahdi, H.R. Ramananarivo, A. Fihri, M. El Achaby, M. Zahouily, A. Barakat, K. Djessas, J. Clark, A. Solhy, Smart designing of new hybrid materials based on brushite-alginate and monetite-alginate microspheres: Bio-inspired for sequential nucleation and growth, Materials Science and Engineering: C 35 (2014) 341-346.
[91] A.A. Mirtchi, J. Lemaitre, N. Terao, Calcium phosphate cements: Study of the β-tricalcium phosphate—monocalcium phosphate system, Biomaterials 10(7) (1989) 475-480.
[92] A.A. Mirtchi, J. Lemaître, E. Munting, Calcium phosphate cements: effect of fluorides on the setting and hardening of β-tricalcium phosphate-dicalcium phosphate-calcite cements, Biomaterials 12(5) (1991) 505-510.
[93] M. Bohner, H. Merkle, J. Lemai, In vitro aging of a calcium phosphate cement, Journal of Materials Science: Materials in Medicine 11(3) (2000) 155-162.
[94] J. Aberg, H. Brisby, H. Henriksson, A. Lindahl, P. Thomsen, H. Engqvist, Premixed acidic calcium phosphate cement: characterization of strength and microstructure, Journal of Biomedical Materials Research Part B: Applied Biomaterials 93(2) (2010) 436-441.
[95] M.H. Alkhraisat, C. Moseke, L. Blanco, J.E. Barralet, E. Lopez-Carbacos, U. Gbureck, Strontium modified biocements with zero order release kinetics, Biomaterials 29(35) (2008) 4691-4697.
[96] T.R. Desai, S.B. Bhaduri, A.C. Tas, A self-setting, monetite (CaHPO 4) cement for skeletal repair, Advances in Bioceramics and Biocomposites II (2007) 61-69.
[97] M. Bohner, U. Gbureck, Thermal reactions of brushite cements, Journal of Biomedical Materials Research Part B: Applied Biomaterials 84(2) (2008) 375-385.
[98] F. Tamimi, D. Le Nihouannen, H. Eimar, Z. Sheikh, S. Komarova, J. Barralet, The effect of autoclaving on the physical and biological properties of dicalcium phosphate dihydrate bioceramics: brushite vs. monetite, Acta biomaterialia 8(8) (2012) 3161-3169.
[99] C. Ribeiro, C. Barrias, M. Barbosa, Calcium phosphate-alginate microspheres as enzyme delivery matrices, Biomaterials 25(18) (2004) 4363-4373.
[100] A. Hirsch, I. Azuri, L. Addadi, S. Weiner, K. Yang, S. Curtarolo, L. Kronik, Infrared absorption spectrum of brushite from first principles, Chemistry of Materials 26(9) (2014) 2934-2942.
[101] R. Štulajterová, Ľ. Medvecký, Effect of calcium ions on transformation brushite to hydroxyapatite in aqueous solutions, Colloids and Surfaces A: Physicochemical and Engineering Aspects 316(1) (2008) 104-109.
[102] E. Stodolak, C. Paluszkiewicz, M. Bogun, M. Blazewicz, Nanocomposite fibres for medical applications, Journal of Molecular Structure 924 (2009) 208-213.
[103] M.T. Jahromi, G. Yao, M. Cerruti, The importance of amino acid interactions in the crystallization of hydroxyapatite, Journal of The Royal Society Interface 10(80) (2013) 20120906.
[104] C. Suryanarayana, M.G. Norton, X-ray diffraction: a practical approach, Springer Science & Business Media2013.
[105] V. Mulley, C. Cavendish, A thermogravimetric method for the analysis of mixtures of brushite and monetite, Analyst 95(1128) (1970) 304-307.
[106] N. Mohan, P.D. Nair, Novel porous, polysaccharide scaffolds for tissue engineering applications, Trends Biomater Artif Organs 18(2) (2005) 219-224.
[107] R.L. Frost, S.J. Palmer, Thermal stability of the 'cave'mineral brushite CaHPO 4· 2H 2 O–Mechanism of formation and decomposition, Thermochimica acta 521(1) (2011) 14-17.

[108] J. Soares, J. Santos, G. Chierice, E. Cavalheiro, Thermal behavior of alginic acid and its sodium salt, Eclética Química 29(2) (2004) 57-64.
[109] R. Russo, M. Malinconico, G. Santagata, Effect of cross-linking with calcium ions on the physical properties of alginate films, Biomacromolecules 8(10) (2007) 3193-3197.
[110] R. Hamai, T. Toshima, M. Tafu, T. Masutani, T. Chohji, Effect of anions on morphology control of brushite particles, Key Engineering Materials, Trans Tech Publ, 2013, pp. 55-60.
[111] T. Toshima, R. Hamai, M. Tafu, Y. Takemura, S. Fujita, T. Chohji, S. Tanda, S. Li, G. Qin, Morphology control of brushite prepared by aqueous solution synthesis, Journal of Asian Ceramic Societies 2(1) (2014) 52-56.
[112] P.D. Reddy, D. Swarnalatha, Recent advances in novel drug delivery systems, International Journal of PharmTech Research 2(3) (2010) 2025-2027.
[113] J. Wu, W. Wei, L.-Y. Wang, Z.-G. Su, G.-H. Ma, A thermosensitive hydrogel based on quaternized chitosan and poly (ethylene glycol) for nasal drug delivery system, Biomaterials 28(13) (2007) 2220-2232.
[114] S. Jabeen, M. Maswal, O.A. Chat, G.M. Rather, A.A. Dar, Rheological behavior and Ibuprofen delivery applications of pH responsive composite alginate hydrogels, Colloids and Surfaces B: Biointerfaces 139 (2016) 211-218.
[115] P. Zhao, H. Liu, H. Deng, L. Xiao, C. Qin, Y. Du, X. Shi, A study of chitosan hydrogel with embedded mesoporous silica nanoparticles loaded by ibuprofen as a dual stimuli-responsive drug release system for surface coating of titanium implants, Colloids and Surfaces B: Biointerfaces 123 (2014) 657-663.
[116] R. Oun, J.A. Plumb, N.J. Wheate, A cisplatin slow-release hydrogel drug delivery system based on a formulation of the macrocycle cucurbit [7] uril, gelatin and polyvinyl alcohol, Journal of inorganic biochemistry 134 (2014) 100-105.
[117] I.S.T. de Figueiredo, M.V. Ramos, N.M.P.S. Ricardo, M.L. da Costa Gonzaga, R.S.P. Pinheiro, N.M.N. de Alencar, Efficacy of a membrane composed of polyvinyl alcohol as a vehicle for releasing of wound healing proteins belonging to latex of Calotropis procera, Process Biochemistry 49(3) (2014) 512-519.
[118] X.J. Loh, P. Peh, S. Liao, C. Sng, J. Li, Controlled drug release from biodegradable thermoresponsive physical hydrogel nanofibers, Journal of Controlled Release 143(2) (2010) 175-182.
[119] M. González-Rodrıguez, M. Holgado, C. Sanchez-Lafuente, A. Rabasco, A. Fini, Alginate/chitosan particulate systems for sodium diclofenac release, International Journal of Pharmaceutics 232(1) (2002) 225-234.
[120] S. Lee, Y.-C. Kim, J.-H. Park, Zein-alginate based oral drug delivery systems: Protection and release of therapeutic proteins, International journal of pharmaceutics 515(1) (2016) 300-306.
[121] Q. Wang, X. Xie, X. Zhang, J. Zhang, A. Wang, Preparation and swelling properties of pH-sensitive composite hydrogel beads based on chitosan-g-poly (acrylic acid)/vermiculite and sodium alginate for diclofenac controlled release, International Journal of Biological Macromolecules 46(3) (2010) 356-362.
[122] H.J. Kim, H. Matsuda, H. Zhou, I. Honma, Ultrasound-Triggered Smart Drug Release from a Poly (dimethylsiloxane)–Mesoporous Silica Composite, Advanced Materials 18(23) (2006) 3083-3088.
[123] C. Viseras, C. Aguzzi, P. Cerezo, M. Bedmar, Biopolymer–clay nanocomposites for controlled drug delivery, Materials Science and Technology 24(9) (2008) 1020-1026.
[124] S.-F. Wang, L. Shen, W.-D. Zhang, Y.-J. Tong, Preparation and mechanical properties of chitosan/carbon nanotubes composites, Biomacromolecules 6(6) (2005) 3067-3072.

[125] A. Ilie, C. Ghiţulică, E. Andronescu, A. Cucuruz, A. Ficai, New composite materials based on alginate and hydroxyapatite as potential carriers for ascorbic acid, International journal of pharmaceutics 510(2) (2016) 501-507.
[126] M.S. Hasnain, A.K. Nayak, M. Singh, M. Tabish, M.T. Ansari, T.J. Ara, Alginate-based bipolymeric-nanobioceramic composite matrices for sustained drug release, International journal of biological macromolecules 83 (2016) 71-77.
[127] S.M.H. Dabiri, A. Lagazzo, F. Barberis, M. Farokhi, E. Finocchio, L. Pastorino, Letter to editor for supporting "Characterization of alginate-brushite in-situ hydrogel composites", Materials Science & Engineering C (74) (2017) 410-412.
[128] S.M.H. Dabiri, A. Lagazzo, F. Barberis, M. Farokhi, E. Finochio, L. Pastorino, Characterization of alginate-brushite in-situ hydrogel composites, Materials Science and Engineering: C 67 (2016) 502-510.
[129] P. Horcajada, C. Márquez-Alvarez, A. Rámila, J. Pérez-Pariente, M. Vallet-Regí, Controlled release of Ibuprofen from dealuminated faujasites, Solid State Sciences 8(12) (2006) 1459-1465.
[130] A. Jubert, M.L. Legarto, N.E. Massa, L.L. Tévez, N.B. Okulik, Vibrational and theoretical studies of non-steroidal anti-inflammatory drugs Ibuprofen [2-(4-isobutylphenyl) propionic acid]; Naproxen [6-methoxy-α-methyl-2-naphthalene acetic acid] and Tolmetin acids [1-methyl-5-(4-methylbenzoyl)-1H-pyrrole-2-acetic acid], Journal of molecular structure 783(1) (2006) 34-51.
[131] S.H. Bjørnøy, D.C. Bassett, S. Ucar, J.-P. Andreassen, P. Sikorski, Letter to the Editor re "Characterization of alginate-brushite in-situ hydrogel composites", Materials Science & Engineering C (70) (2017) 930-931.
[132] S.C. Angadi, L.S. Manjeshwar, T.M. Aminabhavi, Novel composite blend microbeads of sodium alginate coated with chitosan for controlled release of amoxicillin, International journal of biological macromolecules 51(1) (2012) 45-55.
[133] A. Marrella, A. Lagazzo, F. Barberis, T. Catelani, R. Quarto, S. Scaglione, Enhanced mechanical performances and bioactivity of cell laden-graphene oxide/alginate hydrogels open new scenario for articular tissue engineering applications, Carbon 115 (2017) 608-616.
[134] W.F. Lee, R.J. Wu, Superabsorbent polymeric materials. II. Swelling behavior of crosslinked poly [sodium acrylate-co-3-dimethyl (methacryloyloxyethyl) ammonium propane sulfonate] in aqueous salt solution, Journal of applied polymer science 64(9) (1997) 1701-1712.
[135] J. Zhao, X. Zhao, B. Guo, P.X. Ma, Multifunctional interpenetrating polymer network hydrogels based on methacrylated alginate for the delivery of small molecule drugs and sustained release of protein, Biomacromolecules 15(9) (2014) 3246-3252.
[136] P.V. Giannoudis, H. Dinopoulos, E. Tsiridis, Bone substitutes: an update, Injury 36(3) (2005) S20-S27.
[137] J.C. Banwart, M.A. Asher, R.S. Hassanein, Iliac crest bone graft harvest donor site morbidity: a statistical evaluation, Spine 20(9) (1995) 1055-1060.
[138] K. Hing, B. Annaz, S. Saeed, P. Revell, T. Buckland, Microporosity enhances bioactivity of synthetic bone graft substitutes, Journal of Materials Science: Materials in Medicine 16(5) (2005) 467-475.
[139] S. Mokhtari, K. Skelly, E. Krull, A. Coughlan, N. Mellott, Y. Gong, R. Borges, A. Wren, Copper-containing glass polyalkenoate cements based on SiO2–ZnO–CaO–SrO–P2O5 glasses: glass characterization, physical and antibacterial properties, Journal of Materials Science 52(15) (2017) 8886-8903.
[140] W. Brown, A new calcium phosphate cement, J. Dent. Res. 63 (1983) 672.
[141] W. Brown, Dental restoration cement, US patent documents, Patent No. 4518430 (1985).

[142] W. Habraken, P. Habibovic, M. Epple, M. Bohner, Calcium phosphates in biomedical applications: materials for the future?, Materials Today 19(2) (2016) 69-87.
[143] M. EBRA, Calcium phosphate bone cements, Orthopaedic bone cements (2008) 206.
[144] M. Bohner, Reactivity of calcium phosphate cements, Journal of Materials Chemistry 17(38) (2007) 3980-3986.
[145] G. Vereecke, J. Lemaître, Calculation of the solubility diagrams in the system Ca (OH) 2-H3PO4-KOH-HNO3-CO2-H2O, Journal of Crystal Growth 104(4) (1990) 820-832.
[146] F. Tamimi-Marino, J. Mastio, C. Rueda, L. Blanco, E. López-Cabarcos, Increase of the final setting time of brushite cements by using chondroitin 4-sulfate and silica gel, Journal of materials Science: Materials in medicine 18(6) (2007) 1195-1201.
[147] Y. Zhang, H.H. Xu, Effects of synergistic reinforcement and absorbable fiber strength on hydroxyapatite bone cement, Journal of Biomedical Materials Research Part A 75(4) (2005) 832-840.
[148] T.-Y. Chiang, C.-C. Ho, D.C.-H. Chen, M.-H. Lai, S.-J. Ding, Physicochemical properties and biocompatibility of chitosan oligosaccharide/gelatin/calcium phosphate hybrid cements, Materials Chemistry and Physics 120(2) (2010) 282-288.
[149] X. Wang, L. Chen, H. Xiang, J. Ye, Influence of anti-washout agents on the rheological properties and injectability of a calcium phosphate cement, Journal of Biomedical Materials Research Part B: Applied Biomaterials 81(2) (2007) 410-418.
[150] L. Zhao, M.D. Weir, H.H. Xu, An injectable calcium phosphate-alginate hydrogel-umbilical cord mesenchymal stem cell paste for bone tissue engineering, Biomaterials 31(25) (2010) 6502-6510.
[151] M. Tang, W. Chen, M.D. Weir, W. Thein-Han, H.H. Xu, Human embryonic stem cell encapsulation in alginate microbeads in macroporous calcium phosphate cement for bone tissue engineering, Acta biomaterialia 8(9) (2012) 3436-3445.
[152] S.G. Fullana, H. Ternet, M. Freche, J.-L. Lacout, F. Rodriguez, Controlled release properties and final macroporosity of a pectin microspheres–calcium phosphate composite bone cement, Acta biomaterialia 6(6) (2010) 2294-2300.
[153] T. Fuji, T. Anada, Y. Honda, Y. Shiwaku, H. Koike, S. Kamakura, K. Sasaki, O. Suzuki, Octacalcium phosphate–precipitated alginate scaffold for bone regeneration, Tissue Engineering Part A 15(11) (2009) 3525-3535.
[154] J. Esteban, J. Cordero-Ampuero, Treatment of prosthetic osteoarticular infections, Expert opinion on pharmacotherapy 12(6) (2011) 899-912.
[155] P.A. Tran, L. Sarin, R.H. Hurt, T.J. Webster, Opportunities for nanotechnology-enabled bioactive bone implants, Journal of Materials Chemistry 19(18) (2009) 2653-2659.
[156] M. Espanol, R. Perez, E. Montufar, C. Marichal, A. Sacco, M. Ginebra, Intrinsic porosity of calcium phosphate cements and its significance for drug delivery and tissue engineering applications, Acta Biomaterialia 5(7) (2009) 2752-2762.
[157] J. Cabrejos-Azama, M.H. Alkhraisat, C. Rueda, J. Torres, C. Pintado, L. Blanco, E. López-Cabarcos, Magnesium substitution in brushite cements: Efficacy of a new biomaterial loaded with vancomycin for the treatment of Staphylococcus aureus infections, Materials Science and Engineering: C 61 (2016) 72-78.
[158] S. Pujari-Palmer, X. Lu, V.P. Singh, L. Engman, M. Pujari-Palmer, M.K. Ott, Incorporation and delivery of an organoselenium antioxidant from a brushite cement, Materials Letters 197 (2017) 115-119.
[159] C. Chen, Y. Chen, P. Wu, B. Chen, Update on new medicinal applications of gentamicin: evidence-based review, Journal of the Formosan Medical Association 113(2) (2014) 72-82.

[160] L. Montazeri, J. Javadpour, M.A. Shokrgozar, S. Bonakdar, S. Javadian, Hydrothermal synthesis and characterization of hydroxyapatite and fluorhydroxyapatite nano-size powders, Biomedical Materials 5(4) (2010) 045004.
[161] D. Dorset, X-ray diffraction: a practical approach, Microscopy and Microanalysis 4(5) (1998) 513-515.
[162] G. Cama, B. Gharibi, M.S. Sait, J. Knowles, A. Lagazzo, S. Romeed, L. Di Silvio, S. Deb, A novel method of forming micro-and macroporous monetite cements, Journal of Materials Chemistry B 1(7) (2013) 958-969.
[163] F. Fayyazbakhsh, M. Solati-Hashjin, A. Keshtkar, M.A. Shokrgozar, M.M. Dehghan, B. Larijani, Novel layered double hydroxides-hydroxyapatite/gelatin bone tissue engineering scaffolds: Fabrication, characterization, and in vivo study, Materials Science and Engineering: C 76 (2017) 701-714.
[164] M.H. Alkhraisat, F.T. Marino, J.R. Retama, L.B. Jerez, E. López-Cabarcos, Beta-tricalcium phosphate release from brushite cement surface, Journal of Biomedical Materials Research Part A 84(3) (2008) 710-717.
[165] G. Cama, F. Barberis, M. Capurro, L. Di Silvio, S. Deb, Tailoring brushite for in situ setting bone cements, Materials Chemistry and Physics 130(3) (2011) 1139-1145.
[166] C.-H.D. Chen, C.-C. Chen, M.-Y. Shie, C.-H. Huang, S.-J. Ding, Controlled release of gentamicin from calcium phosphate/alginate bone cement, Materials Science and Engineering: C 31(2) (2011) 334-341.
[167] K. Ishikawa, Y. Miyamoto, M. Takechi, T. Toh, M. Kon, M. Nagayama, K. Asaoka, Non-decay type fast-setting calcium phosphate cement: Hydroxyapatite putty containing an increased amount of sodium alginate, Journal of Biomedical Materials Research Part A 36(3) (1997) 393-399.
[168] M. Bohner, J. Lemaître, P.V. Landuyt, P.Y. Zambelli, H.P. Merkle, B. Gander, Gentamicin-loaded hydraulic calcium phosphate bone cement as antibiotic delivery system, Journal of pharmaceutical sciences 86(5) (1997) 565-572.
[169] S.M.H. Dabiri, A. Lagazzo, F. Barberis, A. Shayganpour, E. Finocchio, L. Pastorino, New in-situ synthetized hydrogel composite based on alginate and brushite as a potential pH sensitive drug delivery system, Carbohydrate polymers 177 (2017) 324-333.
[170] A. Sionkowska, B. Kaczmarek, R. Gadzala-Kopciuch, Gentamicin release from chitosan and collagen composites, Journal of Drug Delivery Science and Technology 35 (2016) 353-359.
[171] S.M. Dizaj, F. Lotfipour, M. Barzegar-Jalali, M.-H. Zarrintan, K. Adibkia, Physicochemical characterization and antimicrobial evaluation of gentamicin-loaded CaCO 3 nanoparticles prepared via microemulsion method, Journal of Drug Delivery Science and Technology 35 (2016) 16-23.
[172] D. Lin-Vien, N.B. Colthup, W.G. Fateley, J.G. Grasselli, The handbook of infrared and Raman characteristic frequencies of organic molecules, Elsevier1991.
[173] M.-Y. Shie, D.C.-H. Chen, C.-Y. Wang, T.-Y. Chiang, S.-J. Ding, Immersion behavior of gelatin-containing calcium phosphate cement, Acta Biomaterialia 4(3) (2008) 646-655.
[174] C.-C. Chen, C.-C. Ho, C.-H.D. Chen, W.-C. Wang, S.-J. Ding, In vitro bioactivity and biocompatibility of dicalcium silicate cements for endodontic use, Journal of endodontics 35(11) (2009) 1554-1557.
[175] J. Schnieders, U. Gbureck, R. Thull, T. Kissel, Controlled release of gentamicin from calcium phosphate—poly (lactic acid-co-glycolic acid) composite bone cement, Biomaterials 27(23) (2006) 4239-4249.
[176] H.H. Tønnesen, J. Karlsen, Alginate in drug delivery systems, Drug development and industrial pharmacy 28(6) (2002) 621-630.

[177] M.P. Singh, J. Stefko, J.A. Lumpkin, J. Rosenblatt, The effect of electrostatic charge interactions on release rates of gentamicin from collagen matrices, Pharmaceutical research 12(8) (1995) 1205-1210.